## Department of Precision and Microsystems Engineering

# Development of a vascular model with pre-formed channels to create an alveolar-capillary barrier model integrating flow and stretching

PAULIEN LANINGA

Report no : 2025.007
Supervisors : U. Staufer, S. Koornneef and R. Rottier
Specialisation : Micro and Nano Engineering
Type of report : Thesis Report
Date : 25 February 2025

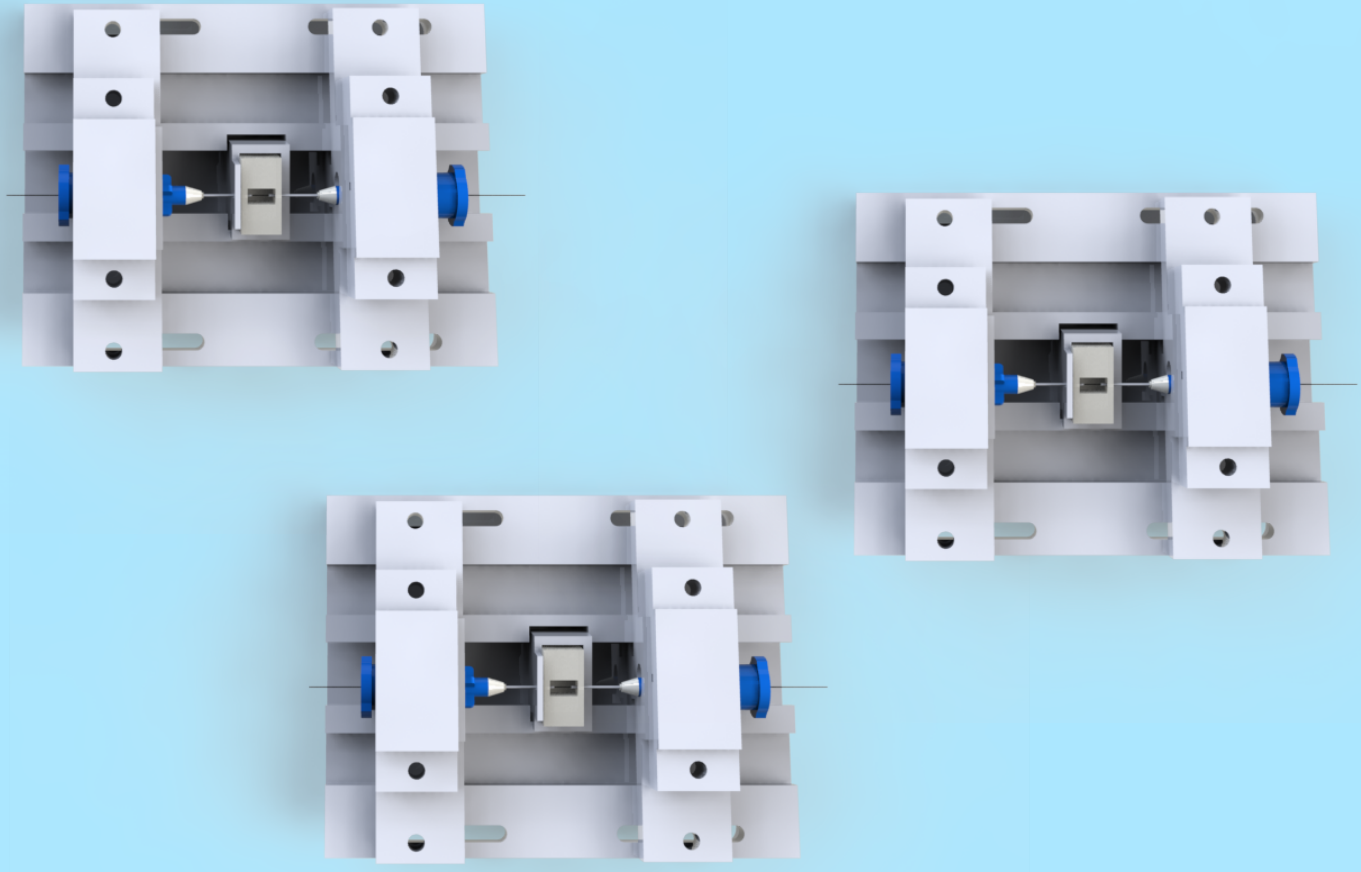

TU Delft Delft University of Technology

Challenge the future

# Development of a vascular model with pre-formed channels to create an alveolar-capillary barrier model integrating flow and stretching

Thesis report

Paulien Laninga

to be publicly defended on:
February 25, 2025 at 10:00 PM.

Thesis committee:

Prof. dr. U. Staufer
Prof. dr. R. Rottier
Dr. P. Fanzio
S. Koornneef MSc



# Preface

This master thesis report is the final part of my master's program High Tech Engineering, part of Mechanical Engineering at the Delft University of Technology. The project was conducted in collaboration with the Erasmus Medical Center in Rotterdam.

The project's success and the joy it brought would not have been possible without the advice, help and invaluable support of my supervisors, friends and family.

I would therefore like to thank the following people in particular. First of all, I would like to thank my main supervisors. Urs Staufer, thank you for all your support and advice. I have enjoyed our interesting discussions and brainstorming sessions during our weekly meetings.

From the Erasmus Medical Center, I would like to thank Sem Koornneef for all your patience and comprehensive explanations about everything related to cell culturing, and for setting up the culturing, maintaining and imaging of all the vessels for this research. I also want to thank Robbert Rottier for your insightful advice and recommendations on related research. Furthermore, I want to thank Floor Benthem for sharing your knowledge on setting up cell cultures.

From the TU Delft, I would like to thank Pieter van Altena for his help with the Nanoindenter and Andrés Hunt for his advice related to the Hydra printer. Moreover, I want to thank all MNE lab staff for their feedback and advice. I thank all the lab technicians of PME, especially Alex van den Bogaard for his assistance in the chemical lab and Gideon Emmaneel for his help with straighting the wires.

Lastly, I want to thank for all the support and encouragement of my friends and family during some challenging times during the project.

# Abstract

This report presents a route map and the first steps to the development of a vascularised alveolar-capillary barrier to study the effects of air pollution on lung-health and chronic respiratory diseases. The ultimate goal is to fabricate a vascularised model of an alveolar-capillary barrier, that mimics the physiology of the human lung more closely than currently used models. Current vascularised alveolar-capillary barrier models are limited by the absence of membrane-free designs and the lack of integration of both fluid flow and membrane stretching. The development of a membrane-free, vascularised model that integrates fluid flow and membrane stretching, requires a reproducible vascularisation method with a lifespan sufficient for epithelial cell differentiation and follow-up experiments. Pre-structured vessels provide more control of the structure of the vessel network and improve the reproducibility of a model compared to a model with a self-assembled vascular network. Therefore, the first step in this study is to establish a method for culturing a lung-derived endothelial vessel in a pre-formed channel within hydrogel as extracellular matrix that can last several weeks. Wire moulding is used to create a hollow channel inside a fibrinogen-based hydrogel between two injection needles. Two diameters of wires, 50 µm and 125 µm, and two concentrations, 1% and 2%, of fibrinogen were used for a total of 10 tests. The endothelial cells were seeded using the capillary effect and after four hours, the perfusion of medium through the channels started. A pre-formed channel in the hydrogel containing 2% hydrogel and seeded with lung-derived endothelial cells remained perfusable for 32 days while withstanding flow leading to a significant amount of shear stress on the endothelial cells. To study the phenomena of gas exchange that accur across larger tissue constructs, the hierarchical dimensions and topological complexity of native vascular beds should be better replicated. Another moulding method is needed to create a structure of hollow channels inside a hydrogel to culture a vascular network rather than one vessel. It was found that with carbohydrate glass, varying structures can be printed and it can be embedded within hydrogel prior to cross-linking without blending into one another. This indicates that sacrificial moulding using carbohydrate glass is a promising technique for creating pre-structured vascularised networks. This potential method to create a pre-structured network combined with our cell seeding method and the 2% fibrinogen hydrogel, is the basis for the development of a reproducible, membrane-free vascularised alveolar-capillary barrier model that incorporates flow and stretching of the barrier.

# Contents

# 1 Introduction

Environmental pollution triggers inflammatory responses in the lungs that affect human lung health and may contribute to the development of chronic lung diseases. Understanding and predicting the progression of chronic lung diseases is important to provide appropriate care. Appropriate cellular models are needed to improve knowledge and understanding of the underlying functional mechanisms of these cellular responses. The use of Lung-on-a-Chip could provide a significant improvement in mimicking the human lung compared to other models. However, several drawbacks and limitations need to be overcome. The structural and dynamic properties of the model should be improved. Erasmus MC and TU Delft are collaborating to obtain a more dynamic and physiologically relevant model to study the effect of environmental pollution on the alveolar-capillary barrier. This report describes the development of a new alveolar-capillary barrier model integrating medium-flow, air-flow and membrane stretching. The initial steps of this development have been taken. A device using wire-moulding has been created for culturing a microvessel model, which is fully described in article form within this report. Additionally, research has begun to explore sacrificial moulding as a potential technique for culturing a vascular network model. Furthermore, possible design options for subsequent development are presented.

# 2 Concept introduction

Based on the findings in literature, a research potential has been identified. These findings are reviewed in detail in the Literature Review, which can be found in Appendix E, and are further discussed in the article presented in Chapter 3.

## 2.1 Research potential

The human alveolar-capillary barrier has a complex physiology. To study the effects of air pollution, such as particle transport and inflammatory responses, on lung health, it is crucial to accurately mimic its physiological environment. While certain simplifications are necessary to create a robust and reproducible model, some parameters are critical and must be included.

Key parameters identified as essential for the model include blood flow, air flow, membrane stretching, and vasculature. Additionally, the model must have a sufficient lifespan to allow for extended culture periods and experimental work. It should also avoid the use of Polydimethylsiloxane (PDMS) and fabricated membranes. Currently, no existing model in the literature fulfils all these requirements.

A reproducible method is therefore needed to culture lung-derived endothelial vessels using preformed channels embedded in hydrogel as the extracellular matrix, designed to last for several weeks. The micro-vessel model should enable the integration of airflow and membrane stretching in subsequent designs, ensuring the relevance of the model.

## 2.2 Research question

The research potential described in section 2.1 leads to the following research question and its sub-questions:
**Can pre-formed channels be used to develop a micro-vessel model to vascularise an alveolar-capillary barrier model integrating flow and stretching?**

- How to create and perfuse hollow channels inside a hydrogel?
  - Which cell seeding method should be used?
  - Which hydrogel should be used?
  - What diameters can be obtained and perfused for several weeks?
- What method can be used to create a perfusable network of hollow channels embedded in a hydrogel?

- Can carbohydrate glass be printed with a fused deposition printer?
- Can carbohydrate glass be embedded within hydrogel prior to cross-linking?

## 2.3 Requirements

Several requirements should be considered when answering the research question and sub-questions mentioned in the 2.2 section. The research question and the requirements will be used to set the objectives. The **device** will be used to culture **models** of an alveolar-capillary barrier to study the effect of pollution on the alveolar-capillary barrier.

To ensure reliable experimental results, the cultured model should be reproducible and include important parameters to accurately mimic the biological environment of the human alveolar-capillary barrier. Reproducing the mechanical environment of the biological tissue is important because of the cellular response to shear stress and strain. The mechanical properties that should be included in this model are listed in the table 2.1.

| Requirements micro-vessel model | Value |
|---|---|
| Shear stress on endothelial cells | 0.1-1 Pa |
| Stiffness of tissue | 1-2 kPa |
| Strain tissue | 10-20% |
| Stretching frequency | 0.2 Hz |
| Perfusability of the vessels | Several weeks |

Table 2.1: Requirements micro-vessel model

In addition to the requirements for the micro-vessel model, there are also requirements for the device used to create the model, which are listed in Table 2.3. To obtain a strain of 10-20% of the membrane, the container in which the model is cultured should also be able to reach this strain. In addition, in order to study the cellular response to environmental stress, it should be possible to assess the cellular response optically, for example with fluoroscopy. An optically transparent device is therefore required. It should also be possible to connect the hollow channels to tubes in order to enable the perfusion of the vessels. Furthermore, it should also be possible to manufacture the device at TU Delft and to transport it and perform the cell culture at Erasmus MC.

| Device requirements |
|---|
| Optical transparency |
| Connection pump to the channels |
| Allow 10-20% strain of the model |
| Create a reproducible model |

Table 2.2: Requirements device

## 2.4 Future design concept

To create a vascularised alveolar-capillary model, a vascular network is preferred over a single straight vessel as it increases the surface area of the model, thereby providing more epithelial cells with sufficient nutrients. Also, with a vascular network the hierarchical dimensions and

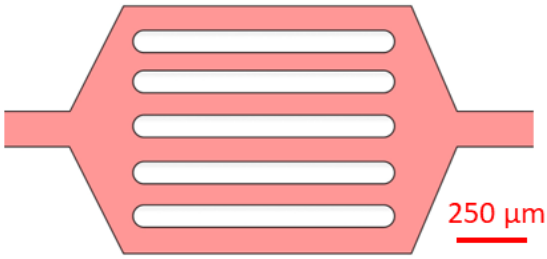


Figure 2.1: Concept of a structure to create a blood vessel network with one inlet and oulet.

topological complexity of native vascular beds can be better replicated. For ease of use and to minimize the amount of tubing needed, a network design with a single inlet and outlet is desirable. A pre-formed structure could therefore have the design shown in Figure 2.1. Additionally, the structure can be optimized to ensure uniformly distributed shear stress on the cells. Another approach can be to focus more on the hierarchical structure of a vascular bed *in vivo*.

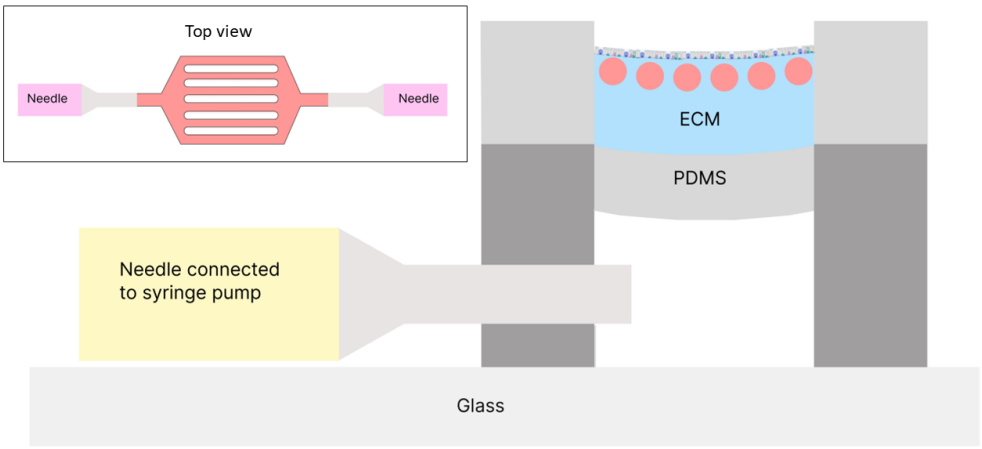


Figure 2.2: Concept of future design. The top view of a blood vessel network is shown. The PDMS structure is attached to a glass substrate, creating a vacuum room underneath the container with the model. A yellow needle is connected to the inside of the vacuum room to control the air pressure and enable stretching of the PDMS layer. This could control periodically stretching of the model which is fully surrounded with hydrogel.

The micro-vessel model should allow the integration of airflow and membrane stretching in future designs to ensure its physiological relevance. To achieve this, a conceptual design for future devices is proposed, allowing for the integration of those parameters. Huh *et al.* demonstrated that a PDMS membrane can achieve a one-axial strain of 10–20% [1]. This makes it a suitable material for our application. This supports the use of a PDMS container to culture the blood vessel, vascular network, and eventually the alveolar-capillary barrier either within or on the

container. In this model, the interface between epithelial and endothelial cells is free of PDMS.

Zamprogno *et al.* used an air pressure differential to generate tri-axial strain in their alveolar-capillary barrier model [2]. A similar approach could be adapted for this design by introducing a vacuum chamber beneath the container housing the vascular network, as illustrated in Figure 2.2. The container should be round to enable tri-axial stretching of the model. The mould used to create this PDMS container is shown in Figures 2.3 and 2.4.

Figure 2.3: Illustration of a closed mould designed to create six round PDMS containers. The mould has a cover that is supported on two opposite sides. This design allows the PDMS to be cut parallel to the two other sides while the cover remains closed. Because this design allows cutting while the cover stays closed, air can enter between the PDMS and the mould, making it easier to remove the PDMS.

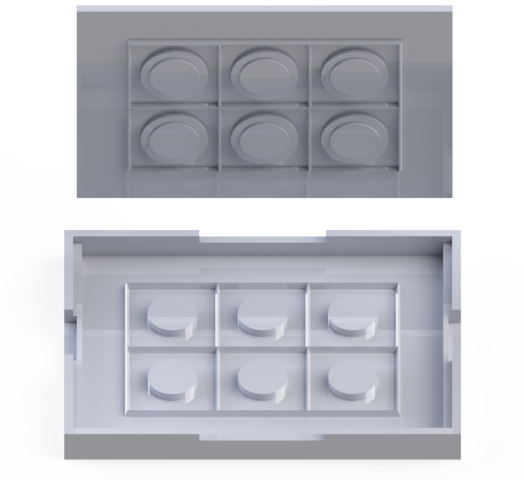

Figure 2.4: The cover is tilted, revealing the inside of the mould. On both sides of the mould, there is a circular thickening. When the lid is closed, a 1 mm gap remains between these thickenings, allowing a thin layer of PDMS to form in that space. As a result, the PDMS develops round cavities on both sides. One of these cavities, which has an edge, can be used for printing a sacrificial mould, while the lower hollow space can function as a vacuum chamber.

Additionally, airflow regulation over the endothelial cells could be implemented using a pharmaceutical tri-clamp to connect a cylindrical PDMS container with tubing, allowing for the integration of airflow and potentially enabling membrane stretching as part of the model.

## 2.5 Research objectives

Despite the concept mentioned, this study focuses on the first step, answering the research questions. The main objective of this study is formulated as:
**Develop a micro-vessel model using pre-formed channels that can serve as a vascularised alveolar-capillary barrier model incorporating flow and stretching.**

**Creating and perfusing a micro-vessel fully embedded within a hydrogel with a pre-formed hollow.**

- Establish a method for fabricating perfusable hollow channels fully embedded within hydrogel.
- Identify a suitable cell seeding method to promote endothelialization of the hollow channels.
- Evaluate different compositions of a hydrogel to determine if they enable long-term perfusion.
- Determine if the cell seeding method and hydrogel lead to a vessel with endothelial cells which can subjected to a relevant shear stress.
- Investigate the range of diameters for hollow channels that can be created, perfused, and maintained for several weeks.

**Determine if sacrificial moulding using carbohydrate glass can be used to create a pre-formed network of hollow channels inside a hydrogel.**

- Develop a protocol for printing carbohydrate glass using a fused deposition printer to form sacrificial moulds for hollow channels.
- Test the feasibility of embedding carbohydrate glass structures within hydrogel prior to cross-linking, ensuring that the sacrificial material does not dissolve or blend into the hydrogel.

## 2.6 Methodology

A methodology is been created to provide an overview of the steps of this study.

To determine the desired cell seeding method, hydrogel and diameters the biological model should be evaluated. Evaluating the performance of the biological model is time-intensive due to the preparation of cells for culture and the need for a model lifespan of several weeks. Developing a 3D-printed sacrificial mould with the desired structure presents significant mechanical challenges. To streamline this research the first step is to start evaluating cell seeding methods, hydrogel formulations, and channel diameters using a simpler fabrication method that does not rely on the immediate success of sacrificial moulding. Also, mechanical development and biological evaluation are carried out in parallel. While the wire-moulding device is being tested and the micro-vessel model is cultured and evaluated, work is been done to develop a sacrificial mould.

### 2.6.1 Creating and perfusing hollow channels in hydrogel

**Fabrication of hollow channels**

- Develop a method based on needle moulding techniques found in literature to create hollow channels within hydrogel which can be connected to tubes.
- Design and fabricate a device which can use this moulding technique and which can alter the diameters of the hollow channel
- Test and optimize the accuracy of the device

**Hydrogel**

- Select 2 suitable fibrinogen-based hydrogel compositions
- Measure the effective young modulus of the hydrogels and compare with the physiological stiffness of lung tissue.

**Cell Seeding**

- Use different cell seeding methods to seed the endothelial cells into the hollow channels and determine an effective technique.

**Test the device and evaluate biological model**

- Assess cell attachment and alignment using fluorescent microscopy.
- Use fluorescence beats to measure flow rate and estimate the shear stress on the endothelial cells within the channels to confirm that it falls within the desired range of 0.1–1 Pa.
- Monitor the perfused channels for several weeks to determine their lifespan

### 2.6.2 Sacrificial moulding using carbohydrate glass

**Printing carbohydrate class**

- Determine a possible composition and a protocol for the preparation of the carbohydrate glass
- Write a G-code for printing carbohydrate glass structures using a fused deposition printer.
- Optimize printing parameters such as temperature, extrusion rate, and printing height to print several structures.

**Embedding carbohydrate glass in hydrogel**

- Embed carbohydrate glass structures within hydrogel prior to cross-linking and test if the materials do not dissolve or blend into each other.

# 3 Vascularization with wire moulding

# Development of a perfused micro-vessel model for studying the alveolar-capillary barrier

P.M. Laninga[1], S. Koornneef[2], R. Rottier[2], and U. Staufer[1a]

[1]Department of Precision and Microsystem Engineering, University of Delft
[2]Department of Pediatric Surgery, Erasmus University Rotterdam
[a]Corresponding author: Mekelweg 2, 2628 CD Delft, u.staufer@tudelft.nl

***Abstract*— Studying the effects of air pollution on lung-health and chronic respiratory diseases requires a model that accurately replicates the mechanical and structural properties of the alveolar-capillary barrier, offering deep insights into their physiology and pathology. It is known that the Lung-on-Chip technology, which integrates tissue engineering and microfluidic technology, has great potential for advancing drug development and personalized disease treatment studies. Current vascularised alveolar-capillary barrier models are limited by the absence of membrane-free designs and the lack of integration of both fluid flow and membrane stretching. To develop a membrane-free, vascularised model that integrates fluid flow and membrane stretching, a method is needed to create a reproducible vascular model with a lifespan sufficient for epithelial cell differentiation and follow-up experiments. In this study the goal is to establish a method for culturing reproducible lung-derived endothelial vessels using pre-formed channels within hydrogel as extracellular matrix that can last several weeks. Wire moulding is used to create a hollow channel inside a fibrinogen-based hydrogel between two injection needles. Two diameters of wires and two concentrations of fibrinogen were used for a total of 10 tests. The endothelial cells were seeded using the capillary effect, and after four hours, the perfusion of medium through the channels was started. A pre-formed channel seeded with lung-derived endothelial cells remained perfusable for 32 days while withstanding both flow and significant shear stress. This pre-structured vessel improves the reproducibility of the model compared to a random self-assembled vessel-network. In addition, this model remains longer perfusable than current vascularised alveolar-capillary barrier models. The lifespan of the model allows for the culture of epithelial cells at the air-liquid interface and follow-up experiments. This model and method enables the creation of pre-structured vascularisation within a hydrogel, providing the basis for a reproducible, membrane-free vascularised alveolar-capillary barrier model that incorporates flow and stretching of the barrier.**

## I. Introduction

A method is developed to culture a vessel perfusable for more than four weeks and fully embedded in a hydrogel simulating the extracellular matrix. This method is promising for creating pre-structured vascularization for an alveolar-capillary barrier. Pre-structured vascular networks provide greater control over flow rates and shear stress distribution in capillaries, potentially extending vessel perfusion times while better mimicking physiological dynamics. Additionally, these networks improve reproducibility, as their structure can be consistently recreated, unlike the randomness inherent in self-assembled networks [1]. A longer lifetime of the capillary network allows the integration of air-liquid-interface (ALI) culture of epithelial cells and follow-up experiments with the model. Compared to a monolayer of endothelial cells, a vascular structure better mimics the mechanical and structural properties of the barrier. A membrane-free model further enhances this replication. In membrane-free models, the term refers specifically to artificially constructed membranes used as scaffolds for culturing epithelial and endothelial cells. This should not be confused with the biological membranes that are components of the alveolar-capillary barrier. A model that better mimics the conditions of the human lung allows pathophysiological processes to be studied with greater accuracy. A model accurately mimicking pathophysiological processes is needed to investigate the effects of air pollution on lung-health and chronic respiratory diseases. To validate the relevance of our model, we first provide background information, starting with an overview of the physiology of the human alveolar-capillary barrier. Parameters that are crucial for the *in vitro* replication of this barrier are discussed, followed by a review of some existing models. Our method is then presented, followed by our results and recommendations for future research.

## II. Theory

This section describes the main considerations of current literature regarding the complex physiology of the human alveolar-capillary barrier. Important parameters are incorporated as requirements into our design process to create a new model that more accurately mimics the alveolar-capillary barrier. A more detailed description of the human alveolar-capillary barrier is given the literature review in Appendix E.

### A. Alveolar-capillary barrier

The permeable alveolar-capillary barrier plays a crucial role in the functioning of the lungs. It ensures gas exchange between the erythrocytes in the blood flowing through the capillaries and the ambient air in the alveoli. The barrier function is to protect the body from harmful substances through epithelial cells and to prevent leakage from the vessel into the airspace through endothelial cells [2]. The barrier also known as the respiratory membrane, consists of two fused basement membranes with an interstitial space between them in certain regions. The human respiratory membrane has an average thickness of $1.1\,\mu m \pm 0.1\,\mu m$. The gas exchange region is smaller, with a

thickness of 0.62 µm ± 0.04 µm [2][3][4]. The two basement membranes within the airway membrane are the endothelial and epithelial basement membranes.

*1) Aveolar epithelium:* The alveolar epithelium is primarily comprised of two types of cells: Type I pneumocytes and Type II pneumocytes, which will be referred to as AT1 (Alveolar Type 1) and AT2 (Alveolar Type 2) cells, respectively. AT1 cells facilitate gas exchange, while AT2 cells produce surfactant, a surface-active agent critical for reducing surface tension and influencing particle retention and movement [5]. AT2 cells are considered stem cells for the alveolus and can rebuild the epithelial layer when AT1 cells are injured [6] [7]. AT2 cells also regulate immune responses against invading pathogens, like bacteria or viruses, by interacting with immune cells present in the alveolar space, including dendritic cells, neutrophils, and resident alveolar macrophages [2] [8]. These macrophages, also known as dust cells, act as the final defence, removing or sequestering unwanted particles, dust, or pathogens [9]. The liquid lining layer has an estimated mean thickness of about 200 nm in the rat lung [10]. Another layer in the epithelium is the epithelial basement membrane which consists of an extracellular matrix and is around 50 nm thick [11].

*2) Interstitial space:* The interstitial space and partly the basement membranes consist of an extracellular matrix, now referred to as ECM, which contains collagen and elastin fibres [2][12]. The ECM is porous and provides structural support for cells. Some reports on animal lungs show that there are two different pore sizes in the membrane, most pores have a diameter of less than 2.5 nm and a small fraction have pores larger than 400 nm [4][13]. Between the alveolar epithelial and capillary endothelial basal laminae fibroblasts can be found. Fibroblasts are cells that can directly connect the endothelium to the epithelium through openings in the basement membranes [10][14]. In some parts of the respiratory system, the basement membranes are fused, thereby reducing the thickness of the barrier to a thickness of 0.62 µm to facilitate gas exchange [4].

*3) Alveoli endothelium:* The basement membrane of the capillary endothelium houses alveolar capillary (aCAP) endothelial cells, specialized for gas exchange, and general capillary (gCap) endothelial cells, which form the capillary network responsible for efficient gas exchange in the alveoli [15]. This network is connected to the broader vessel system, which facilitates the transport of oxygen and nutrients to tissues throughout the body. The capillaries around the alveoli are housed in ECM and have a diameter that can be as small as approximately 6-8 µm [16] [17][18] [19] [20]. Pericytes wrap around the endothelial cells and have finger-like extensions around the capillary wall. They play a crucial role in blood vessel stability and microvascular functions [21]. Blood flow in the capillaries causes shear stress on the endothelial cells, which is in the range of 0.1-1 Pa [22].

### *B. Important parameters modelling the barrier*

Replicating the human physiological environment with accuracy comes with a challenge when modelling the alveoli-capillary barrier. Certain simplifications are necessary to develop a robust and reproducible model. Nonetheless, some parameters are critical to include in the model. Our model is designed for studies investigating the effects of air pollution, such as particle transport and inflammatory reactions, on lung health. Several parameters influencing these processes are discussed.

*1) Blood flow:* The barrier experiences dynamic effects such as the blood flow. This flow affects vascular homeostasis, including the inflammatory response of endothelial cells [23]. Shear stress due to the friction of blood flow on the endothelial layer of capillaries in lungs in around 0.1-1 Pa [22]. This shear stress induces the release of various molecules, including vasoactive substances (such as nitric oxide and endothelin), hormones, and neurotransmitters [19]. These factors collectively control vascular functions like vasomotion (the contraction and relaxation of blood vessels), thrombosis, platelet aggregation, and inflammation [20]. Neurotransmitters can modulate neutrophil activity [24]. Neutrophils are immunocompetent cells that are present in the surfactant. A simple way to create flow in static models is by using rocking platforms. The flow generated by a rocking platform is bidirectional, unlike the unidirectional blood flow in a body. A study using human peripheral blood mononuclear cells (PBMCs), including lymphocytes, monocytes, and dendritic cells, examined the effects of different types of flow. It was found that cells cultured with bidirectional flow have a significant delay in the extravasation of immune cells compared to those cultured with unidirectional flow [25] [26]. Therefore, the direction of flow may influence the model, and to better mimic the barrier, unidirectional flow is preferred.

*2) Air flow:* There is also flow on the epithelial side of the barrier due to breathing. The diaphragm, as the primary respiratory muscle, causes the lungs to expand and contract. Additionally, other respiratory muscles, such as the intercostal muscles, contribute to this process by expanding and stabilizing the ribcage [27]. These rhythmically expanding alveolar walls create a flow inside the alveoli. The type of flow is not only influenced by the geometry of the alveoli, but also by how it is positioned in relation to an alveolar ducts. Radial flow and recirculation flow patterns, such as a vortex, can occur. However, there is still a limited understanding of the three-dimensional chaotic mixing within the alveoli. Furthermore, models are needed to study the effects of these flow patterns on the cells lining the alveolar walls [28].

*3) Stretching:* Another dynamic effect, due to breathing, is the stretching of the membrane. The stretch leads to distortion in cell shape. Stretching also affects the uptake of nanoparticles by the epithelial and endothelial and stimulates their transport across the barrier [29]. Also, the metabolic activity and proliferation are higher when alveolar epithelial cells are stretched [30]. Combining a strain of 10% with a shear stress of 1.5 Pa on the endothelial cells has shown an increase of the transport rate of the nanoparticles [29].

*4) Culture time:* ALI culturing of the epithelial cells is required to let them differentiate. The AT2 cells should be differentiated as it leads to the presence of AT1 cells [31]. AT1 and AT2 cells play an important role in protecting the body from harmful substances and therefore are necessary in a model. Culturing primary alveolar epithelial cells at an air-liquid interface (ALI) remains challenging. To estimate the necessary alveoli epithelial ALI-culture duration, we focus on AT2-to-AT1 differentiation observed in alveolar organoids, which takes 10 to 14 days [31]. The maturation time for small airway epithelial cells can take up to 21 to 28 days. Although, Jung *et al.* reported shortening this time to two weeks by using a model with a capillary network [32][33]. This reduction in maturation time might be because of an efficient nutrient supply and improved cell-cell crosstalk compared to a model with a scaffold or permeable membrane [34].

*5) ECM:* The human alveolar tissue has an elastic modulus in the range of 1 to 2 kPa [4][35]. The ECM provides structural support to the endothelial cells and epithelial cells. To mimic the human extracellular matrix, hydrogels are used. Hydrogel matrixes allow, just like the human ECM, small molecules to diffuse freely [1].

*6) Interstitial space:* As discussed in section II, the thickness of the interstitial space where the gas exchange occurs, can be as thin as $0.62\,\mu m \pm 0.04\,\mu m$. Current models fail to mimic the size of this barrier, as they often use relatively thick porous membranes. Also, models with ECM protein coated or PDMS-based membranes lack cellular crosstalk. This cellular communication is a critical function of the alveolar-capillary barrier, and the presence of such membranes disrupts this process [36]. Therefore, a membrane-free model is preferred as it best mimics the thin layer between the epithelium and endothelium [23]. Additionally, ensuring robust cell attachment is a major challenge when culturing cells on membranes, particularly under flow conditions [37] [38]. Various modification treatments can be applied to improve cell attachment. However, these treatments have both advantages and limitations. For example, some surface modifications can lead to rapid hydrophobic recovery, where the membrane surface quickly reverts to its original state, reducing long-term cell attachment. Furthermore, a single type of modification may not be universally effective for all cell lines, requiring tailored approaches for different applications [37] [38] [39]. Another reason to avoid using a membrane is that materials like Polydimethylsiloxane (PDMS) can affect the diffusion of small molecules due to its non-selective absorption of oxygen and other hydrophobic molecules. Therefore, the interface between epithelial and endothelial cells must be free of PDMS and the cells should only be in contact with hydrogel [1] [23] [38].

*7) Vasculature:* The vasculature is the pathway for transporting nutrients, toxic substances, and body waste throughout the body. It also plays a crucial role in the alveolar-capillary barrier due to the selective permeation of the capillaries. Capillaries are lined with only a single layer of endothelial cells to allow gas exchange [40]. When lung capillaries are damaged, complications like pulmonary hypertension or pulmonary edema can arise [41]. In addition, abnormal pulmonary vessels can lead to the release of cytokines and chemokines, resulting in the appearance of inflammatory cells, including monocytes, T lymphocytes and B lymphocytes. It is well-established that changes in the pulmonary vascular structure and function can contribute to lung disease complications, which are often associated with gas exchange dysfunction. However, a clear understanding of the relationship between pulmonary diseases and vasculature is still lacking [41]. To gain a better understanding of physiological and pathological phenomena, including inflammation and immune responses, related to the vasculature, it is essential to mimic the structural and mechanical properties, of the vasculature of the barrier [41] [42].

### C. Current methods

*1) Alveolar-capillary barrier models:* Transwells are widely used for cell culture. They allow for epithelial cells to be cultured at an air-liquid interface and can be used for co-culturing. Figure 1 shows a transwell with a monolayer of epithelial cells and a monolayer of endothelial cells. This model is a used due to its simplicity. However, this model is static, missing relevant dynamic parameters such as blood and air flow and stretching of the membrane.

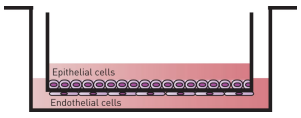


Fig. 1: Transwell co-culture epithelial cells and endothelial cells [48]

Another commercially available model has been developed by Huh *et al.* and is shown in Figure 2. PDMS is used to make a membrane that is $10\,\mu m$ thick and has $10\,\mu m$ wide pentagonal pores. This model includes 2D stretching the PDMS-membrane by mimicking respiration with a strain of 5 to 15% applied to the membrane. It also includes air and

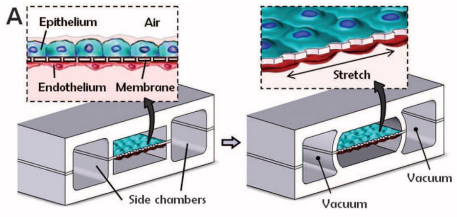


Fig. 2: Device to model alveolar-capillary barrier created by Huh *et al.* [29]

blood flow. Another model was created by Zamprogno *et al.* which integrates 3D membrane stretching into an aveoli-capillary barrier model. They designed a stretchable membrane, that was stretched using a pressure difference [49]. Recently, Iriondo *et al.* developed Simple-Flow, a customizable 3D-printed cell culture plate. Human primary lung-derived PBECs and MVECs were cocultured on an insert membrane for up to 14 days under ALI conditions and medium flow.

This device has medium throughput and is simple to manufacture [37].

Most lung-on-chip models use 2D membranes to culture the cells which differ significantly from the 3D curved alveolar walls and thus result in different cell development processes. Also, a 2D alveolar flow does not fully mimic the 3D phenomena [28].

There are no vascularised alveoli-capillary barrier models commercially or widely available. However research is done with vascularised Lung-on-a-Chip (LoCs), which will now be discussed.

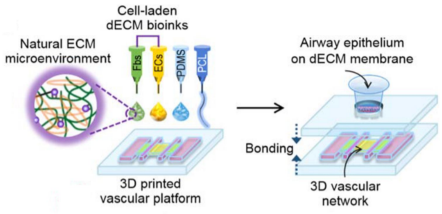


Fig. 3: vascularised network integrated with airway epithelium model created by Park *et al.* [50]

The model of Park *et al.*, shown in Figure 3, contains primary human tracheal epithelial cells (hTEpCs) which are grown on a vitrified membrane. This fully-differentiated *in vitro* airwaymodel is then placed on top of a vascular platform. The vascular platform is created using a 3D cell printing system and with angiogenesis, a biological process which can generate a random network of vessels smaller than 100 µm from pre-existing blood vessels [1] [51]. With this model, Park *et al.* proved that it is possible to create a functional interface between this fully-developed airway epithelium and a vascular network [50]. In our literature review, we found no information on the model's perfusability or lifespan under dynamic conditions. The model created by Jung *et al.* includes

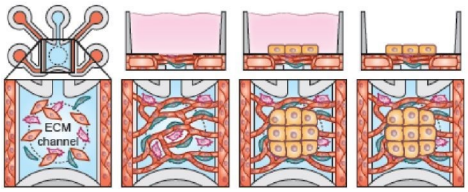


Fig. 4: vascularised network integrated with alveolar or bronchiolar model created by Jung *et al.* [34]

a microvascular network consisting of human primary microvascular endothelial cells, fibroblasts and pericytes and enables the ALI culture of lung epithelial layers on top of the vascularised tissue bed, created by promoting angiogenesis. This network was perfusable however, only 50% of the flow through the main channels, on both sides of the device, flowed through the vascular bed. Those main channels detached from the wall after three weeks (post-seeding) and a decrease in the diameter of the main vessels was observed. This could be due to the non-physiological angle of the channel. Overall, the vascular network had a limited lifetime and remained perfusable no longer than only two weeks after the ALI induction [34].

As discussed, vascularization in LOCs enhances the physiological relevance of the model. Vasculature fully embedded in hydrogel can also eliminate the need for a fabricated membrane, thereby overcoming the challenges of cellular crosstalk and cell attachment [34]. But significant challenges remain regarding perfusability and the lifespan of these models. Self-assembled vascular networks are prone to destabilize after only a few days [52]. Another major limitation is the lack of structural control of these self-assembled capillary networks. Which can result in non-optimized channel structures, high resistance, and vessel damage [34]. To induce self-assembly, angiogenic growth factors are introduced. However, their effects on capillary sprouting can vary making it challenging to determine the appropriate concentration for engineered systems. Knowledge of their independent and collective influence on angiogenesis is lacking. Furthermore, the optimal concentration for their application in engineered systems depends on several factors, including tissue type, vascular density, and the cellular microenvironment [53]. Another critical limitation is the inability of self-assembled networks to replicate the hierarchical dimensions and topological complexity of native vascular beds, therefore they are not suitable to study the phenomena of gas exchange that accur across larger tissue constructs [40] [52]. The challenges of a self-assembled vascular network include low reproducibility, poor control over vascular geometry, and long fabrication times [1]. In contrast, pre-structured vascular networks provide greater control over flow rates and shear stress distribution in capillaries, potentially extending vessel perfusion times while better mimicking physiological dynamics. Additionally, these networks improve reproducibility, as their structure can be consistently recreated, unlike the randomness inherent in self-assembled networks [1]. To gain more knowledge about the creation of such pre-structured networks, several scaffold based vascularization methods are discussed.

*2) Scaffold-based vascularisation methods:* There are several known methods to create scaffold based vascularised models, PDMS moulds created with soft

| **Hydrogel** | **Cells** | **Viability** | **Perfusability** | **Source** |
|---|---|---|---|---|
| Fibrinogen solution mixed with thrombin | HUVECs | At least 14 days | At least 7 days | Paek *et al.* 2019 [43] |
| Fibrin mixed with type I collagen | hAMECs | Over 40 days | - | Paek *et al.* 2019 [43] |
| PEG hydrogel | HUVECs | At least 3 days | - | Miller *et al.* 2012 [44] |
| Agarose | HUVECs | At least 8 days | - | Miller *et al.* 2012 [44] |
| Fibrin gel (10 mg mL$^{-1}$) | HUVECs | - | At least 9 days | Miller *et al.* 2012 [44] |
| Collagen gel | HUVECs | - | At least 1 week | Chrobak *et al.* 2006 [45] |
| Collagen I with plasmin and VitroGel | HUVECs | - | For 2 days | Lin *et al.* 2023 [46] |
| TG gelatin* | HUVECs | - | At least 4 days | Shimizu *et al.* 2020 [19] |
| Collagen I with 25% Matrigel | HUVECs | At least 2 days | At least 2 days | Bischel *et al.* 2013 [47] |

Notes: * Pre-gel solution of transglutaminase cross-linked gelatin

Tab. 1. Hydrogels Compared with Cell Viability and Perfusion Capabilities

litography, scaffold wrapping, needle moulding and sacrificial moulding [1]. A more detailed review of these methods can be found in the literature review in Appendix E. Our aim is to combine the vessel with alveolar epithelial cells, with only a hydrogel mimicking the ECM in between. With PDMS moulding the vessel is surrounded with PDMS and therefore this method can not be used for our application [47]. Scaffold wrapping is a method where a cylindrical structure is encapsulated with endothelial cells and a tube is formed by vasculogenesis, the formation of new blood vessels, after the scaffold is degraded. This method results in vessel formation with a diameter as small as 30 µm. However, the capillaries remain perfusable for only a few days [46]. This could be related to the degradation of the surface material to which the endothelial cells are attached to. Sacrificial moulding is another approach for fabricating capillaries with diameters ranging from 150 to 750 µm. It is a fast method because it only takes a few minutes for the mould to dissolve, after which the hollow channels are ready to be seeded with cells. Biocompatible materials such as carbohydrates and PVA, which are cost-effective, can be used as sacrificial templates. Studies have shown with this method that capillaries can be cultured and remain perfusable for at least a few days [19] [44]. Needle moulding is another fast and inexpensive method to create straight vessels with a diameter between 55 to 400 µm [43] [45] [54]. Chrobak *et al.* and Peak *et al.* were able to reach perfusability for 1 week, whereas some remained perfusable for 3 weeks.

*3) Hydrogel:* Hydrogels are used to mimic the human ECM. Several types of hydrogels are used for vascularised models. Due to the limited data available on the lifespan of vascularised models using MVECs, as we plan to use, we instead focus on the existing data regarding the lifespan of vascularised models using human umbilical vein endothelial cells (HUVECs). The results of several studies are shown in table 1. A wide range of materials are used but no clear conclusion can be made. However, hydrogels with fibrinogen or fibrin show viability for a long time [43]. Besides the composition of hydrogels, their mechanical properties are important as well. Such as microstructure, density and elastic moduli, these parameters influence not only the duration of perfusability and cell viability but also the angiogenic activity, as demonstrated by Park *et al.* [54]. Mechanical properties can be influenced by varying the concentration of materials within a hydrogel. A higher concentration of fibrinogen results in a higher elastic modulus and provides more mechanical stability for endothelial cells [1] [55] [56]. However, the concentration of fibrinogen also affects mass transport and pore dimensions. A low concentration of fibrinogen leads to a higher porosity, which promotes cell migration and mass transport [1] [56] [57]. Also, lower concentrations of collagen, which also affect hydrogel ligand density, may result in endothelial cells invading the hydrogel rather than forming an intact monolayer lining the hydrogel [47]. In this study, the priority is to create strong aligned vessels rather than a random self-assembled vascularised network. The optimal parameters to achieve this are unknown, but the phenomena described suggest that changing the concentration, and therefore the mechanical properties, has an effect on the success of growing stable vessels.

### *D. Summary of the theory and research approach*

Blood flow, air flow, membrane stretching, and vasculature have been identified as important parameters to integrate into our model. The model should also have a sufficient lifetime to allow for culture time and experiments. The interface between epithelial and endothelial cells must be free of PDMS to prevent interference with the transport process. Furthermore, a membrane-free model is preferred to overcome the challenges of cellular crosstalk and cell attachment. No model in the literature meets all these requirements. As a prerequisite, a reproducible method is needed for culturing lung-derived endothelial vessels. Pre-structured vascular networks provide greater control over flow rates and shear stress distribution and improve reproducibility compared to self-assembled vessel networks. Therefore, a scaffold-based method is used. The scaffold-based method of culturing the vessel should create a vessel model that allows airflow and membrane stretching to be integrated into later designs. In addition, it should be capable of producing vessels with diameters ranging from 50 to 150 µm to mimic small capillaries while minimizing the risk of clogging [58] [59]. Furthermore, the method should provide vessels with a long duration of perfusability and cell viability. Among the available techniques, needle moulding stands out as the most suitable approach to meet these requirements. This method has proven to be a straightforward method to culture vessels with sufficient longevity [43] [45] [54].

In our device, we wanted to use the needle not only as a mould but also as a connection point on both sides, connecting the hollow channels to tubes for improved user-friendliness. However, challenges arose due to the misalignment of the needles, which would create sharp angles within the hollow cylindrical channel. In addition, the removal process proved to be sensitive to handling, resulting in vibration and unintended deflections of the needles. Through empirical research during development, we have developed a modified version of the needle moulding technique. The needles are fixed in one position and a wire is threaded through the needles. The wire acts as a mould to form a smooth, hollow channel while still allowing the needles to connect to the tubes. This adaptation ensures the formation of hollow cylindrical channels while increasing ease of use. To further establish a method for creating a microvessel model, a cell seeding method, hydrogel and diameter should be determined. The literature does not provide us with an optimised cell seeding method, hydrogel or diameter. Through empirical research during testing, it was found that the fluid containing the cells had already entered the hollow channels before pressure was applied. This showed that using the capillary effect could be an effective method of cell seeding.

To determine the most suitable hydrogel, we compared other scaffold-based micro-vessel studies. These studies suggest that fibrinogen-based hydrogels produce vessels with longer viability and perfusability, so a fibrinogen-based hydrogel will be used." To investigate the effect of the mechanical properties of a fibrinogen-based hydrogel, the concentration of fibrinogen is varied. In addition, to gain further insight into the preferred diameter, the wire diameter is varied.

## III. Methods

Ten experiments were conducted in this study to test a device and method to create a micro-vessel model. Hollow channels were formed within a hydrogel-filled container using wires as moulds. The hollow channels were seeded with microvascular endothelial cells to form vessel. Two different wire diameters were used: 50 µm and 125 µm. Additionally, two hydrogel compositions were evaluated, containing 1% and 2% fibrinogen.

### *A. Fabrication PDMS container and wire preparation and placement*

The PDMS container, shown in white in Figure 5, is designed as a container. PDMS is a two-part resin, consisting of a base and a curing agent, mixed in a 7:1 ratio. To fabricate the container, the PDMS-

Fig. 5: Two injection needles are inserted into the PDMS container with a wire pulled through, to serve as a mould. The needles are spaced approximately 2.5 mm apart.

mixture is poured into the 3D-printed mould shown in Figure 6 and cured for 24 hours at room temperature. Once cured, the PDMS is removed from the mould and cut into eight containers. Inside the container, a straight wire is placed between two injection needles, as shown in Figure 6. This wire is the mould to create a hollow channel in the hydrogel that is poured into the container. To straighten the tungsten wires with a diameter of 125 µm, two methods of cold work hardening are used in sequence. Cold work hardening involves straining the material beyond its yield strength. The tungsten wires with a diameter of 50 µm were prone to breaking during the hardening process. Therefore, these were replaced by molybdenum wires with a diameter of 50 µm. A detailed description of the hardening methods is given in Appendix B.1. To place the wire in the container, two identical injection needles are used. Initially, one needle is inserted through the wall of the PDMS box. The wire is then threaded almost entirely through this needle. Subsequently, the second needle is inserted through the wall. The wire is pushed from the first needle through the opposite

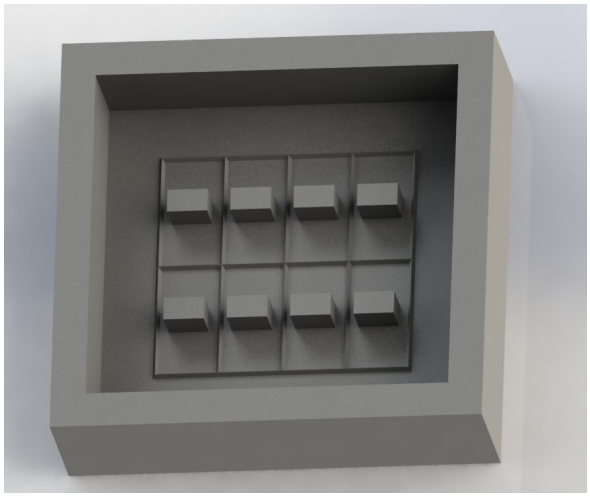

Fig. 6: 3D-printed PLA mould for 8 PDMS containers. The mould is filled with PDMS, and after curing, the PDMS is removed and cut into 8 individual containers.

needle, by placing the needles close to each other. Once the wire is threaded through both needles, the needles are gradually pulled apart, roughly leaving a 2 to 3 mm spanned wire between them as shown in Figure 5. This part of the wire acts as the mould to create the hollow channel within the hydrogel. When pushing the needles through the PDMS-walls of the container, large deflections of the PDMS-wall were prevented by using a puncture-support, shown in Figure 7. The rectangular surface serves as a handle, while the smaller segment is positioned within the PDMS container. It is pressed against the PDMS wall to counteract the force of the needle insertion, preventing excessive stretching of the PDMS before it ruptures. During this process, both needles need to

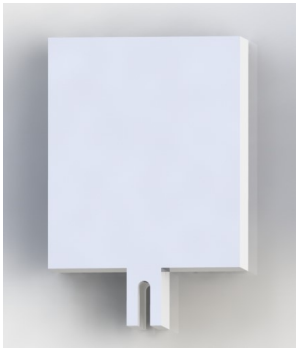

Fig. 7: Puncture-support to prevent stretching of the PDMS container when injecting the needles. It is 3D-printed with PLA. The rectangular surface is the handle and the smaller segment is positioned within the PDMS container.

be precisely aligned, which will be discussed in more detail later in this section. This is made possible by 3D-printed polylactic acid (PLA) rails and fixators, shown in Figure 8. The performance of this alignment is evaluated in the Results section.

### *B. ECM Hydrogel preparation and placement*

To mimic the extra-cellular matrix two hydrogels with different fibrinogen concentrations are tested, shown in table 2. The number of pericyte cells used is $0.63 \times 10^6$ cells/mL of saline. The pericyte cells were trypsinized, counted and spun down, then re-suspended in the calculated amount of saline 0.9%

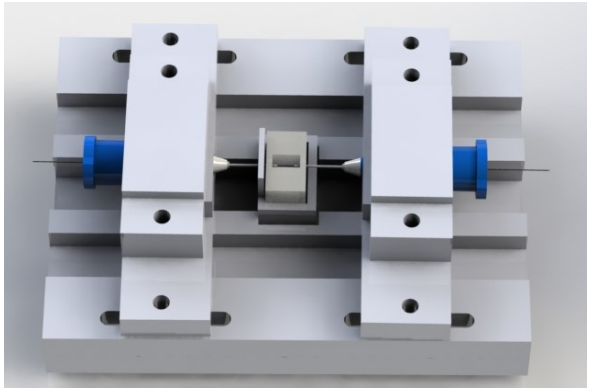

Fig. 8: A PLA 3D-printed device designed to slide and align two injection needles through a PDMS container. The device functions as a rail system to ensure proper alignment of the needles. A wire, acting as a mould, is threaded through both needles. Once the needles are correctly positioned, they can be secured in place using bolts.

| Composition 1 | Composition 2 |
|---|---|
| 70 µL salines with pericytes | 45 µL saline with pericytes |
| 25 µL fibrinogen 40 mg/mL | 50 µL fibrinogen 40 mg/mL |
| 3 µL aprotinin | 3 µL aprotinin |
| 2 µL thrombin | 2 µL thrombin |

Tab. 2. Compositions of ECM Hydrogels

solution. In each test, the hydrogel contained $10^4$ pericytes. The devices, including the PDMS, were first fully immersed in 70% Isopropanol for 5 minutes. Followed by rinsing with phosphate-buffered saline (PBS) and air drying in the fume hood. The PBS increases the wettability of the container, avoiding trapped air bubbles between the wall of the container and the hydrogel. Then the hydrogel was carefully pipetted into the PDMS box, and the container was then sealed with a glass coverslip and incubated at 37 degreeCelsius for 30 to 60 minutes to solidify.

### *C. Wire moulding, seeding and culturing cells*

In this study, human donor microvascular endothelial cells (MVECs) at Passage 3 to Passage 4 (P3-P4), were used. When the hydrogel was solidified, 100 µL of MVEC medium (EGM-2MV Catalog #: CC-3202) containing $3.76 \times 10^6$ cells/mL was pipetted into one of the injection needles. Subsequently, the wire was carefully removed by pulling it out from the opposite side, allowing the cells to naturally enter the hollow channel due to the capillary effect. To further enhance this process, the device was tilted. In cases where cells were not visible in the channel, a 2 mL syringe was used to apply pressure, forcing the MVEC solution into the channel. The devices with seeded channels were incubated in different orientations, being rotated every 45 minutes for approximately 3 hours to promote uniform endothelial cell attachment on all surfaces. Before connecting the devices to the tubing connected to a peristaltic pump, all tubes and connectors were flushed with 70% IPA at a flow rate of 11 µL/s for 10 minutes. The tubes were then emptied and flushed with PBS for an additional 10 minutes to remove residual IPA. After the 3-hour seeding period, the channels were connected to the peristaltic pump and perfused with microvascular endothelial cell growth medium-2 (Cat. No. CC-3202) at a constant flow rate.

### *D. Measuring effective Young's modulus hydrogel*

The effective Young's modulus of the hydrogels was measured using the Optics11 Life Piuma Nanoindenter (Optics11 Life, the Netherlands). The setup is shown in Figure 9. The measurements were taken four days after the hydrogels were compounded, during this time the samples were stored at room temperature. For the measurement, the hydrogels were placed in saline 0.9% solution and a cantilever with a stiffness of 0.023 N/m and a probe with a tip radius of 25 µm was used. The probe was slowly lowered to locate the surface and then indented into the hydrogel, causing the cantilever to bend. After one second of indentation, the probe was retracted. The Piuma system recorded a force-displacement curve, which was used to calculate the effective Young's modulus, based on the Hertz model. The effective Young's modulus, $E_{\text{eff}}$, is calculated with equation 1, with $F$, $R$ and $h$, being the force, radius and indentation depth, respectively.

$$F = \frac{4}{3} * E_{\text{eff}} * \sqrt{R} * h^{\frac{3}{2}} \tag{1}$$

Fig. 9: Sample of hydrogel with composition 2 in saline 0.9% solution on Petri dish placed under the Piuma nanoindenter

### *E. Live cell staining and immunofluorescent staining*

To provide information on the viability of the endothelial cells during culture, 70 nm lysotracker red was diluted in the endothelial medium and incubated for a period of 4 h at 37 °C. Fluorescent images were taken using an ECHO revolve microscope from the endothelial tubes. Fluorescent beads (GFP BrightComp eBeads™ Compensation Bead Kit, 6 µm, Catalog No. A10514) were used to provide information about the flow. The beads were directly injected into the tubing before the device. Subsequently, videos were captured using the ECHO Revolve to visualize the movement speed through the endothelial tube.

Immunofluorescence staining was performed to detect and localize cell-specific antigens for endothelial cells and pericytes. The cells were fixed by placing the PDMS container in 1% PFA over the weekend. A cross-section with a width of 300 µm in width, was made from the PDMS container using a vibratome (Leica VT1200S). The slices were placed in 0.1% tween dilution overnight for permeabilization of the fixed cells. Slices were blocked with 5% BSA, 5% Normal Donkey serum and 0.1% Triton- X in PBS for 6 h at RT. The slices were washed 3 times for 10 minutes 0.03% Triton-X in PBS before the primary antibodies were incubated. Primary antibodies of vimentin (1:500 dilution, Abcam, Cat. No. Ab92547) and CD31

(1:100 dilution, BioLegend, Cat. No. 303101) were incubated overnight at 4 °C and subsequently washed 3 times for 10 minutes with 0.03% Triton-X in PBS. Secondary antibodies were 1:500 diluted (Alexa Fluor 488 donkey anti-Mouse, Jackson ImmunoResearch, Cat. No 715-545-151, Alexa Fluor 647 donkey anti-Rabbit, Jackson ImmunoResearch, Cat. No 711-605-152) and DAPI 1:2000 (bdBioscience, Cat. No. 564907) were incubated overnight at 4 °C and subsequently washed 3 times for 10 minutes with 0.03%Triton-X in PBS before imaging.

### F. Analyses images and vessels

*1) Flow analysis:* The fluorescence beads were captured in a video, and their speed was determined by measuring the time and distance between their entry and exit from the frame. With 20 measurements, the average velocity of the beads is calculated. To measure the volume flow rate, $Q$, formula 2 was used, with $v_{\text{avg}}$ the rate of the medium through the tube and $A$ the cross-section of the tube [60].

$$Q = A v_{\text{avg}} \tag{2}$$

To calculate the shear stress on the endothelial cells the maximum velocity is needed. In a parabolic, fully developed laminar flow, the maximum speed is twice the average speed, $v_{\text{avg}}$, so formula 3 was used [61].

$$v_{\text{max}} = 2 v_{\text{avg}} \tag{3}$$

The flow in a capillary is considered to be a fully developed Poiseuille flow in a cylindrical tube with a parabolic velocity profile. Therefore Poiseuille's law is often used to calculate the shear stress on the walls of capillaries [62]. The formula that is derived for the parabolic velocity profile of Poiseuille flow is shown in equation 4 [60]. For $D$, diameter the average and smallest diameter are used and the viscosity coefficient of the cell growth medium is for simplification estimated to be 1 mPa s [63].

$$\tau_w = \frac{2 \mu v_{\text{max}}}{R} \tag{4}$$

*2) Diameter vessel analysis:* The width of the channels is measured to determine the diameter of the cultured vessels. One image was taken from each vessel on the day of cell seeding. The image is rotated to place the vessel horizontally. A Matlab script, which can be found in Appendix D.3, is used to draw two lines on the border of the vessel on each image. Figure 10 shows the picture before and after the two lines are drawn. The points are defined by marking the edge of the channel. The line is then interpolated to provide a value from its vertical position at each pixel between the defined points. Then the vertical distance between the two lines is measured for each pixel. The uncertainty of these measurements is estimated to be ±13 µm.

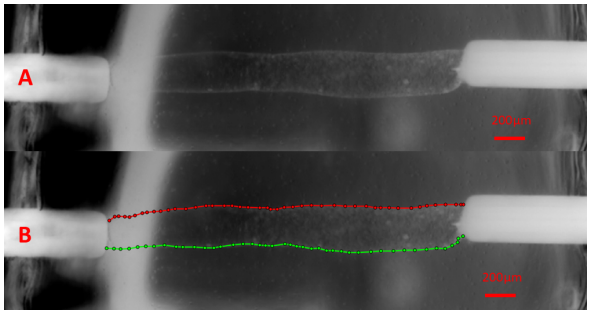

Fig. 10: Points are selected along both edges of capillary 7, and interpolated lines are generated to determine the vessels' width.

*3) Injection needles alignment analysis:* To provide information on the accuracy of this device, the angular difference between the two needles and the positional offset of the two needles on the vertical axis is evaluated. The primary goal of a good alignment is to ensure that the wire mould can be smoothly guided from one needle through the other when the mould is being positioned. Proper alignment of the needles significantly speeds up this process. Another critical goal is to guide the wire mould carefully during its removal to prevent damage to the hollow channels. Due to its stiffness, the end of the wire may deviate as it exits one of the needles. This deviation could cause the wire to widen the hollow channel rather than follow its intended path. The inner diameter of the smallest injection needles is 102 µm, while our wire has a diameter of 50 µm. To achieve both goals, smoothly guiding the wire mould through the needles and preventing enlarging the diameter of the hollow channel, a maximum offset of 50 µm and an angular difference of 1.2° was set. This angular difference results in an approximate offset of 50 µm over a distance of 2.5 mm. To measure the angular difference and positional offset, Matlab scripts are used which can be found in Appendices D.4 and D.5. Figure 11 shows how two lines are drawn parallel to the needle, extended by a dashed line. The angular difference is shown in blue.

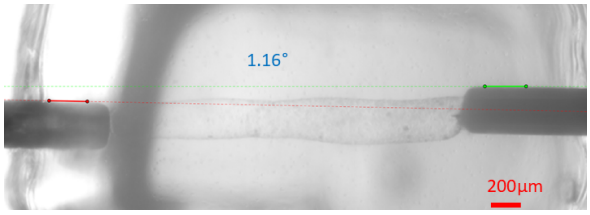

Fig. 11: Two lines are drawn along the needles to measure the angular difference between them.

To determine the positional offset of the needles, the values of the vertical axis on the picture, of two points on the tip of each needle are compared, this is shown in Figure 12. The points are indicated with a small circle, and a horizontal line is drawn through to visualize the difference, the positional offset is shown in blue.

The perfusability of the channels was examined under a microscope. If leakage occurred or the channels were no longer visible, the vessels were no longer considered perfusable.

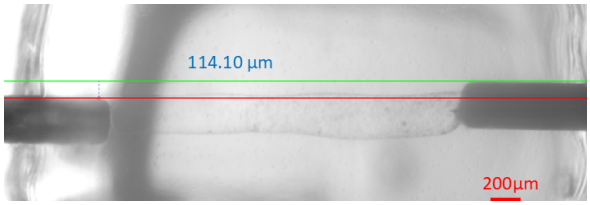


Fig. 12: Two points are selected at the tips of both needles to determine the positional offset between them.

## IV. Results

### A. Effective Young's modulus fo the hydrogel

The effective Young's modulus of the hydrogels with composition 1 and 2 were tested, see Table 2 for specifications. The force-displacement curve of all measurements with the hydrogel with composition 1 showed an unexpected unloading curve, that was not aligned with the loading curve. Therefore, the effective Young's modulus measurements were unreliable and not presented. Because hydrogels are soft materials, multiple measurements are performed to account for variability and ensure accuracy. For the hydrogel with composition 2, three reliable measurements were obtained, all using a maximum force of 0.04 µN. The effective Young's modulus values, provided by the Piuma software, were 1.97 kPa, 3.50 kPa, and 3.13 kPa. Taking the mean provides a more reliable representation of the material's mechanical properties, resulting in a mean Young's modulus of 2.87 kPa. One of the Load-Indentation plots is shown in Figure 13, while the other plots from the measurements are provided in Appendix C.1.

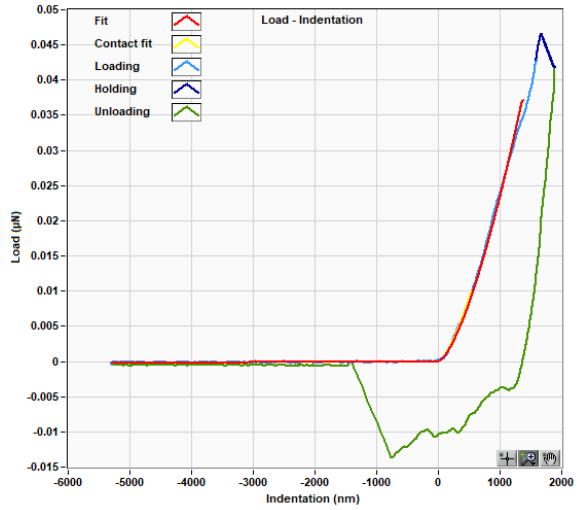


Fig. 13: Indentation plot of the nanoindenter in the hydrogel with composition 2, showing hysteresis between the loading and unloading curves.

### B. Performance of the device and the method

Hollow channels were successfully created in all devices using wire moulding, regardless of the hydrogel composition or wire diameter. Several results offer a detailed evaluation of the device and methods, followed by findings on the performance of the capillaries.

*1) Alignment needles:* The results regarding the alignment of the needles, including the angular difference and positional offset are presented in Figure 14. The angular difference varies between 0.21° and 2.73°, with many values being within the preferred range, below the maximum of 1.2°. The positional offset ranges between 5 µm and 202 µm, where many are well below the maximum of 50 µm. The distance between the needles, and therefore the length of the vessels, varies between 2041 µm and 2692 µm.

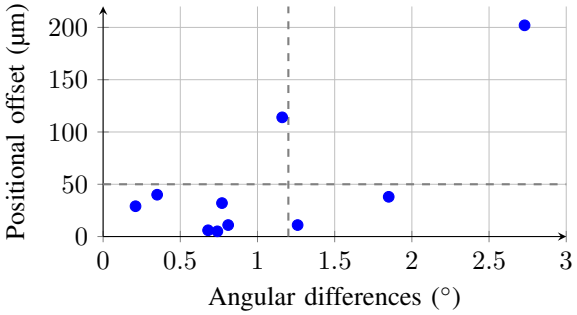


Fig. 14: The accuracy and alignment of the needle placement inside the PDMS container. The two dashed lines represent the preferred maximum positional offset of 50 µm and angular difference of 1.2°

*2) Cell seeding:* Cell seeding was achieved using the capillary effect in 3 out of 10 devices (devices 1, 2, 3, 5, 6, 8, and 10). For the other 3 devices (devices 4, 7, and 9) a 2 mL-syringe was used to apply additional pressure to push the MVEC solution into the channel. The capillary effect was possibly hindered by an air bubble in the channel. In 6 devices (devices 2, 4, 5, 7, 9, and 10), including the 3 that required a syringe for the cell seeding, the air bubbles were initially present within the channels. In each case, the flow eventually removed the bubbles, which can be seen in Figure 15.

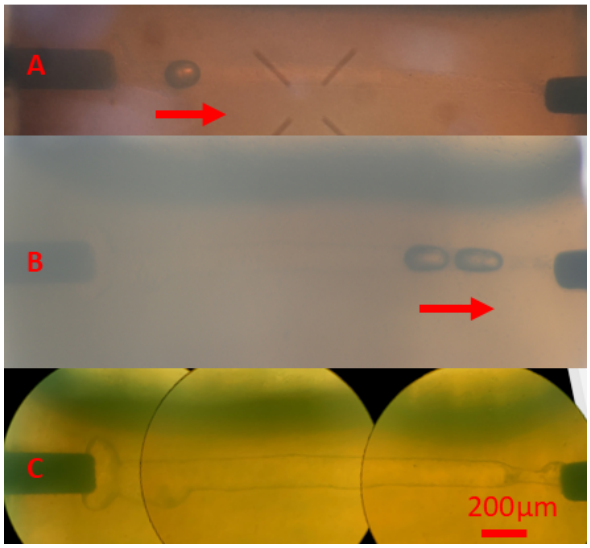


Fig. 15: Airbubbels visible inside on of the channels. The flow is in the direction of the arrow. (A) Vessel within minutes after the cell seeding with airbubble on the left side of the channel. (B) Vessel after 3 to 4 hours with moved airbubbles. (C) Vessel after 5 days without airbubble.

*3) Diameter created channels:* Two different wires are used as mould to create hollow channels. Figure 16 shows two boxplots of the diameters of the vessels, with on the left the vessels created using the wire with a diameter of 50 µm and on the right the vessels created using the wire with a diameter of 125 µm. The results indicate that, for both types of wire, the

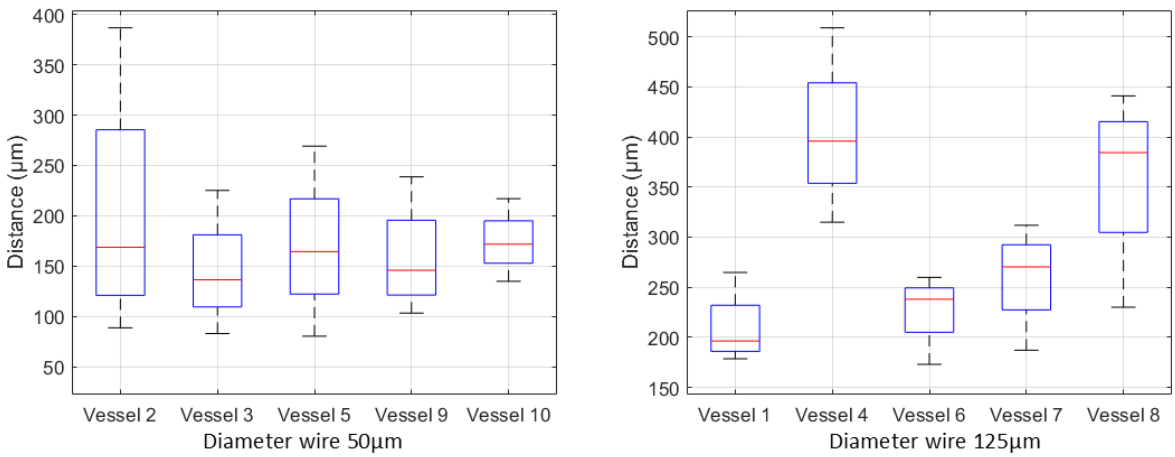


Fig. 16: On the left the a boxplot showing the width of vessels made with a 50 µm wire, based on 298-485 measurements (including interpolated points). All measurements have an associated uncertainty of ±13 µm. On the right, a boxplot showing the width of vessels made with a 125 µm wire, based on 380 to 470 measurements (including interpolated points). All measurements have an associated uncertainty of ±13 µm.

channels have a larger diameter than the moulds used, with some vessels showing substantial variation in their widths. The effect of air bubbles was analyzed to better understand these results.

Figure 15 contains three images taken at different times, that show the same channel that contains an air bubble. The channel initially appears wider and irregularly shaped on the left side, corresponding to the location of the air bubble during the early minutes of cell seeding. Over time, the air bubble shifts position, as observed in images B. The channel on the left side of the air bubbles is wider compared to the right side, and the air bubbles themselves appear to be altered in shape compared to the round form observed in image A. Later, on day 5, as shown in image C, the air bubbles completely moved through and exited the channel. Despite the air bubble's transit, the width of the channel on the right side remains narrow. Those images reveal that the air bubble may initially deform the channel, as seen in images A. However, at a later moment, when images B were captured, the air bubble itself became deformed, potentially indicating an interaction between the air bubble and the channel structure that evolves over time.

### C. Performance vessels

*1) Cell viability and growth:* Figure 19 shows a contrast and fluorescence image of channel 5 on day 2 which was incubated with Lysotracker. The channel is clearly visible in the fluorescence image, indicating that the endothelial cells form a viable vessel. Fluorescence images were also taken of vessel 4 on day 9 and of vessel 1 on day 16 and showed viable vessels, results are not shown. Figure 20 shows a cross section slice of the PDMS container with a thickness of 300 µm. Inside the hydrogel, there is a hole which is the vessel. Within the hydrogel, pericytes are observed primarily surrounding the vessel and at the base of the gel, see Figure 20. The brightfield image of Figure 21 shows the pericytes surrounding the endothelial tube. Post-fixation results from the lysotracker stainings are displayed in Figure 17, indicating a circle of endothelial cells.

Figure 18 shows immunostainings of the fixated cross-section of the vessel. Vimentin visualizes the pericytes while CD31 the endothelial cells. The LysoTracker shown in 18B had been used before and is still visible after the cells are fixated. The vimentin marks the pericytes, shown in Figure 18A, which are clearly visible. CD31, the endothelial cell marker in 18C, does show several green dots and a clear circle of the endothelial cells. DAPI stains DNA, thereby marking the nuclei, shown in Figure 18D, only partially marked the cells. Figure 18 shows pericytes attached to the vessel, at the top and the bottom left.

*2) Flow:* The velocities of 20 fluorescence beads are tracked on day 16 flowing through one of the vessels. Those measurements can be found in Appendix C.5. The average velocity of the beads was found to be 1215 µm/s. The average diameter of this vessel is measured to be 199 µm. The volume flow rate, $Q$ = 2.27 µL/min, calculated with formula 2. With formulas 3 and 4 the shear stress is calculated and shown in table 3.

| Used values | Shear stress |
|---|---|
| Average diameter and average velocity | 0.049 Pa |
| Smallest diameter and average velocity | 0.054 Pa |

Tab. 3. The shear stress on the endothelial cells measured in one of the vessels, based on the average velocity of twenty fluorescence beads

*3) Smallest diameter and perfusable days of cultured capillaries:* 10 endothelial tubes were created under different conditions varying the width of the mould and hydrogel composition. Three cultured vessels (vessels 1, 4, and 5) were still in good condition when fixated on days 16, 10, and 10, respectively. The loss of perfusion in the remaining seven capillaries was due to channel rupture or leakage. To see if shear stress or high pressure affects the lifespan of the capillary, the minimum width of the capillary and its relationship to its lifespan is examined and shown in Figure 22. The dots are spread out without indicating a relation between the minimum width and perfusable days.

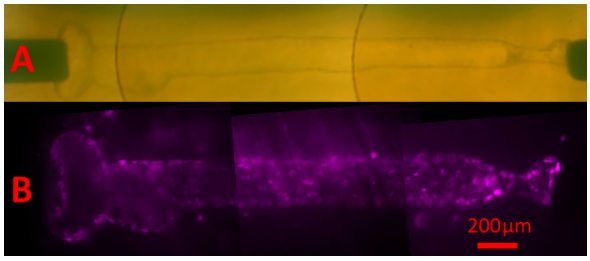


Fig. 19: (A) Contrast image of vessel 5, 1 day after cell seeding. (B ) Enhanced confocal fluorescence microscopy image of vessel 5, 9 days after cell seeding. The channel with endothelial cells was incubated with 70 nm Lysotracker for 4 hours to assess viability.

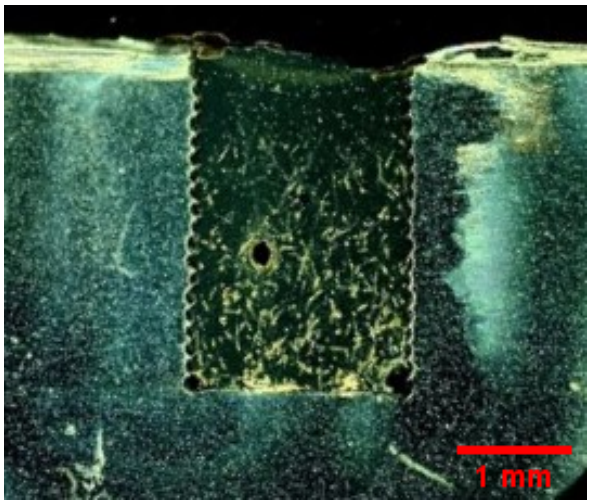


Fig. 20: Slice of 300 µm of PDMS container filled with hydrogel containing a vessel. In the middle of the hydrogel a whole is visible which is the cross section of the vessel. The pericytes are visible throughout the hydrogel, most of them are around this vessel or on the lower part in the hydrogel.

*4) Compostion hydrogel and perfusable days of cultured capillaries:* The lifespan of the capillaries and the composition of their hydrogel are shown in Figure 23. All the vessels perfusable for 10 or more days were cultured in the hydrogel with composition 2. All capillaries that were perfusable for 6 days or less,

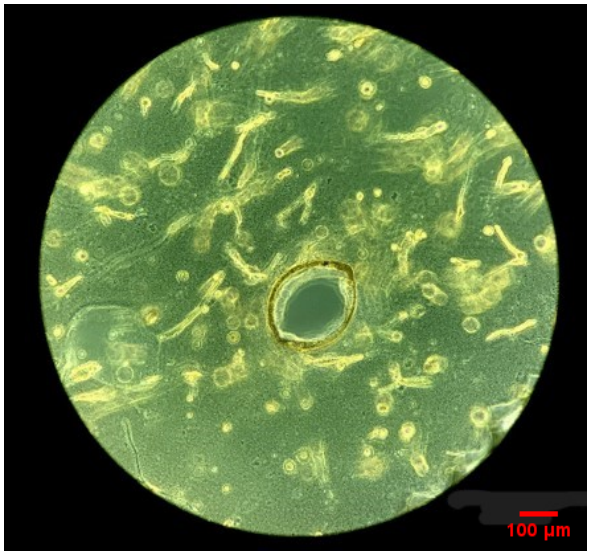


Fig. 21: Slice of 300 µm of PDMS container filled with hydrogel containing a vessel. The whole in the middle is the cross-section of a vessel, around the vessel are pericytes which seem to align around the wall of the vessel.

with one exception, were cultured in the hydrogel with composition 1. This indicates a correlation between the lifespan and the hydrogel composition.

## V. Discussion

The results of each section are discussed first, followed by an analysis of the significance of the findings.

### A. *Effective Young's modulus ECM Hydrogel*

This hydrogel was designed to mimic the human lung tissue and therefore should have a low effective Young's modulus. Measuring samples with low elastic moduli, soft materials, comes with challenges. Soft materials can exhibit viscoelasticity, meaning they have a time-dependent strain and have high surface adhesion forces to the indenter [64]. The soft material of the fabricated hydrogel composition 1 is likely to

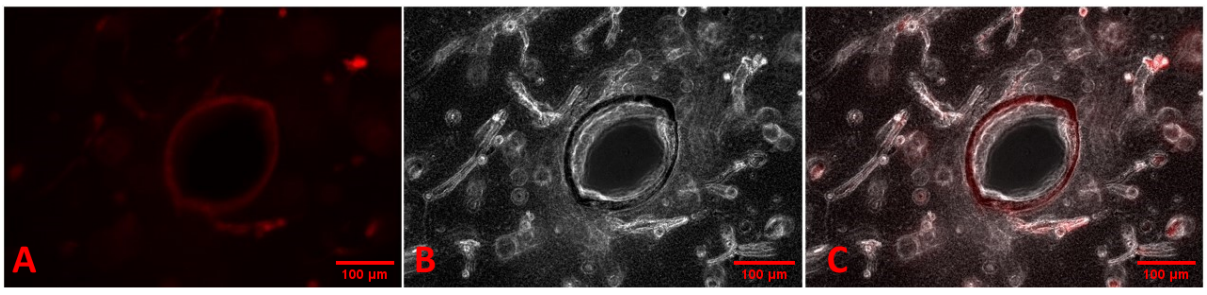


Fig. 17: LysoTracker Red labelling lysosomes within pericytes and alveolar endothelial cells of vessel 1 which is fixated day 16. (A) LisoTracker signal marking a circle of endothelial cells and some pericytes. (B) Contrast image, showing surrounding pericytes (C) Overlay of both images A and B.

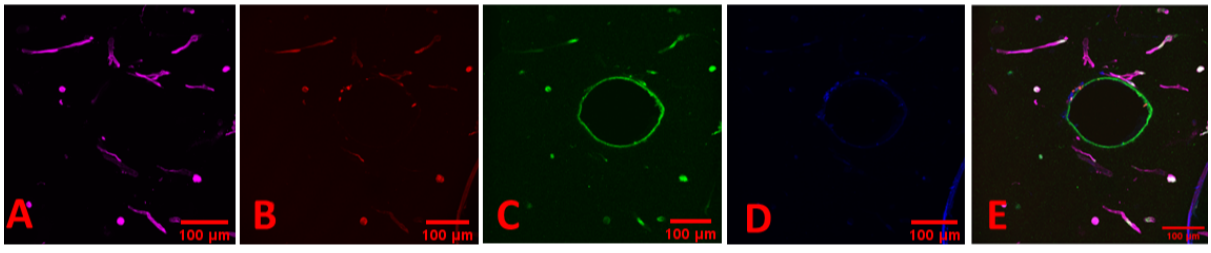


Fig. 18: Enhanced images of the cross-section from vessel 1 fixated on day 16. (A) Vimentin marking several pericytes (B) LysoTracker Red still partly visible after fixation process, (C) CD31 marking endothelial cells (D) DAPI to mark DNA, it only partially marking the endothelial cells and pericytes (E) Overlay image of images A to D

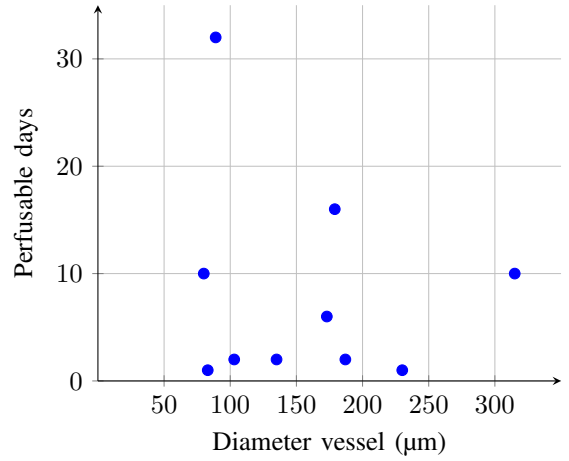


Fig. 22: Scatter diagram to compare the smallest width of 10 vessels with their lifespan.

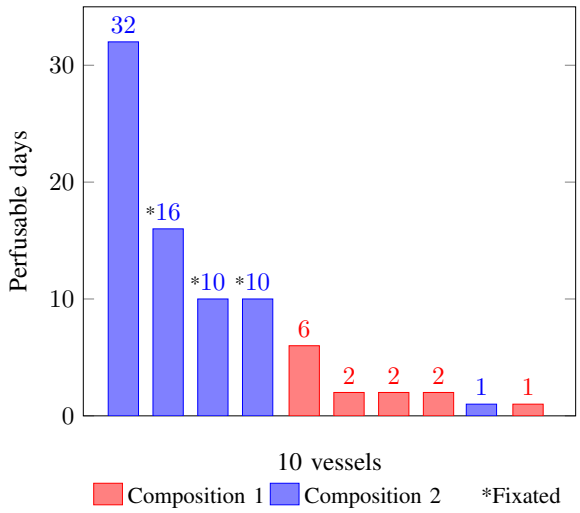


Fig. 23: Bar chart showing the lifespan comparison of 10 vessels cultured in different hydrogel compositions. The vessels with 10 and 16 days of perfusion were fixated.

have failed because of the softer viscosity and its higher surface adhesion forces. These phenomenona could explain as well the hysteresis, the misaligning of the unloading curve to the loading curve, in the hydrogel with composition 2. Although both aspects might have affected our measurement, a result of 2.87 kPa is in the range of 2-3 kPa. This is the range of the elastic modulus of human lung tissue, as mentioned in section II, indicating that this mechanical aspect of the lung tissue is accurately mimicked.

### B. Performance device and method

*1) Alignment needles:* The alignment of the needles provides insight into the reproducibility of the model. The positional offset and angular differences are measured using a 2D picture from a single viewpoint. This means that they do not represent the absolute offset or difference, but give an indication of the accuracy of the alignment. By designing and printing needle holders in various dimensions, the clearance was successfully minimized between the needle holder and the rails while still allowing smooth movements. The relatively thin injection needles themselves could explain the offset, as these needles are relatively prone to bending. When an injection needle bends, this bending typically occurs at the base of the stainless steel section, right where it transitions from the polyester component. Inserting the needles through the PDMS could lead to some angular difference and positional offset. This could be due to the impact of being pushed against the PDMS container before penetrating. Also, PDMS is very flexible and tends to stretch before it ruptures. Before the PDMS ruptures, the position of the created hole in the PDMS might have been slightly shifted, leading to a deflection of the needle when it pierces through. This effect was largely counteracted by using the puncture-support and fast movement of the needles. A fast movement of the needles is preferred because the material has less time to deform and behaves more brittle, this leads to a clean rupture. It also requires less force, compared to a slow movement, preventing more bending of the needle. When both needles experience the previously discussed force, this can further amplify angular differences and, consequently, their positional offsets especially if they bend in opposite directions. Despite these effects, the measured offsets and angular differences remain relatively small. The relatively limited offsets leads to the expectation that the interaction between the needles and the PDMS is the primary cause and that other factors minimally contribute to the limitation of the accuracy of the aligning. To minimise the effects of the insertion, the needles could be retracted further back to the container wall, reducing the length of the needle that sticks out. This, in turn, limits the offset caused by bending due to a shifted position of the created hole. The different distances between the needles resulted in a variation of the length of the vessels. This parameter was not a priority and not a specific length was required for our research but it should be consistent to provide more reproducible vessels. Retracting the needle further back to the edge of the container wall will improve the consistency in the length of the vessels.

*2) Cell seeding:* Using the capillary effect for cell seeding provides an easy and fast method. It avoids the risk of applying a high pressure leading to a wider or ruptured channel. It can not be considered completely reliable yet, as for 3 out of 10 channels it did not lead to the desired result. To avoid air bubbles the device was wetted, including the inside of the propylene part of the needles. However, it might be that the stainless steel part was not wet enough or that air bubbles were trapped in this part of the needle. This would explain why other studies where needle moulding is used, do not mention the presence of air bubbles. If this method did not suffer from this phenomenon, it could be explained by the difference between the methods. This is the presence of the wire inside the needle, a place where air bubbles can be trapped.

*3) Diameter created channels:* The measured width represents an approximation of the diameter as it is captured from a single perspective in a top-down view. The smallest width in the channels is 80 µm, created with a wire of 50 µm and 173 µm created with a wire of 125 µm. The average mean width of the channels created was 161 µm and 296 µm made with wires 50 µm and 125 µm respectively. This variation

could be explained by several limiting factors. Observations and the shapes of some channels tell us that the maximum width can be explained by the presence of air bubbles, which also leads to a larger mean and median width. However, the larger minimum width could be explained by two other factors. One of these is the adhesiveness of the hydrogel to the wire. This became visible because of another test where wires were reused without being cleaned, so probably containing rests of hydrogel. It clearly showed that the hydrogel was being stretched when the wires were pulled out of the hydrogel. The stickiness of the reused wires was noticed when these wires were pulled from the hydrogel container. This indicated that the stickiness, influenced by surface roughness and hydrophilic properties, can affect the width of the channel. A hydrophobic wire with a smooth surface might reduce this stickiness, this might be done using a hydrophobic coating. Another factor is the deflection of the wire. The tungsten and molybdenum wires are strong and stiff. So when the wire is pulled out of the hydrogel, it does not bend following the hollow channel and due to its deflections, it creates a wider channel. This could be avoided by using more flexible wires or more straight wires. The variation in width makes our model less reproducible but does not directly affect other important parameters of the vessels. However, it can be a problem when implementing an epithelial layer with the vessels because it leads to an altering distance between the endothelial and epithelial which is a parameter that should be consistent in a model.

### C. Performance vessels

The cell seeding of vessel 1 was exclusively done via the capillary effect. The endothelial structural integrity of this vessel of the endothelial cells was confirmed by the presence of CD31 at cell-cell junctions throughout the circle in the cross-section. The pericytes were able to attach around the vessel which is crucial as they provide structural support to microvessels [21]. LysoTracker, as shown in Figure 17 highlights the circular arrangement of endothelial cells forming the vessel wall. In Figure 18 the visibility of Lysotracker is reduced due to the washing process related to the other markers. CD31, a marker for endothelial cells, reveals several green dots around the vessel, potentially indicating endothelial cells proliferation into the ECM. DAPI, which marks DNA, also shows the circular arrangement of endothelial cells. Together, these markers confirm that endothelial cells properly adhered to the hollow channel and aligned to form a vessel. In particular, DAPI provides insight into cell-cell junctions, indicating a strong connection between the endothelial cells. It was measured that vessel 1 was able to withstand a shear stress of 0.054 Pa. However, endothelial cells in the human lung typically experience higher shear stresses, ranging from 0.1 to 1 Pa, as discussed earlier. Since human capillaries are smaller and generally experience higher shear stresses, this model, with a larger diameter than human lung capillaries, demonstrates significant shear stress exposure. Nonetheless, it remained perfusable and viable for an extended duration, indicating robust vessels with strong cell attachment. Three vessels, vessel 1, 4, and 5, were subjected to fixation. As a result, their lifespan may have been extended by several days or even weeks. The smallest diameter determines the highest pressure and shear stress on the vessels. We assume that the channels tend to fail due to ruptures created by high pressure, therefore it seemed interesting to see if there was a relation between the smallest width and the lifespan. However, there does not seem to be a relation indicating that a high shear stress did not lead to the rupturing of the channels and that the high pressures might have had another origin. The fibrinogen concentration in the hydrogel could enhance the lifespan of the endothelial tube, as higher fibrinogen concentration was found to support prolonged culture periods for the vessels. This is possibly due to the different mechanical properties of the hydrogel, which provide greater structural support to the endothelial cells [1].

### D. Significance of the findings

The results shown are based on one test and one donor, which is a limitation to the foundation of the conclusions drawn. Also, the permeable functionality of the vessels is unknown. However, the study shows the potential of a relatively cheap and basic fabricated device to create a micro-vessel model. A new method of moulding is invented and this study shows that wire moulding can be used to create vessels fully embedded in the hydrogel. This device also demonstrates a convenient method of connecting those vessels with tubes to a peristaltic pump, using the injection needles. The limitation of this device is that only one straight vessel can be cultured per device. One vessel can probably provide limited nutrients to the potential epithelial cells above. Another limitation is the unwanted widening and high variation in diameters of the vessels, although this may be resolved as this method is improved. The lifespan of some of the endothelial tubes greatly exceeded that of other microchannel tubes formed by scaffolds found in literature [43] [45] [47] [54] [65]. This lifespan indicates that this method might be combined with the ALI culturing of a layer of alveolar epithelial cells. With this method vessels are surrounded by hydrogel which allows the culture of epithelial cells on top, preventing the use of a fabricated membrane. The device is robust, but for now, the varying diameter compromises its reproducibility. The main cause for this is the presence of air bubbles, leading to wider and greater variation in the diameter of the vessels, and it limits the cell seeding method. However, the results of this cell seeding method and this hydrogel composition are still applicable.

## VI. Conclusion

The main goal is to create an organs-on-chip system which best reproduces the *in vivo* conditions and can be used to study the effect of air pollution on our lung health. A model that integrates blood flow, air flow, membrane stretching and vasculature is preferred. The

model should also have a sufficient lifetime to allow for culture time and experiments and should be free of PDMS and membranes. In this study, a vessel model was created using a new moulding method. This wire moulding method provides an inventive and robust method to supply the vessels with medium flow by using injection needles. Cell seeding through the capillary effect offers a simple approach. However, while it often works, the cell seeding method is not completely reliable yet. The cultured vessels are fully embedded in hydrogel allowing for further designs to be integrated with epithelial cells without a fabricated and PDMS-free membrane. With the model, a vessel with a lifespan of 32 days was created in a 2% fibrogen hydrogel. This indicates that those vessels can be co-cultured with alveolar epithelial cells and allowing them to fully differentiate and also have time for follow-up experiments. The fibrinogen concentration in the hydrogel could enhance the lifespan of the endothelial tube, as higher concentration, 2% compared to 1% fibrinogen, was found to support prolonged culture periods for the vessels. Possible due to the changed mechanical properties therefore, the higher effective youngs modules might provide more structural support for the endothelial cells to adhere to the wall of the membrane. The hydrogel with 2% fibrinogen has an elastic modulus that is corresponding to the elastic modulus of the human lung tissue. The microvascular endothelial cells were able to withstand significant shear stress, although lower than in vivo condidtions. It was confirmed that endothelial cells properly adhered to the hollow channel, were strong connected to each other and were aligned to form a vessel. The vessels have varying and enlarged diameters compared to the diameter of the mould. This might be due to the stiffness of the wires and the presence of air bubbles after cell seeding. To make the model more reproducable the presence of air bubbles should be avoided. These methods and results can be used as a step towards a membrane-free vascularised alveolar-capillary barrier model, which incorporates flow and stretching of the barrier.

## VII. Recommendations

In this study the 2% fibrinogen hydrogel provides a longer lifespan of the endothelial tubes then the 1% fibrinogen hydrogel. Further research should be done with a larger test group to see if similar result can be obtained. Also, other compositions of hydrogel can be compared and further research can be done on the underlying cause of the longer lifespan of those vessels. To further improve this model several changes can be made. To decrease the diameter of the channels, other biocompatible wires with a higher flexibility should be used. To overcome the biggest challenge, the presence of air bubbles, it is recommended to try wetting the stainless steel part of the needle. An alternative approach involves first removing the wire before introducing the endothelial cell solution into the needles, rather than placing the solution inside and then removing the wire. This may prevent air bubbles from forming or being trapped between the wire and the inner surface of the needle.

This study is a first step towards a vascularised alveolar-capillary barrier model incorporating flow and stretch. The goal was to gather information about which cell seeding method, hydrogel composition and diameters to use. Methods to combine capillaries with epithelial cells, creating a capillary network and applying stretch to the barrier are the next challenges. Combining the vessel with the epithelial cells could be initiated once the model is more reproducible. The next challenge is to obtain a small layer of hydrogel between the capillaries and the epithelial cells. The capillaries could be cultured just below the surface of the hydrogel by aligning the needles higher in the PDMS container to decrease the gel volume above the needles. When a larger area of epithelial cells is desired, alternative moulding techniques such as sacrificial moulding are recommended, as they can create a network of vessels rather than a single tube, thereby providing a broader nutrient supply to a greater number of cells. The same diameters, the 2% fibrinogen hydrogel and cell seeding method can then be used. In a follow-up design to implement air flow and stretching of the membrane, the principle of using a pressure difference as was done in the model of Zamprogno *et al.* could be a good starting point. The bottom of the PDMS container could then be designed circular instead of rectangular to obtain tri-axial stretching of the membrane.


## Acknowledgements

We would like to thank Pieter van Altena for his assistance with the nanoindenter and Floor Benthem for culturing the MVECs and pericytes, as well as for her help in preparing the hydrogels.


## References


[1] S. Fleischer, D. N. Tavakol, and G. Vunjak-Novakovic, (2020), "From arteries to capillaries: approaches to engineering human vasculature," *Advanced functional materials*, vol. 30, no. 37, p. 1910811. https://doi.org/10.1002/adfm.201910811

[2] A. Kadyrova, P. Kanabekova, A. Martin, D. Begimbetova, and G. Kulsharova, (2022), "Evaluation of membranes for mimicry of an alveolar-capillary barrier in microfluidic lung-on-a-chip devices," *Materials Today: Proceedings*, vol. 71, pp. 7–12. https://doi.org/10.1016/j.matpr.2022.05.582

[3] P. Gehr, M. Bachofen, and E. R. Weibel, (1978), "The normal human lung: Ultrastructure and morphometric estimation of diffusion capacity'," *Respiration Phyvsiology*, vol. 32, pp. 121–140. https://doi.org/10.1016/0034-5687(78)90104-4

[4] A. Doryab, S. Tas, B. Taskin, L. Yang, A. Hilgendorff, J. Groll, D. E. Wagner, and O. Schmid, (2019), "Review www.afm-journal.de evolution of bioengineered lung models: Recent advances and challenges in tissue mimicry for studying the role of mechanical forces in cell biology," *Advanced functional materials*, vol. 29, no. 39. https://onlinelibrary.wiley.com/doi/10.1002/adfm.201903114

[5] B. E. Isakson, G. J. Seedorf, R. L. Lubman, W. H. Evans, and S. Boitano, (2003), "Cell–cell communication in heterocellular cultures of alveolar epithelial cells," *American journal of respiratory cell and molecular biology*, vol. 29, no. 5, pp. 552–561. https://doi.org/10.1165/rcmb.2002-0281OC

[6] W. F. Boron and E. L. Boulpaep. Elsevier health sciences, (2012), *Medical physiology, 2e updated edition e-book: with student consult online access*, ,ISBN: 1455711810, 9781455711819.

[7] C. E. Barkauskas, M. J. Cronce, C. R. Rackley, E. J. Bowie, D. R. Keene, B. R. Stripp, S. H. Randell, P. W. Noble, B. L. Hogan *et al.*, (2013), "Type 2 alveolar cells are stem cells in adult lung," *The Journal of clinical investigation*, vol. 123, no. 7, pp. 3025–3036. https://doi.org/10.1172/JCI68782

[8] V. Kumar, (2020), "Pulmonary innate immune response determines the outcome of inflammation during pneumonia and sepsis-associated acute lung injury," *Frontiers in immunology*, vol. 11, p. 1722. https://doi.org/10.3389/fimmu.2020.01722

[9] Y. S. Khan and D. T. Lynch. StatPearls Publishing, Treasure Island (FL), (2022), *Histology, Lung*. http://europepmc.org/books/NBK534789

[10] L. Knudsen and M. Ochs, (2018), "The micromechanics of lung alveoli: structure and function of surfactant and tissue components the structural components for gas exchange," *Histochemistry and Cell Biology*, vol. 150, pp. 661–676. https://doi.org/10.1007/s00418-018-1747-9

[11] E. R. Weibel, (1970), "Morphometric estimation of pulmonary diffusion capacity: I. model and method," *Respiration physiology*, vol. 11, no. 1, pp. 54–75. https://doi.org/10.1016/0034-5687(70)90102-7

[12] O. T. Guenat and F. Berthiaume, (2018), "Incorporating mechanical strain in organs-on-a-chip: Lung and skin," *Biomicrofluidics*, vol. 12. https://doi.org/10.1063/1.5024895

[13] C. Hermans and A. Bernard, (1998), "Pneumoproteinaemia: a new perspective in the assessment of lung disorders," *European Respiratory Journal*, vol. 11, pp. 801–803. https://erj.ersjournals.com/content/11/4/801

[14] A. Doryab, M. B. Taskin, P. Stahlhut, A. Schröppel, D. E. Wagner, J. Groll, and O. Schmid, (2021), "A biomimetic, copolymeric membrane for cell-stretch experiments with pulmonary epithelial cells at the air-liquid interface," *Advanced Functional Materials*, vol. 31. https://doi.org/10.1002/ADFM.202004707

[15] H. Watanabe-Takano, K. Kato, E. Oguri-Nakamura, T. Ishii, K. Kobayashi, T. Murata, K. Tsujikawa, T. Miyata, Y. Kubota, Y. Hanada *et al.*, (2024), "Endothelial cells regulate alveolar morphogenesis by constructing basement membranes acting as a scaffold for myofibroblasts," *Nature Communications*, vol. 15, no. 1, p. 1622. https://doi.org/10.1038/s41467-024-45910-y

[16] M. G. Levitzky, *Blood Flow to the Lung, Pulmonary Physiology, 9e*. McGraw-Hill Education, (2017). accessmedicine.mhmedical.com/content.aspx?aid=1160936239

[17] D. F. Tees, P. Sundd, and D. J. Goetz, 1 (2006), "A flow chamber for capillary networks: Leukocyte adhesion in capillary-sized, ligand-coated micropipettes," *Principles of Cellular Engineering*, pp. 213–231. https://doi.org/10.1016/B978-012369392-1/50011-5

[18] E. R. Weibel, (2017), "Lung morphometry: the link between structure and function introduction: searching for the structural basis of lung physiology," *Cell and tissue research*, vol. 367, pp. 413–426. https://doi.org/10.1007/s00441-016-2541-4

[19] A. Shimizu, W. H. Goh, S. Itai, M. Hashimoto, S. Miura, and H. Onoe, (2020), "Lab on a chip devices and applications at the micro-and nanoscale ecm-based microchannel for culturing in vitro vascular tissues with simultaneous perfusion and stretch †," *Lab on a Chip*, vol. 20, no. 11, pp. 1917–1927. https://doi.org/10.1039/d0lc00254b

[20] A. Sandoo, J. J. V. van Zanten, G. S. Metsios, D. Carroll, and G. D. Kitas, 2 (2010), "The endothelium and its role in regulating vascular tone," *The Open Cardiovascular Medicine Journal*, vol. 4, p. 302. https://doi.org/10.2174/1874192401004010302

[21] E. M. Meijer, C. G. V. Dijk, R. Kramann, M. C. Verhaar, and C. Cheng, 2 (2022), "Implementation of pericytes in vascular regeneration strategies," *Tissue Engineering - Part B: Reviews*, vol. 28, pp. 1–21. http://dx.doi.org/10.3390/cells10071602

[22] T. J. Bennet, A. Randhawa, J. Hua, K. C. Cheung, T. J. . Bennet, A. . Randhawa, J. . Hua, K. C. Cheung, T.-L. Hackett, and E. T. Osei, 6 (2021), "Airway-on-a-chip: Designs and applications for lung repair and disease," *Cells 2021*, vol. 10, p. 1602. https://doi.org/10.3390/cells10071602

[23] S. Pun, L. C. Haney, and R. Barrile, 10 (2021), "Modelling human physiology on-chip: Historical perspectives and future directions," *Micromachines*, vol. 12. https://doi.org/10.3390/mi12101250

[24] A. Kanashiro, C. H. Hiroki, D. M. da Fonseca, A. Birbrair, R. G. Ferreira, G. S. Bassi, M. D. Fonseca, R. Kusuda, G. C. M. Cebinelli, K. P. da Silva, C. W. Wanderley, G. B. Menezes, J. C. Alves-Fiho, A. G. Oliveira, T. M. Cunha, A. S. Pupo, L. Ulloa, and F. Q. Cunha, 1 (2020), "The role of neutrophils in neuro-immune modulation," *Pharmacological Research*, vol. 151, p. 104580. https://doi.org/10.1016/j.phrs.2019.104580

[25] L. van Os, J. Yeoh, G. Witz, D. Ferrari, P. Krebs, Y. Chandorkar, S. Zeinali, A. Sengupta, and O. T. Guenat, 8 (2023), "Immune cell extravasation in an organ-on-chip to model lung inflammation," *European Journal of Pharmaceutical Sciences*, vol. 187, p. 106485. https://doi.org/10.1016/j.ejps.2023.106485

[26] C. R. Kleiveland, 1 (2015), "Peripheral blood mononuclear cells," *The Impact of Food Bioactives on Health: In Vitro and Ex Vivo Models*, pp. 161–167. https://doi.org/10.1007/978-3-319-16104-4_15

[27] A. De Troyer, P. A. Kirkwood, and T. A. Wilson, (2005), "Respiratory action of the intercostal muscles," *Physiological reviews*, vol. 85, no. 2, pp. 717–756. https://doi.org/10.1152/physrev.00007.2004

[28] J. Dong, Y. Yang, and Y. Zhu, 3 (2022), "Recent advances in the understanding of alveolar flow," *Biomicrofluidics*, vol. 16, p. 021502. https://doi.org/10.1063/5.0084415

[29] D. Huh, B. D. Matthews, A. Mammoto, M. Montoya-Zavala, H. Y. Hsin, and D. E. Ingber, 6 (2010), "Reconstituting organ-level lung functions on a chip," *Science*, vol. 328, pp. 1662–1668. https://doi.org/10.1126/science.1188302

[30] A. O. Stucki, J. D. Stucki, S. R. R. Hall, M. Felder, Y. Mermoud, R. A. Schmid, T. Geiser, and O. T. Guenat, (2014), "From chip-in-a-lab to lab-on-a-chip: towards a single handheld electronic system for multiple application-specific lab-on-a-chip (asloc)," vol. 15, p. 1302. https://doi.org/10.1039/C4LC01252F

[31] Y. Li, Y. S. Prakash, Q. Tan, and D. Tschumperlin, 4 (2024), "Defining signals that promote human alveolar type i differentiation," *American Journal of Physiology - Lung Cellular and Molecular Physiology*, vol. 326, pp. L409–L418. https://doi.org/10.1152/ajplung.00191.2023

[32] D. Cozens, E. Grahame, E. Sutherland, G. Taylor, C. C. Berry, and R. L. Davies, 12 (2018), "Development and optimization of a differentiated airway epithelial cell model of the bovine respiratory tract," *Scientific Reports*, vol. 8, p. 853. https://doi.org/10.1038/s41598-017-19079-y

[33] M. R. Staudt, L. J. Buro-Auriemma, M. S. Walters, J. Salit, T. Vincent, R. Shaykhiev, J. G. Mezey, A. E. Tilley, R. J. Kaner, M. W. Ho, and R. G. Crystal, 10 (2014), "Airway basal stem/progenitor cells have diminished capacity to regenerate airway epithelium in chronic obstructive pulmonary disease," *American Journal of Respiratory and Critical Care Medicine*, vol. 190, pp. 955–958. https://doi.org/10.1164/rccm.201406-1167LE

[34] O. Jung, Y. T. Tung, E. Sim, Y. C. Chen, E. Lee, M. Ferrer, and M. J. Song, 2 (2022), "Development of human-derived, three-dimensional respiratory epithelial tissue constructs with perfusable microvasculature on a high-throughput microfluidics screening platform," *Biofabrication*, vol. 14, p. 025012. https://doi.org/10.1088/1758-5090/AC32A5

[35] N. Khalilgharibi and Y. Mao, (2021), "To form and function: on the role of basement membrane mechanics in tissue development, homeostasis and disease," *Open biology*, vol. 11, no. 2, p. 200360. https://doi.org/10.1098/rsob.200360

[36] A. Doryab and J. Groll, 3 (2023), "Biomimetic in vitro lung models: Current challenges and future perspective," *Advanced Materials*, vol. 35, p. 2210519. https://doi.org/10.1002/adma.202210519

[37] C. Iriondo, S. Koornneef, K.-P. Skarp, M. Buscop-van Kempen, A. Boerema-de Munck, and R. J. Rottier, (2024), "Simple-flow: A 3d-printed multiwell flow plate to coculture primary human lung cells at the air–liquid interface," *ACS Biomaterials Science & Engineering*. https://doi.org/10.1021/acsbiomaterials.4c01322

[38] F. Akther, S. B. Yakob, N.-T. Nguyen, and H. T. Ta, (2020), "Surface modification techniques for endothelial cell seeding in pdms microfluidic devices," *Biosensors*, vol. 10, no. 11, p. 182. https://doi.org/10.3390/bios10110182

[39] H. H. Chung, M. Mireles, B. J. Kwarta, and T. R. Gaborski, (2018), "Use of porous membranes in tissue barrier and co-culture models," *Lab on a Chip*, vol. 18, no. 12, pp. 1671–1689. https://doi.org/10.1039/C7LC01248A

[40] C. O'Connor, E. Brady, Y. Zheng, E. Moore, and K. R. Stevens, (2022), "Engineering the multiscale complexity of vascular networks," *Nature Reviews Materials*, vol. 7, no. 9, pp. 702–716. https://doi.org/10.1038/s41578-022-00447-8

[41] H. Nam, Y. mi Choi, and J. Jang, 1 (2020), "Vascularized lower respiratory-physiology-on-a-chip," *Applied Sciences 2020, Vol. 10, Page 900*, vol. 10, p. 900. https://doi.org/10.3390/app10030900

[42] W. H. Wu, T. H. Punde, P. C. Shih, C. Y. Fu, T. P. Wang, L. Hsu, H. Y. Chang, and C. H. Liu, 3 (2015), "A capillary-endothelium-mimetic microfluidic chip for the study of immune responses," *Sensors and Actuators B: Chemical*, vol. 209, pp. 470–477. https://doi.org/10.1016/j.snb.2014.11.123

[43] J. Paek, S. E. Park, Q. Lu, K. T. Park, M. Cho, J. M. Oh, K. W. Kwon, Y. S. Yi, J. W. Song, H. I. Edelstein, J. Ishibashi, W. Yang, J. W. Myerson, R. Y. Kiseleva, P. Aprelev, E. D. Hood, D. Stambolian, P. Seale, V. R. Muzykantov, and D. Huh, 7 (2019), "Microphysiological engineering of self-assembled and perfusable microvascular beds for the production of vascularized three-dimensional human microtissues," *ACS Nano*, vol. 13, pp. 7627–7643. https://doi.org/10.1021/acsnano.9b00686

[44] J. S. Miller, K. R. Stevens, M. T. Yang, B. M. Baker, D. H. T. Nguyen, D. M. Cohen, E. Toro, A. A. Chen, P. A. Galie, X. Yu, R. Chaturvedi, S. N. Bhatia, and C. S. Chen, 7 (2012), "Rapid casting of patterned vascular networks for perfusable engineered three-dimensional tissues," *Nature Materials 2012 11:9*, vol. 11, pp. 768–774. https://doi.org/10.1038/nmat3357

[45] K. M. Chrobak, D. R. Potter, and J. Tien, (2006), "Formation of perfused, functional microvascular tubes in vitro," *Microvascular research*, vol. 71, no. 3, pp. 185–196. whttps://doi.org/10.1016/j.mvr.2006.02.005

[46] Y. T. Lin, Y. T. Tung, J. Y. Wong, and G. J. Wang, 3 (2023), "Fabrication of perfusable microvessel networks by mimicking in vivo vasculogenesis using a novel scaffold-wrapping method," *Materials and Design*, vol. 227, p. 111707. https://doi.org/10.1016/j.matdes.2023.111707

[47] L. L. Bischel, E. W. Young, B. R. Mader, and D. J. Beebe, 2 (2013), "Tubeless microfluidic angiogenesis assay with three-dimensional endothelial-lined microvessels," *Biomaterials*, vol. 34, p. 1471. https://doi.org/10.1016/j.biomaterials.2012.11.005

[48] K. R. Short, J. Kasper, S. Van Der Aa, A. C. Andeweg, F. Zaaraoui-Boutahar, M. Goeijenbier, M. Richard, S. Herold, C. Becker, D. P. Scott *et al.*, (2016), "Influenza virus damages the alveolar barrier by disrupting epithelial cell tight junctions," *European Respiratory Journal*, vol. 47, no. 3, pp. 954–966. https://doi.org/10.1183/13993003.01282-2015

[49] P. Zamprogno, S. Wüthrich, S. Achenbach, G. Thoma, J. D. Stucki, N. Hobi, N. Schneider-Daum, C. M. Lehr, H. Huwer, T. Geiser, R. A. Schmid, and O. T. Guenat, 12 (2021), "Second-generation lung-on-a-chip with an array of stretchable alveoli made with a biological membrane," *Communications biology*, vol. 4. https://doi.org/10.1038/s42003-021-01695-0

[50] J. Y. Park, H. Ryu, B. Lee, D.-H. Ha, M. Ahn, S. Kim, J. Y. Kim, N. L. Jeon, and D.-W. Cho, (2018), "Development of a functional airway-on-a-chip by 3d cell printing," *Biofabrication*, vol. 11, no. 1, p. 015002. https://doi.org/10.1088/1758-5090/aae545

[51] A. G. Monteduro, S. Rizzato, G. Caragnano, A. Trapani, G. Giannelli, and G. Maruccio, (2023), "Organs-on-chips technologies–a guide from disease models to opportunities for drug development," *Biosensors and Bioelectronics*, vol. 231, p. 115271. https://doi.org/10.1016/j.bios.2023.115271

[52] J. T. Morgan, J. Shirazi, E. M. Comber, C. Eschenburg, and J. P. Gleghorn, (2019), "Fabrication of centimeter-scale and geometrically arbitrary vascular networks using in vitro self-assembly," *Biomaterials*, vol. 189, pp. 37–47. https://doi.org/10.1016/j.biomaterials.2018.10.021

[53] J. J. Tronolone and A. Jain, (2021), "Engineering new microvascular networks on-chip: ingredients, assembly, and best practices," *Advanced functional materials*, vol. 31, no. 14, p. 2007199. https://doi.org/10.1002/adfm.202007199

[54] S. Park, T. H. Kim, S. H. Kim, S. You, and Y. Jung, 8 (2021), "Three-dimensional vascularized lung cancer-on-a-chip with lung extracellular matrix hydrogels for in vitro screening," *Cancers*, vol. 13. https://doi.org/10.3390/cancers13163930

[55] H. Duong, B. Wu, and B. Tawil, 2009, "Modulation of 3d fibrin matrix stiffness by intrinsic fibrinogen–thrombin compositions and by extrinsic cellular activity," *Tissue Engineering Part A*, vol. 15, no. 7, pp. 1865–1876. https://doi.org/10.1089/ten.tea.2008.0319

[56] A. Montero, C. Quílez, L. Valencia, P. Girón, J. L. Jorcano, and D. Velasco, (2021), "Effect of fibrin concentration on the in vitro production of dermo-epidermal equivalents," *International journal of molecular sciences*, vol. 22, no. 13, p. 6746. https://doi.org/10.3390/ijms22136746

[57] C. L. Chiu, V. Hecht, H. Duong, B. Wu, and B. Tawil, (2012), "Permeability of three-dimensional fibrin constructs corresponds to fibrinogen and thrombin concentrations," *BioResearch open access*, vol. 1, no. 1, pp. 34–40. https://doi.org/10.1089/biores.2012.0211

[58] Z. Wang, S. M. Mithieux, and A. S. Weiss, (2019), "Fabrication techniques for vascular and vascularized tissue engineering," *Advanced healthcare materials*, vol. 8, no. 19, p. 1900742. https://doi.org/10.1002/adhm.201900742

[59] R. M. Linville, N. F. Boland, G. Covarrubias, G. M. Price, and J. Tien, (2016), "Physical and chemical signals that promote vascularization of capillary-scale channels," *Cellular and molecular bioengineering*, vol. 9, pp. 73–84. https://doi.org/10.1007/s12195-016-0429-8

[60] D. Katritsis, L. Kaiktsis, A. Chaniotis, J. Pantos, E. P. Efstathopoulos, and V. Marmarelis, 3 (2007), "Wall shear stress: Theoretical considerations and methods of measurement," *Progress in Cardiovascular Diseases*, vol. 49, pp. 307–329. https://doi.org/10.1016/j.pcad.2006.11.001

[61] F. M. White, "Fluid mechanics 8th edition in si units," (2016), ,ISBN:978-9-814-72017-5.

[62] B. J. Ballermann, A. Dardik, E. Eng, and A. Liu, 9 (1998), "Shear stress and the endothelium," *Kidney International*, vol. 54, pp. S100–S108. https://doi.org/10.1046/j.1523-1755.1998.06720.x

[63] C. Poon, 2 (2022), "Measuring the density and viscosity of culture media for optimized computational fluid dynamics analysis of in vitro devices," *Journal of the mechanical behavior of biomedical materials*, vol. 126. https://doi.org/10.1016/j.jmbbm.2021.105024

[64] Y. M. Efremov, T. Okajima, and A. Raman, 12 (2019), "Measuring viscoelasticity of soft biological samples using atomic force microscopy," *Soft Matter*, vol. 16, pp. 64–81. https://doi.org/10.1039/C9SM01020C

[65] A. Tan, K. Fujisawa, Y. Yukawa, and Y. T. Matsunaga, 10 (2016), "Bottom-up fabrication of artery-mimicking tubular co-cultures in collagen-based microchannel scaffolds," *Biomaterials Science*, vol. 4, pp. 1503–1514. https://doi.org/10.1039/C6BM00340K

# 4 Vascularisation by sacrificial moulding

To create the structure described in Chapter 2, an alternative moulding technique to wire moulding is needed. Our literature review revealed that, in addition to needle moulding, sacrificial moulding has been used to culture vessels with a relatively longer lifespan compared to those created using other scaffold-based methods.

## 4.1 Theory

To gain more knowledge about sacrificial moulding, further research was conducted and is discussed here.

### 4.1.1 Sacrificial moulding

3D-printable sacrificial moulding offers a reproducible fabrication technique and enables the creation of a more complex structures than those achievable with needle moulding. Various materials can be used for sacrificial moulding. However, for our application, it is essential to dissolve the mould without relying on toxic solvents. While PLA and PCL are commonly used as printing filaments in fused deposition modelling (FDM) printers and are suitable for sacrificial moulding, they are not applicable in this context. These materials require organic solvents, such as chloroform and dichloromethane, which can cause cell damage [3].

Polyvinyl Alcohol (PVA) is another commonly used material for sacrificial moulding. Shimizu *et al.* fabricated a PVA mould using 200 µm nozzles and employed it within a gelatin hydrogel to create hollow channels. However, they achieved a minimum channel width of 300 µm [4]. PVA has a high solubility in water but has been shown to swell in water-containing environments such as hydrogels [3]. For our application, it is important to create small channels, preferably with diameters smaller than 150 µm. Therefore, the alternative sacrificial material, carbohydrate glass, is further explored.

Miller *et al.* used a mixture of sucrose, glucose and dextran and reversed osmosis water to create vessels with a diameter of 150 - 750 µm [5]. After Miller *et al.* printed their sacrificial moulding also Pollet *et al.* used this method. Pollet *et al.* used it for a PDMS mould. But interestingly, they were able to fabricate a structure with a diameter of 120 µm with in-plane bifurcations [6]. Moeun *et al.* aimed to improve the glass made by Miller *et al.* They showed that they made a stronger network using only sucrose or a mixture of sucrose and glucose.

To give an overview of these studies, the materials print settings and diameter of the moulds are collected in Table 4.1.

| Variable article | Miller *et al.*, 2012 [5] | Pollet *et al.*, 2019 [6] | Pollet *et al.*, 2019 [6] | Moeun *et al.*, 2023 [7] | Moeun *et al.*, 2023 [7] |
|---|---|---|---|---|---|
| Diameter printed glass | 200$\mu$m | 200$\mu$m | 120±12$\mu$m | 400-3100$\mu$m | 400-3100$\mu$m |
| Material | 25g glucose, 53g sucrose, 10g dextran, 50 ml reverse osmosis water | 53g sucrose, 25g glucose | 25g glucose, 53g sucrose, 10g dextran | sucrose | 20g Sucrose, 10g glucose |
| Nozzle temperature | NR | NR | NR | 95 | 80 |
| Barrel temperature | 110 | 90 | 90 | 110 | 110 |
| Nozzle size | 1.2 mm or 0.84 mm | 0.15 mm | 0.15 mm | 1 mm | 1 mm |
| Velocity of nozzle | 50 mm/s | 4.17 mm/s | 3 mm/s | 0.067-2.3 mm/s | 0.067-2.3 mm/s |
| Viscosity | NR | 44.2 Pa s at 90 °C (measured at 1 Hz) | 163.9 Pa s at 90 °C (measured at 1 Hz) | 529 Pa s at 95 °C (measured at 0.5 Hz) | 529 Pa s at 80 °C (measured at 0.5 Hz) |

Notes: NR, information was not reported

Table 4.1: Comparison print settings of printed carbohydrate glass or sugerglass

Table 4.1 shows that the composition of the glass and the print settings result in different diameters of the mould. To further explore this, different compositions of the glass will be discussed.

### 4.1.2 Composition of the glass

**The materials which are used to create the glass**

The materials used to make sugar glass are glucose and sucrose and to make carbohydrate glass are glucose, sucrose and dextran. Glucose is a monosaccharide, sucrose is a disaccharide and dextran is a polysaccharide comprising glucose units linked together [8].

The glass temperature and melting point the materials are presented in 4.2

| Component | Glass temperature | Melt temperature |
|---|---|---|
| Glucose | 35 °C [9] | 155 °C [9] |
| Sucrose | 70 °C [9] | 185 °C [9] |
| Dextran* | 220 - 225 °C [10] | 483 °C** |

Notes: *characteristics depend on molecular weight, we use dextran with $70 \times 10^3$ g/mol. **Melting temperature obtained from our supplier Merck.

Table 4.2: Glass temperature and melt temperature of materials used in carbohydrate glass

To be able to print a structure with a small diameter it is needed to understand the relationship between the viscosity, temperature and used materials.

**The viscosity depends on the composition and the temperature**

Moeun *et al.* printed multiple structures with different compositions. They first optimised the print settings for the 2:1 sucrose:glucose glass. To use the same optimised print settings for glass with other components, it was preferred to have a the same viscosity. They used the Williams-Landel-Ferry model to create temperature-dependent viscosity data of sugar glass formulations. The viscosity data for two mixtures, one containing only sucrose and the other, referred to as 'Original,' being sugar glass, are shown in Figure 4.1. The data was used to determine the nozzle temperature for each glass.

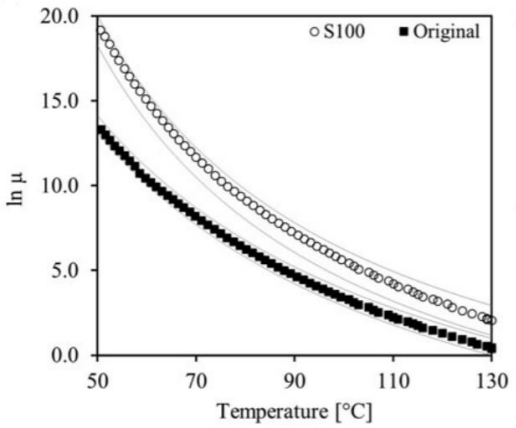


Figure 4.1: S100 means that the material is only sucrose. The mixture called 'Original' consists of sucrose and glucose, using a 2:1 sucrose-to-glucose mass ratio [7].

Pollet *et al.* determined that the viscosity of carbohydrate glass is higher compared to sugar glass. The viscosity of sugar glass and carbohydrate glass over a range of temperatures is shown in figure 4.2. The difference between the mixtures is that carbohydrate glass contains dextran. Dextran has a high glass temperature ranging from 150-225 °C depending on the chain length. Dextran is a polysaccharide and therefore has a higher molecular weight compared to glucose and sucrose, which are a monosaccharide and a disaccharide, respectively. The higher glass temperature and the higher molecular weight explain the higher viscosity of carbohydrate glass [6].

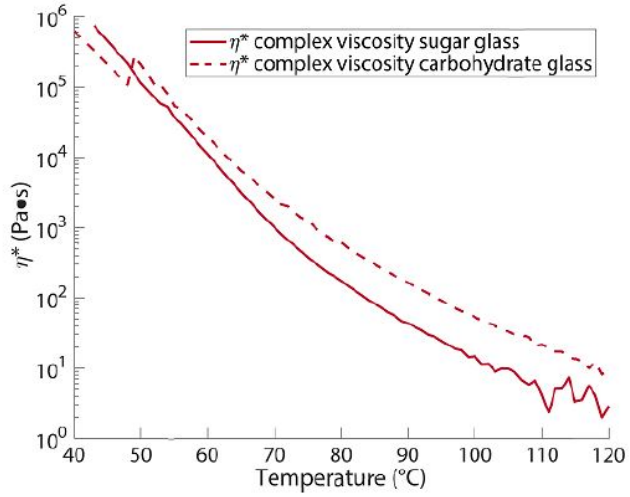


Figure 4.2: Pollet *et al.* measured the viscosity of the carbohydrate glass at several temperatures: 90 °C, 95 °C, 100 °C and 105 °C the measured viscosities are 163.9 Pa s, 93.23 Pa s, 54.26 Pa s and 33.29 Pa s. The viscosity of the carbohydrate glass is higher than the viscosity of sugar glass [6]

Pollet *et al.* demonstrated that printing carbohydrate glass at 90 °C results in structures with smaller diameters compared to printing at 105 °C [6]. This suggests that a lower printing temperature, and consequently a higher viscosity, can lead to the formation of structures with smaller diameters. And Pollet *et al.* showed that when printing a structure with bifurcations the sugar glass performed better compared to carbohydrate glass because of the lower viscosity at constant printing temperatures, which improves creating in-plane junctions [6].

**The composition of glass affects the stability of the structure**

The composition of the glass also affects its stability. Sucrose is unstable in supersaturated solutions, the addition of glucose prevents recrystallization and therefor facilities the formation of a stable glass [5]. Miller *et al.* also used dextran because it improved the temperature stabillity [5]. This is substantiated by the calculations of Moeun *et al.*. calculated the glass temperature of several mixtures, this is shown in figure 4.3. It can be seen that adding dextran results in a higher glass temperature. A higher glass temperature leads to an improvement in printing a stable 3D structure supported by itself. Because a high glass temperature results in rapid solidification. The printed filaments are then strong enough to withstand the forces during printing, for example, caused by cooling air jets, and the weight of its own structure [7].

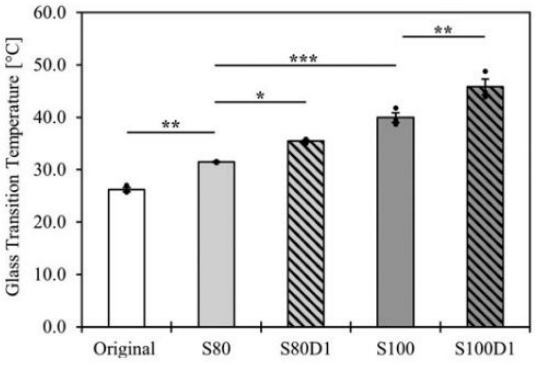


Figure 4.3: The mixture referred to as 'Original' consists of sucrose and glucose in a 2:1 sucrose-to-glucose mass ratio. The mixture S80 contains a 4:1 sucrose-to-glucose mass ratio. S100 indicates that the material is composed entirely of sucrose. The label D1 refers to the addition of 1% dextran to the mixture [7].

**Composition of the glass affects the strength of the structure**

Not using dextran also has it advantages. As Moeun *et al.* have shown, it will result in a higher strength of the structure [7]. Moeun *et al.* have compared a mixture of only sucrose and a mixture of sucrose and glucose, both have shown a higher strength and flexural modules compared to the mixture of Miller *et al.*. This could be due to a higher degree of caramelization and decreased water content [7].

**Preparation glass**

Not only the composition of the glass is an important factor. Heating pure sucrose and glucose separately leads to a mass decrease of the material [9]. The heating temperature of a mixture

is therefore a parameter which will influence the material properties. Also, Dextran is often added after the heating process. Adding Dextran beforehand might increase the water content and affect the degree of caramelisation which leads to lower glass temperature values than when Dextran is stirred in after the heating process [7].

### 4.1.3 Discussion and conclusion theory sacrificial moulding

A high stiffness, stable material and a low viscosity to allow extrusion through small nozzles are prerequisites for a sacrificial mould.

Deciding the composition of the glass involves a trade-off. Adding glucose and dextran leads to a lower strength of the printed structure and an undesired increase in viscosity. However, it also improves the stability of the printed structure by increasing the glass transition temperature.

In our study, the goal is to create a network of small channels, approximately 50 µm to 150 µm, within a hydrogel. Since the hydrogel is a water-based environment, it is crucial that the structure remains stable while the hydrogel is crosslinking. Also, the structure we aim to print is shorter than the 40 mm length reported by Moeun *et al.*, so reduced strength might not become an issue.

Therefore, the addition of glucose and dextran might provide us with the best results. Moreover, Pollet *et al.* achieved the smallest printed diameter of 120 µm when using the mixture with all the three components, demonstrating that this mixture provides the best performance among the three studies we compared.

With a higher velocity of the nozzle, the speed of the movement of the printhead, smaller diameters can be obtained [6]. However, faster is not always better, as ruptures of the glass structure during printing need to be avoided. In table 4.1 is shown that printing carbohydrate glass with a diameter of 120 µm was done with a nozzle temperature of 90 °C and with a nozzle velocity of 3 mm/s. While this information serves as a useful guideline, the optimal printing velocity and extrusion rate for successfully producing smaller structures should be determined through testing.

## 4.2 Method

Al steps were taken at ME at the TU Delft. The carbohydrate mixture was made and poured into the syringe inside the chemical lab. The printing was done at the Multiscale Lab. The Hydra 21 printer from Hyrel3D was used with the KR2-15 printhead.

### 4.2.1 Preparation carbohydrate glass

A mixture with 25 g glucose, 53 g sucrose, 10 g destran 86 kDa and 50 mL demi water was haeted to 90° on a hotplate while stirring using a magnetic stir bar. Then it was placed in an oven at 165 °C for 30 minutes. The hot mixture was poured in a stainless steel syringe that was then placed in the printhead of the printer. The nozzle had a diameter of 1.5 mm.

### 4.2.2 Printer settings

Two structures were printed using different print settings. For both structures, a custom G-code was written to precisely control the printing parameters. The scripts for these prints are provided in Appendices D.1 and D.2.

#### Square

The height of the printhead was calibrated using a thin piece of paper placed between the petri dish and the printhead to ensure proper alignment. The X and Y coordinates in the G-code were determined based on the position of the petri dish. The temperature of the printhead was set to 90 °C. The printhead height was adjusted to 20 mm. The printhead then moved to the first and second points of the square with a nozzle velocity of 560 mm/min, while for the third and fourth points, the velocity was reduced to 180 mm/min. For each side of the square, the extrusion rate was set to 3 mm, ensuring consistent deposition of the material.

#### Line with overhang

For this structure, the temperature of the printhead was again set at 90 °C, and the printhead height was again set to 20 mm. A single line was printed across two petri dishes placed at a distance from each other. This setup caused the printed carbohydrate glass to be partially extruded into air, creating an overhang. To facilitate cooling and hardening of the material at the point of deposition, the nozzle velocity was reduced to 80 mm/min. The extrusion rate was set to 2 mm. Additionally, the filament was slightly retracted at the end of the print to prevent extra material at the endpoint.

### 4.2.3 Embedding carbohydrate glass in hydrogel

To test whether the carbohydrate glass would dissolve or blend into the hydrogel prior to cross-linking, red-coloured carbohydrate glass was embedded in a 2% fibrinogen-based hydrogel and tested at three different temperatures: 4 °C, 21 °C, and 37 °C.

The test at 4 °C was conducted using a cooling block. The next test was performed at room temperature, at 21 °C. The other test was carried out by placing the embedded carbohydrate glass in an incubator at 37 °C for a few minutes.

After a short period, the samples were inspected to observe whether the red-coulored carbohydrate glass had mixed with the hydrogel. Additionally, the firmness of the carbohydrate glass was assessed to determine whether it remained hard or had softened, indicating it was melting.

## 4.3 Results

### 4.3.1 Square

The carbohydrate glass was printed in a square shape. The printing process began at the bottom-right corner, the starting position, followed by the bottom-left corner, the second position. A large volume of carbohydrate glass was deposited at the starting position. The first printed line had the smallest width among all the lines in the square.

### 4.3.2 Line with overhang

The carbohydrate glass was printed in a single line across two petri dishes placed at a distance from each other, resulting in an overhang of the carbohydrate glass. The width of the overhang is ranging from 3.2 - 5.8 mm.

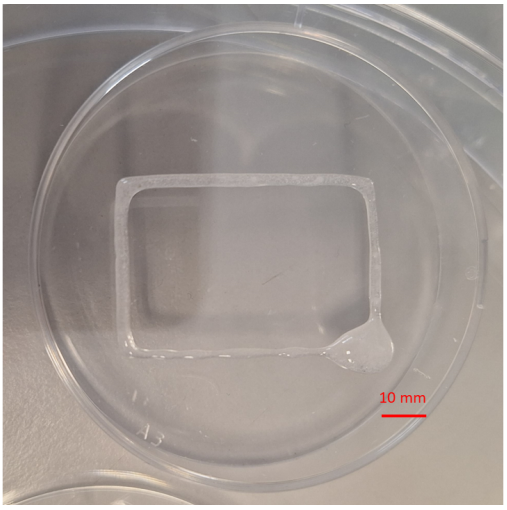


Figure 4.4: Printed carbohydrate glass structure in the shape of a square with widths in ranging from 1.5 - 3.5 mm.

### 4.3.3 Embedding carbohydrate glass in hydrogel

The carbohydrate glass did not dissolve or blend into the hydrogel at temperatures 4 °C and 21 °C. At both temperatures, the hydrogel was able to solidify. At 37 °C the hydrogel was softened and some blending was visible at 37 °C.

## 4.4 Discussion and conclusion

The results obtained were based on a single composition and without optimisation of the printing parameters. Despite this being the first and only attempt, we successfully printed structures with a width matching the nozzle diameter and achieved an overhang.

A preliminary protocol for printing carbohydrate glass was developed, suggesting it is possible to create structures with a width of approximately 1.5 mm. However, further optimisation of the print settings is required to produce structures with a consistent and smaller diameter. Smaller diameters can also be achieved by using finer nozzles. The printer used in this study allows for the connection of injection needles to the nozzle head, enabling further reduction of the printhead diameter. With a sufficiently low-viscosity mixture, this setup could enable the printing of carbohydrate glass with significantly reduced diameters.

Active cooling of the print area could also improve the printing process by producing more cylindrical structures and prolonging the stability of overhangs. Testing different compositions of carbohydrate glass may further enhance the structural quality of the printed objects.

For applications requiring the printed carbohydrate glass to remain stable for extended periods, especially when not immediately embedded in the hydrogel, certain measures can be taken. Exposing the printed structure to nitrogen gas could help keep the carbohydrate glass dry, preventing moisture from affecting its shape. Additionally, storing the printed structures at lower temperatures may improve stability over time.

Our experiments showed that the carbohydrate glass did not dissolve or blend into the hydrogel at

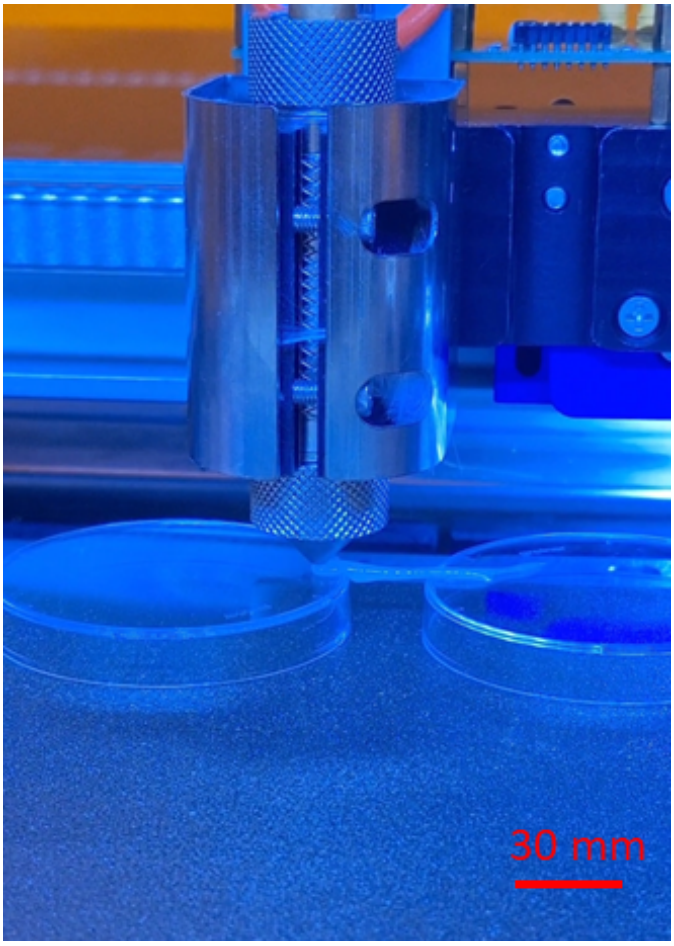


Figure 4.5: Carbohydrate glass printed with overhang with widths ranging from 3.2 - 5.8 mm.

4 °C. However, the impact of such temperature shifts on the pericytes embedded in the hydrogel remains uncertain. Further research is needed to determine if these cells can tolerate exposure to these temperature shifts.

This study demonstrates a proof of concept for printing carbohydrate glass using a fused deposition modelling (FDM) printer available at TU Delft. It also confirms that carbohydrate glass can be embedded into hydrogel prior to cross-linking. These findings indicate that sacrificial moulding with carbohydrate glass could be a promising method for creating networks of hollow channels inside hydrogels.

# 5 Discussion

The structure presented in Chapter 2 has not yet been fabricated, and its development will present additional challenges, such as ensuring cylindrical shapes at the junctions. Furthermore, depending on the PDMS container design for future devices, the need for a large overhang may arise. This requirement, combined with a small diameter, comes with challenges as the structure must support its own weight. Additionally, dissolving a complex structure with multiple small cylinders embedded within a hydrogel may prove difficult, and further research is needed to determine which designs are feasible.

The wire-moulding technique, combined with our cell-seeding method and hydrogel, has shown promise in creating a micro-vessel model that meets all requirements. However, it remains uncertain whether these techniques can be effectively combined with sacrificial moulding. For example, cell seeding within a hydrogel containing a network of hollow channels may require increased force, particularly for longer structures. When seeding cells into a network of hollow channels, such as the one presented in Chapter 2, it is important to evaluate whether all channels within the structure are adequately seeded with cells.

The lifespan of the vessel models created using the wire moulding technique suggests that culturing vessels in pre-formed channels enhances the lifespan of the model compared to models with random blood vessel networks. With vasculogenesis, it is possible to create capillaries with a diameter as small as 10 µm, which might be challenging to achieve using wire or sacrificial moulding. However, despite this, these techniques offer the advantage of control over the structure and a greater control over shear stress on endothelial cells, which may provide a strong justification for their use in this application.

Conducting a study with a large number of tests will require many assembled devices. Fabricating and assembling the wire moulding device presented in Chapter 3 is time-consuming. While 3D printing the rails and other components is straightforward and easily scalable, fabricating multiple PDMS containers can also be done efficiently. However, threading the wire through both needles is relatively time-consuming and may limit scalability. This challenge could potentially be resolved by using straighter wires or by transitioning to the sacrificial moulding technique. The PDMS container can be designed to allow for the direct printing of carbohydrate glass onto the container, which would significantly reduce the assembly time and improve the overall efficiency of the process. Such a development would streamline the fabrication process and make the method more practical for large-scale applications. As the number of devices increases, the quantity of tubes required will also grow, potentially leading to a more complex and disorganized setup. However, integrating flow into the system inherently necessitates such complexity as part of the process.

Future designs that integrate stretching and airflow aim to better mimic the mechanical and

dynamic environment of the human lung tissues. While these improvements enhance the physiological relevance of the model, they may also introduce additional complexities. The parameters associated with stretching and airflow are likely to affect cellular responses. However, it is difficult to predict if these changes influence the biological reaction to air pollution, the primary focus of this model. This uncertainty is particularly significant if stretching is modified from uniaxial to tri-axial.

# 6 Conclusion and recommendations

The main goal is to create an organ-on-chip system which best reproduces the in vivo conditions and can be used to study the effect of air pollution on our lung health. A model which integrates blood flow, air flow, membrane stretching and vasculature is preferred. Additionally, the model should have a sufficient lifetime to allow for culture time and follow-up experiments, and should be free of fabricated membrane.

As a first step, a vessel model with a sufficient lifespan was successfully developed, allowing us to answer our research questions. This study demonstrates that seeding primary endothelial cells into pre-formed channels can be used to develop a micro-vessel model with a lifespan exceeding those of current alveolar-capillary barrier models with random vessel networks. Hollow channels with average mean diameters of 161 µm and 296 µm were created using wire-moulding, with 50 µm and 125 µm wires, respectively. The use of a 2% fibrinogen hydrogel, combined with cell seeding facilitated by the capillary effect, resulted in well-adhered endothelial cells. These cells formed strong interconnections, aligned to form a vessel, and remained perfusable for up to 32 days.

Additionally, several carbohydrate glass structures were successfully printed. The carbohydrate glass was not compromised by embedding it with the hydrogel prior to crosslinking. Therefore, sacrificial moulding with carbohydrate glass demonstrated its potential to enhance the relevance of the micro-vessel model.

Improving the reproducibility of models created with our wire moulding device can be achieved by using an alternative material for the wires. An innovative option could be using human hair, which is flexible and biocompatible, has a high breaking strength of more than 200 MPa and a diameter of approximately 60 µm [11].

Several recommendations are proposed for the development of subsequent devices. Sacrificial moulding can be used when a larger model surface is required than what is achievable with wire moulding, or when it is desired to replicate the complex structure of native blood vessel networks in a model. In this case, the next steps involve optimizing the protocol for printing carbohydrate glass to create a network with small diameters and cylindrical hollow channels. Additionally, the process for resolving the challenges in removing the carbohydrate glass from within the hydrogel should be tested and refined.

For future designs, the visual observation of the cultured model can be enhanced. In the current device, glass can be used as the base of the container. Moreover, when membrane stretching is incorporated, the vacuum chamber could be built on a glass substrate by attaching PDMS directly onto the glass surface.

The network structure presented with our future concept allows for a larger surface area of the model and with only one inlet and outlet, the number of required tubes is minimized. However,

the shape of the sacrificial mould should be carefully designed to ensure that the flow generates a uniform shear stress on the endothelial cells throughout the entire network.

The findings of this study, particularly the extended lifespan of this model, may also be relevant to other applications. The vessel model created using wire moulding demonstrates that culturing endothelial cells in pre-formed channels not only improves the lifespan compared to random blood vessel networks but also provides greater control over the shear stress experienced by endothelial cells. This enhanced control could be valuable for other research areas, such as studies on blood vessel diseases or investigations into other human barriers, including the blood-brain barrier or the skin barrier.

# Bibliography


[1] D. Huh, B. D. Matthews, A. Mammoto, M. Montoya-Zavala, H. Y. Hsin, and D. E. Ingber, 6 (2010), "Reconstituting organ-level lung functions on a chip," *Science*, vol. 328, pp. 1662–1668. https://doi.org/10.1126/science.1188302

[2] P. Zamprogno, S. Wüthrich, S. Achenbach, G. Thoma, J. D. Stucki, N. Hobi, N. Schneider-Daum, C. M. Lehr, H. Huwer, T. Geiser, R. A. Schmid, and O. T. Guenat, 12 (2021), "Second-generation lung-on-a-chip with an array of stretchable alveoli made with a biological membrane," *Communications biology*, vol. 4. https://doi.org/10.1038/s42003-021-01695-0

[3] S. Li, H. Li, X. Shang, J. He, and Y. Hu, 9 (2023), "Recent advances in 3d printing sacrificial templates for fabricating engineered vasculature," *MedComm – Biomaterials and Applications*, vol. 2, p. e46. https://doi.org/10.1002/mba2.46

[4] A. Shimizu, W. H. Goh, S. Itai, M. Hashimoto, S. Miura, and H. Onoe, (2020), "Lab on a chip devices and applications at the micro-and nanoscale ecm-based microchannel for culturing in vitro vascular tissues with simultaneous perfusion and stretch †," *Lab on a Chip*, vol. 20, no. 11, pp. 1917–1927. https://doi.org/10.1039/d0lc00254b

[5] J. S. Miller, K. R. Stevens, M. T. Yang, B. M. Baker, D. H. T. Nguyen, D. M. Cohen, E. Toro, A. A. Chen, P. A. Galie, X. Yu, R. Chaturvedi, S. N. Bhatia, and C. S. Chen, 7 (2012), "Rapid casting of patterned vascular networks for perfusable engineered three-dimensional tissues," *Nature Materials 2012 11:9*, vol. 11, pp. 768–774. https://doi.org/10.1038/nmat3357

[6] A. M. Pollet, E. F. Homburg, R. Cardinaels, and J. M. den Toonder, 12 (2019), "3d sugar printing of networks mimicking the vasculature," *Micromachines 2020, Vol. 11, Page 43*, vol. 11, p. 43. https://doi.org/10.3390/mi11010043

[7] B. N. Moeun, S. A. Fernandez, S. Collin, G. Gauvin-Rossignol, T. Lescot, M. A. Fortin, J. Ruel, A. Bégin-Drolet, R. L. Leask, and C. A. Hoesli, 10 (2023), "Improving the 3d printability of sugar glass to engineer sacrificial vascular templates," *3D Printing and Additive Manufacturing*, vol. 10, pp. 869–885. https://doi.org/10.1089/3dp.2021.0147

[8] S. Priya, M. Choudhari, Y. Tomar, V. M. Desai, S. Innani, S. K. Dubey, and G. Singhvi, (2024), "Exploring polysaccharide-based bio-adhesive topical film as a potential platform for wound dressing application: A review," *Carbohydrate Polymers*, vol. 327, p. 121655. https://doi.org/10.1016/j.carbpol.2023.121655

[9] S. Jeong-Ah, K. Hyun-Joung, H. K. Kim, and Y.-H. Hwang, 7 (2012), "Caramelization processes in sugar glasses and sugar polycrystals," *New Physics: Sae Mulli*, vol. 62, pp. 761–767. https://doi.org/10.3938/NPSM.62.761

[10] C. Asgreen, M. M. Knopp, J. Skytte, and K. Löbmann, (2020), "Influence of the polymer glass transition temperature and molecular weight on drug amorphization kinetics using ball milling," *Pharmaceutics*, vol. 12, no. 6, p. 483. https://doi.org/10.3390/pharmaceutics12060483

[11] W. Yang, Y. Yu, R. O. Ritchie, and M. A. Meyers, )2020), "On the strength of hair across species," *Matter*, vol. 2, no. 1, pp. 136–149. https://doi.org/10.1016/j.matt.2019.09.019

# Appendices

# A Self-reflection on my thesis

Throughout my thesis, I regularly reflected on my progress, including key aspects such as time management, ownership, and communication. I believe these are essential elements to be mindful of during such a complex project. Honest self-reflection was crucial for me, as it allowed me to track my development and make necessary adjustments. Moreover, self-reflection is something I naturally engage in and enjoy doing. From the start, I set a personal goal: to create something I would be proud of, not only in terms of the final outcome but also the process leading to it.

I chose this research topic primarily because I was excited about the opportunity to collaborate with another discipline. Additionally, the topic of Organ-On-a-Chip, was entirely new to me. This provided me with the chance to take a deep dive into a new area and the high potential for learning a lot of new things.

Furthermore, this project involved both brainstorming and prototype fabrication. Two aspects I was looking forward to because they allowed me to engage in hands-on problem-solving. However, this also introduced some uncertainty, as I questioned whether I had the necessary skills to contribute meaningful new insights.

At the start of my literature review, it was challenging to understand the biological terminology used in other studies. However, as time passed, I became more comfortable with the subject matter. I also spend time in the lab at Erasmus MC, observing processes first hand and asking questions about why certain techniques were used and how they worked. This approach, combined with a structured method for gathering and synthesizing information, significantly deepened my understanding of the field. As my knowledge grew, so did my enthusiasm for the project. I started to imagine ambitious possibilities and it felt like the sky was the limit.

Once my literature review was complete, I moved on to testing my initial design. However, this phase took longer than I had anticipated. Through multiple iterations, I refined my first prototype into a functional design. Each iteration brought practical challenges that required problem-solving, and while this sometimes felt frustrating, I enjoyed the process. My focus was always on the next step and how to get there, constantly seeking improvements.

One of the things that surprised me most about myself was how positively I handled practical challenges. Rather than feeling discouraged, my first instinct was always to think of possible solutions. The main challenge for me was accepting that good solutions often require time. Therefore, I frequently felt as if I was racing against the clock, eager to move on to my final design while struggling with the time-consuming steps required to get there.

During the development process, I encountered challenges that I couldn't solve on my own. Initially, I hesitated to ask for help, because I wanted to solve problems independently or because I was not sure whom to approach. However, as I started reaching out to lab support and other

experts, I quickly realized how much time I could save by asking for help sooner. I also learned that people are often happy to assist when they see curiosity and engagement.

Toward the end of my thesis, my available working time became more limited due to my recovery. This forced me to set clear priorities and make difficult decisions about what to leave out. I now recognize this as one of the most valuable lessons of my thesis: that I can still be proud of my work, even the things I had to let go of.

A key takeaway from my thesis journey is the importance of asking for help. At the same time, I realized that while I approached literature critically, constantly questioning and analysing sources, I did not always apply the same level of critical thinking when receiving direct answers from experts. I have come to understand that carefully evaluating information in discussions is essential, not to challenge the expertise of others, but to ensure that I extract the insights most relevant to my research. This is something I am now more aware of and will continue to develop.

Another important lesson I learned was the value of keeping people informed about my work, even when I wasn't actively seeking help. Simply ensuring that others knew what I was working on created opportunities for valuable discussions and feedback.

Throughout my thesis, I frequently received feedback that my plans were ambitious but that time was limited. While I acknowledged the validity of these warnings, I found it difficult to fully accept them and I still do. Learning to set realistic expectations and balance ambition with feasibility remains a challenge for me, and it is something I aim to continue working on. My supervisor's feedback helped me realize the impact of my self-criticism: while my constant self-reflection pushed my work to a higher level, it also made me overly focused on what could still be improved. As a result, I sometimes found it difficult to appreciate my own progress, which affected my confidence.

The most valuable lesson I learned during my thesis is that, not knowing everything does not mean that I cannot contribute to a field. I have also realized the importance of balancing my critical thinking. While self-reflection and a high standard for my work have been beneficial, I need to place my critical perspective in context and also acknowledge my achievements.

Moving forward, I want to improve my ability to step back and appreciate my contributions. The results I achieved were primarily due to three key strengths: my problem-solving mindset, perseverance in overcoming challenges, and enthusiasm for learning new concepts. However, in a future research project, I would like to further improve in three areas: setting more realistic expectations, carefully evaluating information in discussions, and learning to recognize my progress rather than focusing solely on areas for improvement.

# B Detailed manufacturing device process

## B.1 Straightening wires

The wire is placed through the needles and serves as a mould within the hydrogel. The diameter of the wire determines the diameter of the hollow channels which will be formed. When a wire is pulled out of the hydrogel its deflection will also impact the shape and diameter of the channel. To mitigate this effect the deflection of the wires should be minimized.

The aim is to achieve a maximum deflection as large as its own diameter. For the wire with a diameter of 0.125 mm, two different methods of cold work hardening were done in sequence. With cold work hardening the material is strained beyond its yield point.

The 0.125 mm diameter wire is first manipulated by a wire straightener consisting of three nylon rolling cylinders. This nylon clamp is shown in Figures B.1 and B.2. Some parts of the cylinders are wider, creating bumps. As the wire is pulled through the straightener, these protrusions bend the wire past its elastic point, causing plastic deformation of the wire. This occurs in several directions, resulting in the straightening of the wire.

Figure B.1: A wire straightener is shown on the left and a clamper on the right. The wire straightener consists of three nylon rolling cylinders connected to each other. Some parts of the cylinders are wider, creating bumps. As the wire is pulled through the straightener, these protrusions bend the wire past its elastic point, causing plastic deformation of the wire. This occurs in several directions, resulting in the straightening of the wire.

Figure B.2: A wire straightener is shown on the left and a clamper on the right. The wire straightener consists of three nylon rolling cylinders connected with each other. The rolling cylinders are clamped in the position as shown in this Figure. The wire is pulled through the centre of the three cylinders.

After this first manipulation, the wire had less curvature and no bumps, but still had more deflection than desired. Another method of cold work hardening is used. The wire is twisted by clamping the wire to a bench and using the drill to twist the wire alternately in both directions. The setup of this manipulation is shown in Figure B.3. When twisting the wire, the wire is under tension, so the wire is hardened as it is pulled straight.

Figure B.3: The wire is twisted by clamping the wire to a bench and using the drill to twist the wire alternately in both directions. When twisting the wire, the wire is under tension, so the wire is hardened as it is pulled straight.

Twisting the wire also causes plastic deformation by creating defects in the crystal lattice. As the defects, or dislocation density, increase, they create a barrier to further dislocation movement, increasing the hardness of the material.

Care must be taken with both methods as the hardening of the material makes the wire even more vulnerable to breakage

The same methods were tested using the 0.05 mm wire. The wire straightener deformed the 0.05 mm wire as it was pulled through, but the deformation was not equal on all sides, resulting in a more crulled wire than before. The twisting method requires sufficient tension in the wire to straighten it. However, the required tension could not be achieved without breaking the wire.

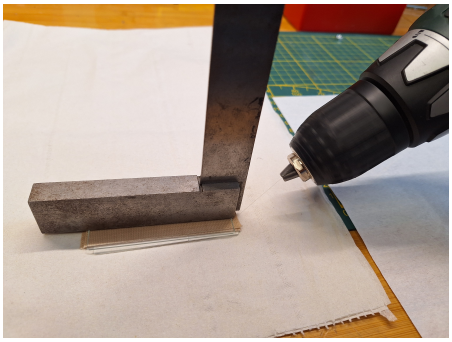

Figure B.4: Two flat pieces of glass with a piece of Teflon tape on each, were placed on top of each other with the wire between them. A 400 gram weight was placed on top. The wire was pulled out at a 45° angle using a dill.

So, the two methods used for the thicker wire could not be used for the thinner wire.

Based on the theory that the wire must be bent beyond its yield point in all directions and that the wire is easily broken, a new method was used, the setup of this method is shown in Figure B.4. Two flat pieces of glass with a piece of Teflon tape on each, were placed on top of each other with the wire between them. A 400 gram weight was placed on top. The wire was pulled out at a 45° angle using a dill.

## B.2 Fabrication of the containers

Several PDMS containers can be created using the mould shown in Figure B.6. This design is chosen to facilitate the removal of PDMS from the mould without causing damage to either the PDMS or the mould. When the PDMS is taken out of the mould, it can be cut in 8 peaces, as shown in Figure B.5, the cut lines are visible on the PDMS due to small high differences in the mould.

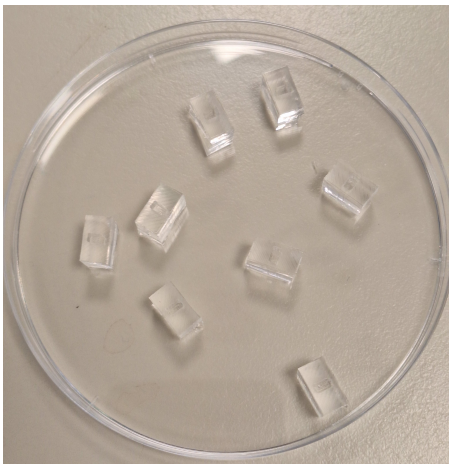

Figure B.5: PDMS box

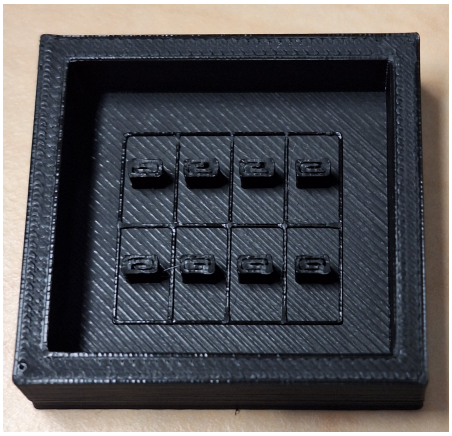

Figure B.6: 3D-printed PDMS mould to make 8 containers.

## B.3 Rails for sliding and fixing the needles

Figure B.7 shows the 3D-printed rails. Within the rails, there is a rectangle compartment designed to hold the PDMS container. This compartment is open at the bottom to allow visibility from beneath. Figure B.8 shows the initial step of placing the mould, where the wire is almost fully threaded through one needle. The next step involves inserting both injection needles through the PDMS container and guiding the wire through them. In Figure B.7, this process is completed, and the needles are secured in place on the rails with the bolts. This state of the device allows transportation to the Erasmus MC.

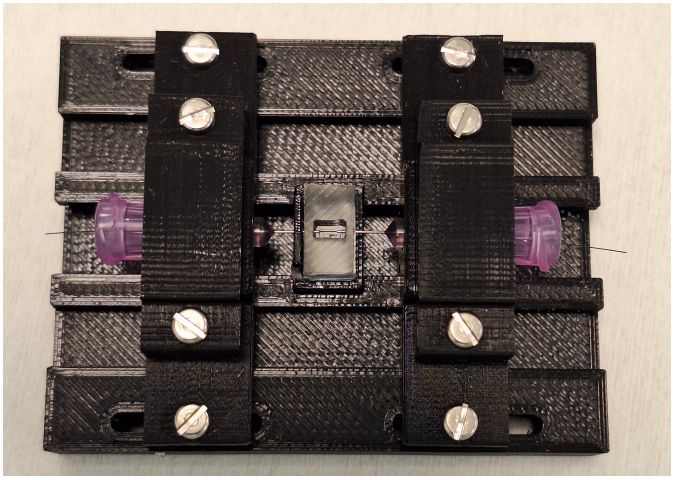

Figure B.7: The wire is threaded through both injection needles, which are then pulled apart, leaving the wire in place and spanning as mould within the container.

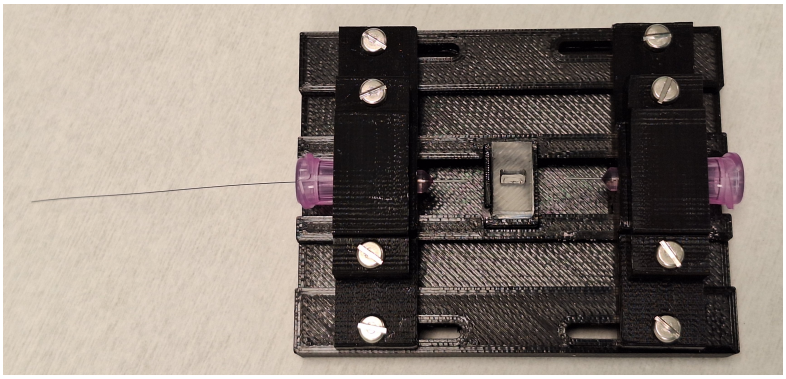

Figure B.8: Wire through one of the injection needles

# C Results

## C.1 Elastic modulus ECM Hydrogel

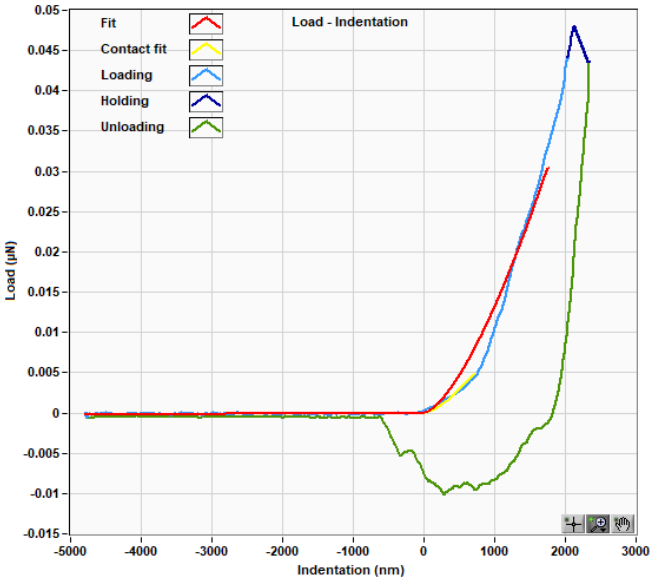


Figure C.1: Young's modulus 1.97kPa

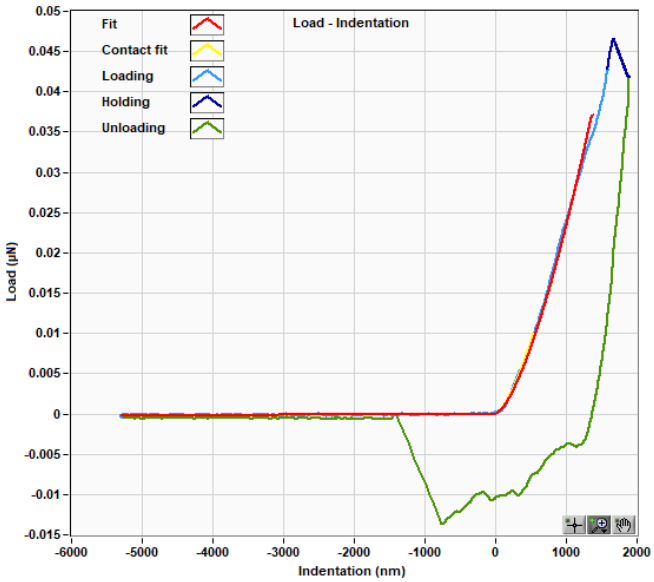


Figure C.2: Young's modulus 3.50kPa

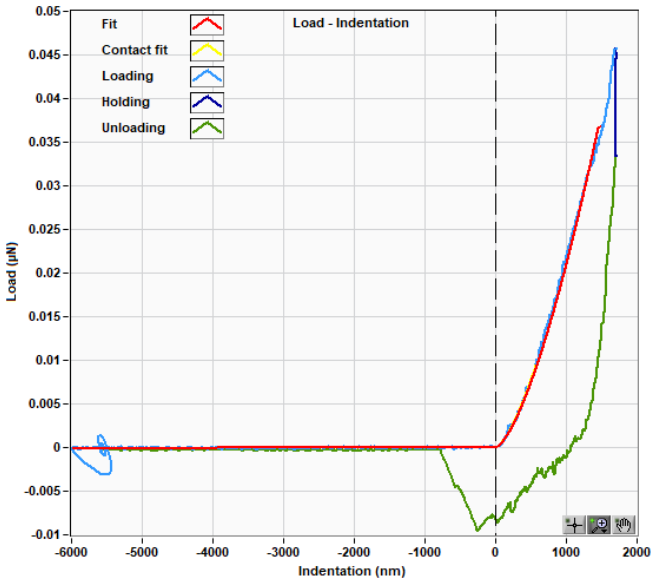


Figure C.3: Young's modulus 3.13kPa

## C.2 Diameter

**Diameter created channels**

Two different wires are used as mould to create hollow channels. The width of the channels is compared to the used wires. Table C.1 shows the mean, median and smallest width of the channels created using the wire with a diameter of 125 µm. In table C.2, this information of the channels created using the wire with a diameter of 50 µm is shown.

| Vessel | Hydrogel | Mean width | Median width | Smallest width |
|---|---|---|---|---|
| 1 | 2 | 199 µm | 193 µm | 179 µm |
| 4 | 2 | 399 µm | 393 µm | 315 µm |
| 6 | 1 | 237 µm | 239 µm | 173 µm |
| 7 | 1 | 268 µm | 273 µm | 187 µm |
| 8 | 1 | 379 µm | 390 µm | 230 µm |
| average | - | 296 µm | 298 µm | 217 µm |

Table C.1: Width capillaries, channels made with wires of 125 µm. All measurements have an associated uncertainty of ±13 µm.

| Vessel | Hydrogel | Mean width | Median width | Smallest width |
|---|---|---|---|---|
| 2 | 2 | 184 µm | 153 µm | 89 µm |
| 3 | 2 | 135 µm | 137 µm | 83 µm |
| 5 | 2 | 164 µm | 164 µm | 80 µm |
| 9 | 1 | 152 µm | 139 µm | 103 µm |
| 10 | 1 | 171 µm | 173 µm | 135 µm |
| average | - | 161 µm | 153 µm | 98 µm |

Table C.2: Width capillaries, channels made with wires of 50 µm. All measurements have an associated uncertainty of ±13 µm.

## C.3 Allignment needles

In Table C.3 the results about the accuracy and alignment of the needle placement are presented.

| **Device** | **Anglur difference** | **positional offset** | **Distance in between** |
|---|---|---|---|
| 1 | 0.81 ° | 11 µm | 2474 µm |
| 2 | 0.74 ° | 5 µm | 2424 µm |
| 3 | 0.21 ° | 29 µm | 1666 µm* |
| 4 | 2.73 ° | 202 µm | 2187 µm |
| 5 | 0.77 ° | 32 µm | 2692 µm |
| 6 | 1.26 ° | 11 µm | 2176 µm |
| 7 | 1.16 ° | 114 µm | 2380 µm |
| 8 | 0.35 ° | 40 µm | 2204 µm |
| 9 | 0.68 ° | 6 µm | 2572 µm |
| 10 | 1.85 ° | 38 µm | 2041 µm |

Note: *This result is incorrect due to an air bubble obstructing the view of half the vessel.

Table C.3: Results about the accuracy and alignment of the needle placement

## C.4 Lifespan

| Test | Diameter | Wire | Composition | Perfusable for | Comment |
|---|---|---|---|---|---|
| 2 | 50 | tungsten | 20 | 32 days | |
| 1 | 125 | tungsten | 20 | 16 days | Fixated |
| 5 | 50 | tungsten | 20 | 10 days | Fixated |
| 4 | 125 | tungsten | 20 | 10 days | Fixated |
| 6 | 125 | tungsten | 10 | 6 days | |
| 9 | 50 | molybdenum | 10 | 2 days | |
| 10 | 50 | molybdenum | 10 | 2 days | |
| 7 | 125 | tungsten | 10 | 2 days | |
| 3 | 50 | molybdenum | 20 | 0-1 day | |
| 8 | 125 | tungsten | 10 | 0-1 day | |

Table C.4: Perfusable days of cultured capillaries

## C.5 Flow measurements

Table C.5: Velocity measurements across films.

| Film | Time (s) | Distance (m) | Velocity (m/s) | Velocity (mm/s) | Velocity (µm/s) |
|---|---|---|---|---|---|
| 1 | 1.03 | 0.00087 | 0.00084466 | 0.844660 | 844.660194 |
| | 0.58 | 0.00087 | 0.0015 | 1.500000 | 1500.000000 |
| | 0.83 | 0.00087 | 0.001048193 | 1.048193 | 1048.192771 |
| | 1.36 | 0.00087 | 0.000639706 | 0.639706 | 639.705882 |
| | 1.42 | 0.00087 | 0.000612676 | 0.612676 | 612.676056 |
| | 0.65 | 0.00087 | 0.001338462 | 1.338462 | 1338.461538 |
| 2 | 0.33 | 0.00087 | 0.002636364 | 2.636364 | 2636.363636 |
| | 1.05 | 0.00087 | 0.000828571 | 0.828571 | 828.571429 |
| | 0.51 | 0.00087 | 0.001705882 | 1.705882 | 1705.882353 |
| | 0.73 | 0.00087 | 0.001191781 | 1.191781 | 1191.780822 |
| | 1.02 | 0.00087 | 0.000852941 | 0.852941 | 852.941176 |
| | 0.48 | 0.00087 | 0.0018125 | 1.812500 | 1812.500000 |
| | 0.45 | 0.00087 | 0.001933333 | 1.933333 | 1933.333333 |
| | 0.74 | 0.00087 | 0.001175676 | 1.175676 | 1175.675676 |
| | 1.08 | 0.00087 | 0.000805556 | 0.805556 | 805.555556 |
| | 1.01 | 0.00087 | 0.000861386 | 0.861386 | 861.386139 |
| | 0.71 | 0.00087 | 0.001225352 | 1.225352 | 1225.352113 |
| 3 | 1.30 | 0.00087 | 0.000669231 | 0.669231 | 669.230769 |
| | 0.65 | 0.00087 | 0.001338462 | 1.338462 | 1338.461538 |
| | 0.68 | 0.00087 | 0.001279412 | 1.279412 | 1279.411765 |
| | | | **Average** | 1215.007 137 µm/s | |
| | | | **Max** | 2636.363 636 µm/s | |

## C.6 Height difference between needles

The ten figures are shown which are used to determine the positional offset of the needles for each device.

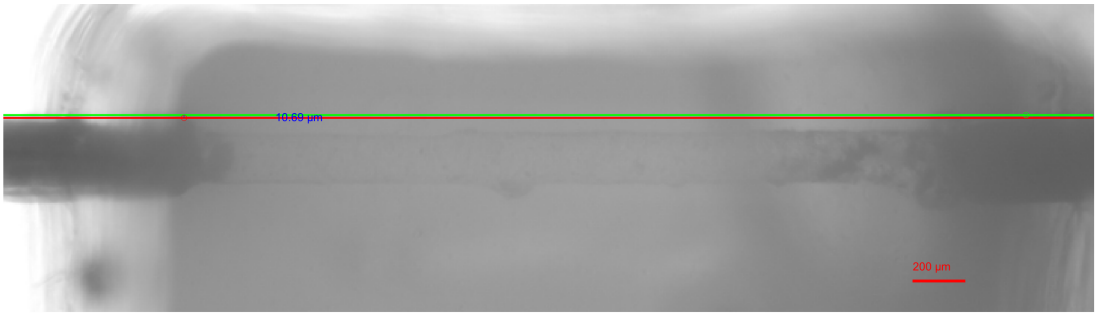


Figure C.4: Height difference between needles of vessel 1

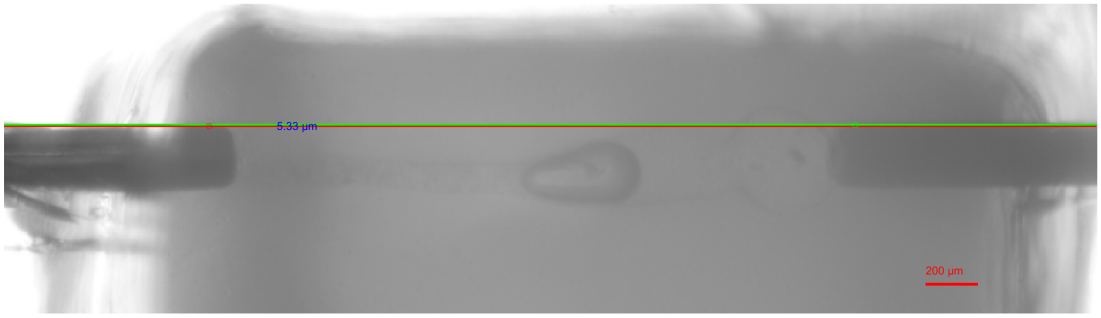


Figure C.5: Height difference between needles of vessel 2

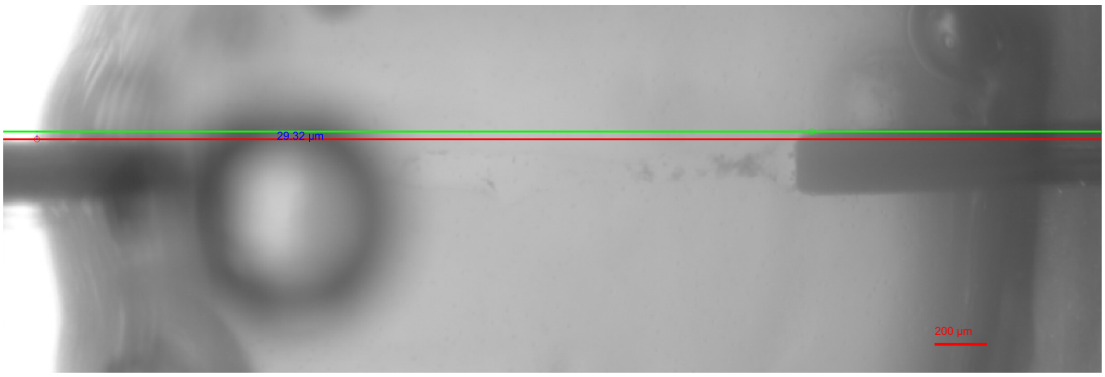


Figure C.6: Height difference between needles of vessel 3

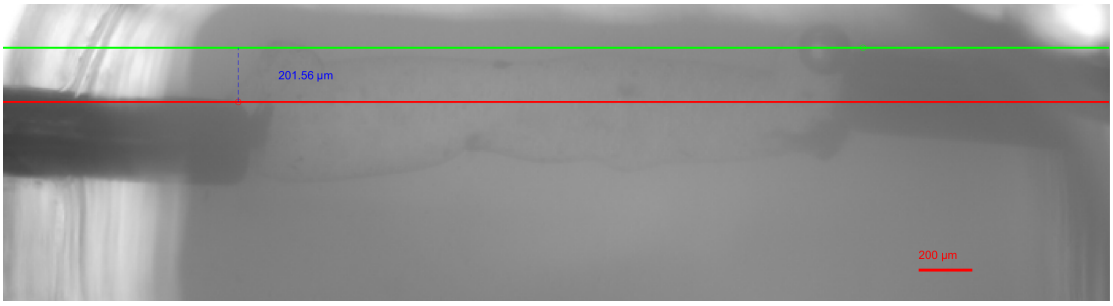


Figure C.7: Height difference between needles of vessel 4

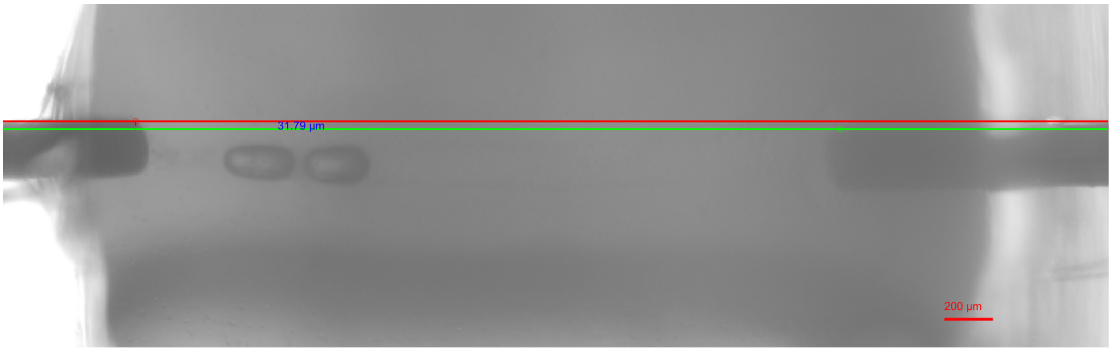


Figure C.8: Height difference between needles of vessel 5

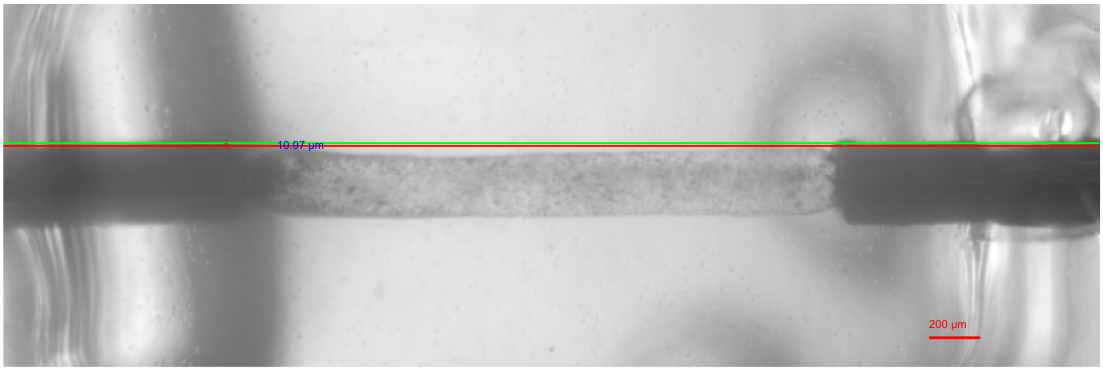


Figure C.9: Height difference between needles of vessel 6

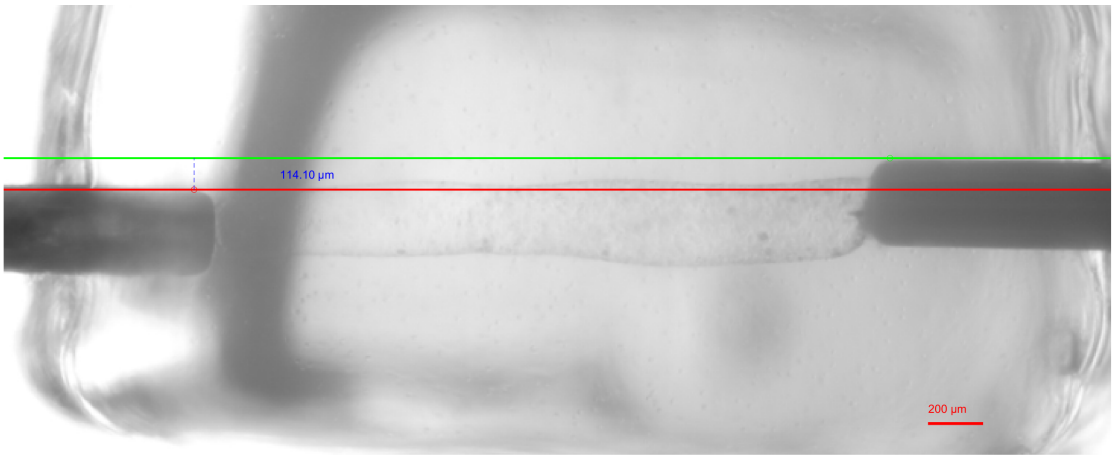


Figure C.10: Height difference between needles of vessel 7

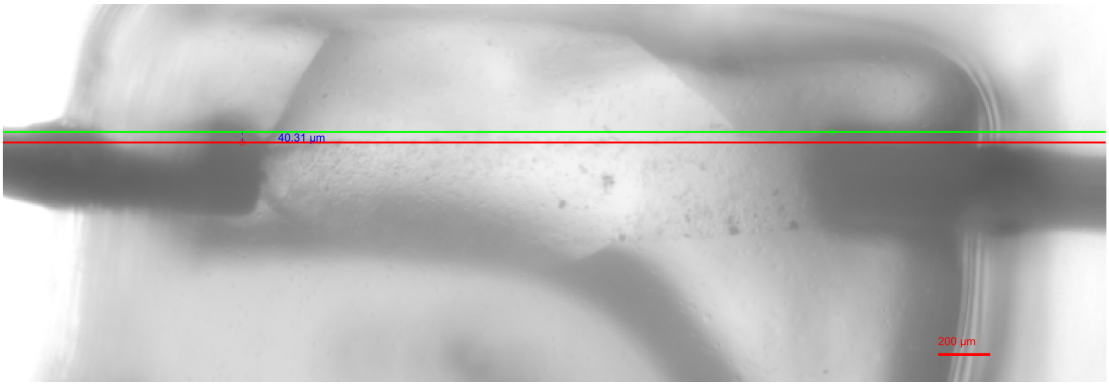


Figure C.11: Height difference between needles of vessel 8

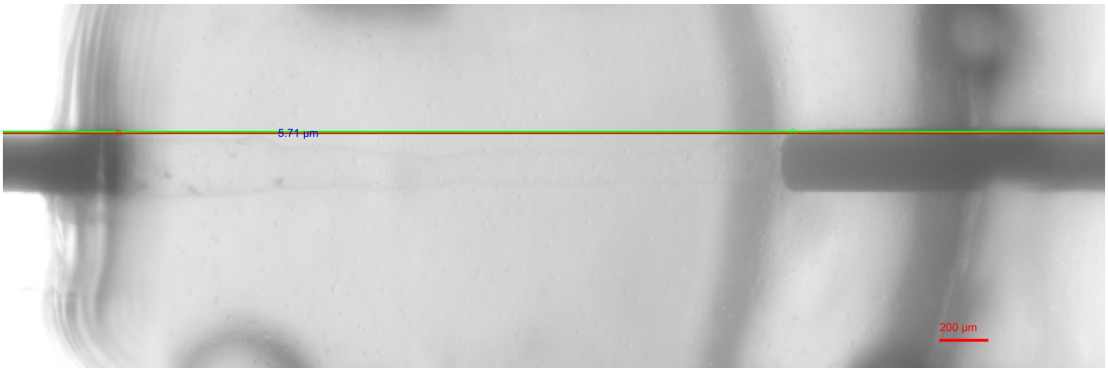


Figure C.12: Height difference between needles of vessel 9

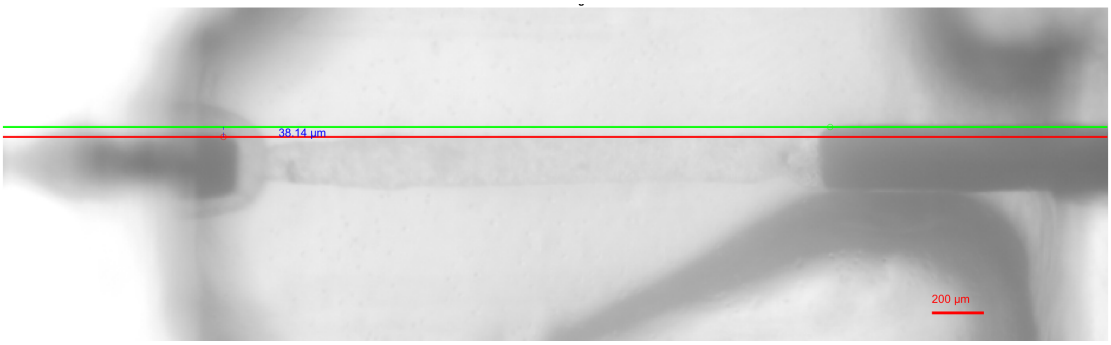


Figure C.13: Height difference between needles of vessel 10

## C.7 Angles between needles

The ten figures are shown which are used to determine the angular differences of the needles for each device.

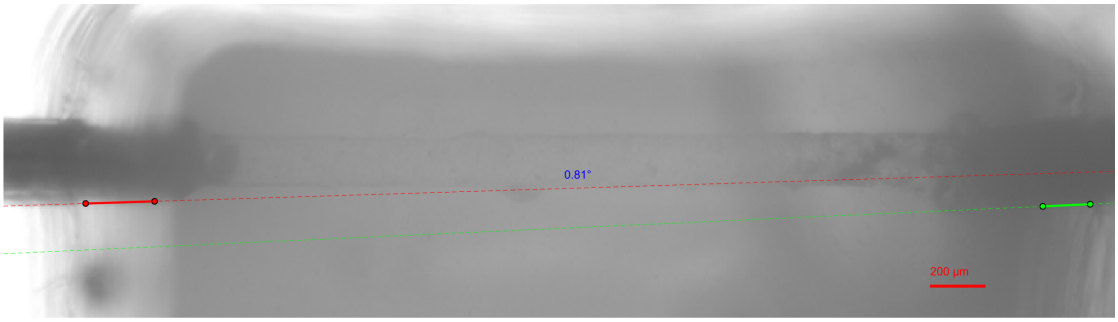


Figure C.14: Angle between needles of test 1

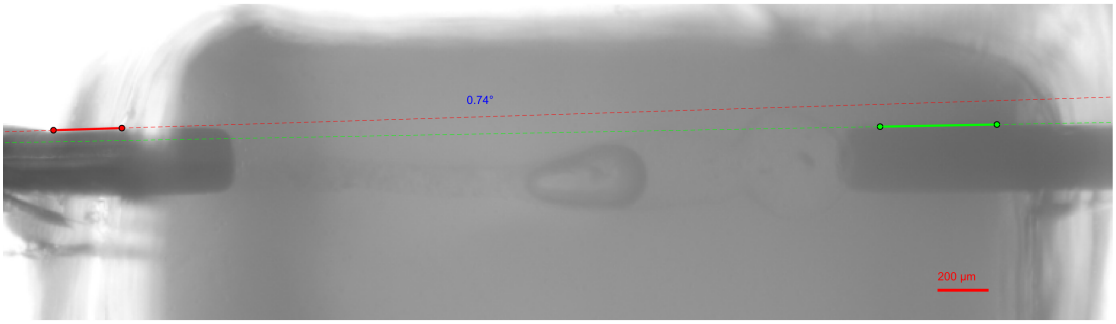


Figure C.15: Angle between needles of test 2

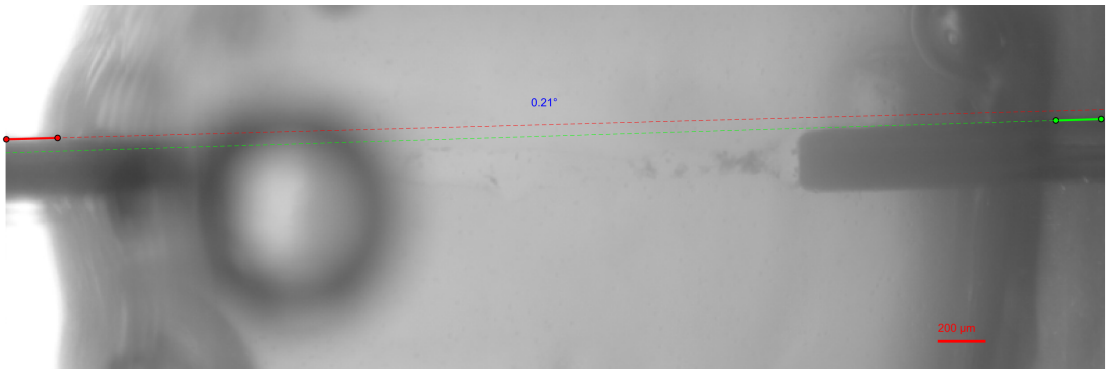


Figure C.16: Angle between needles of test 3

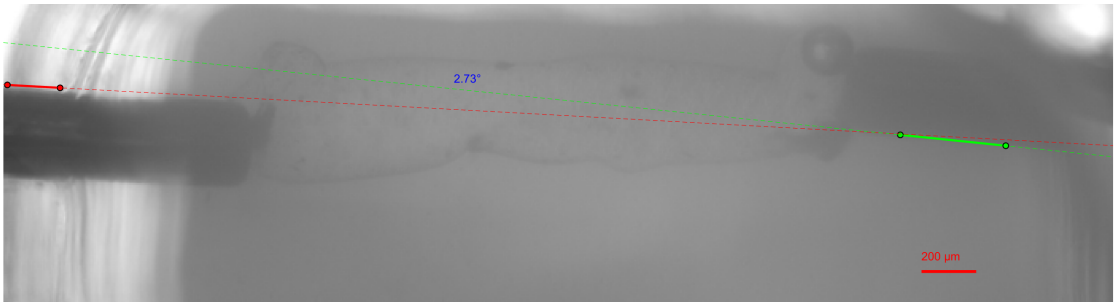


Figure C.17: Angle between needles of test 4

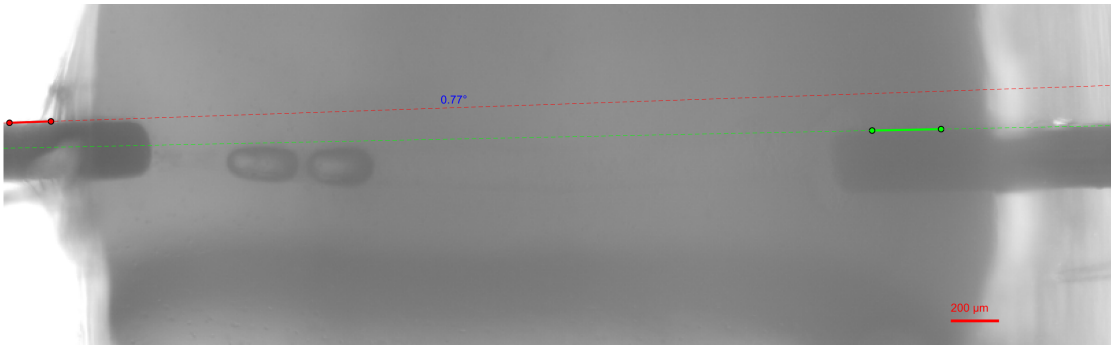


Figure C.18: Angle between needles of test 5

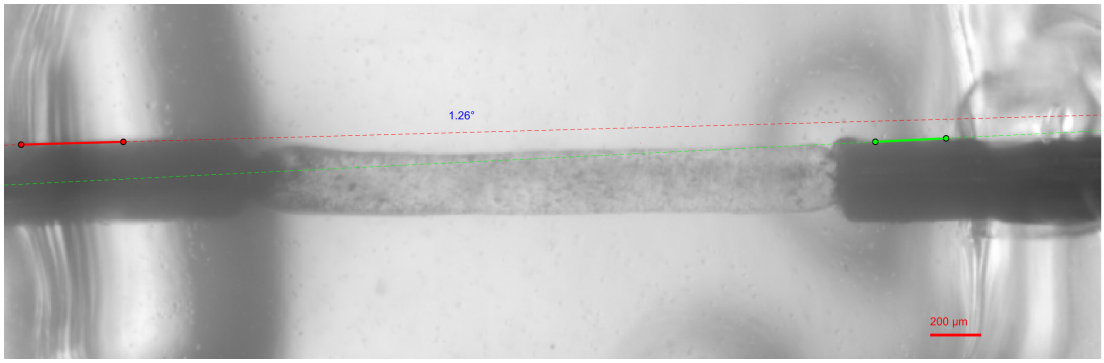


Figure C.19: Angle between needles of test 6

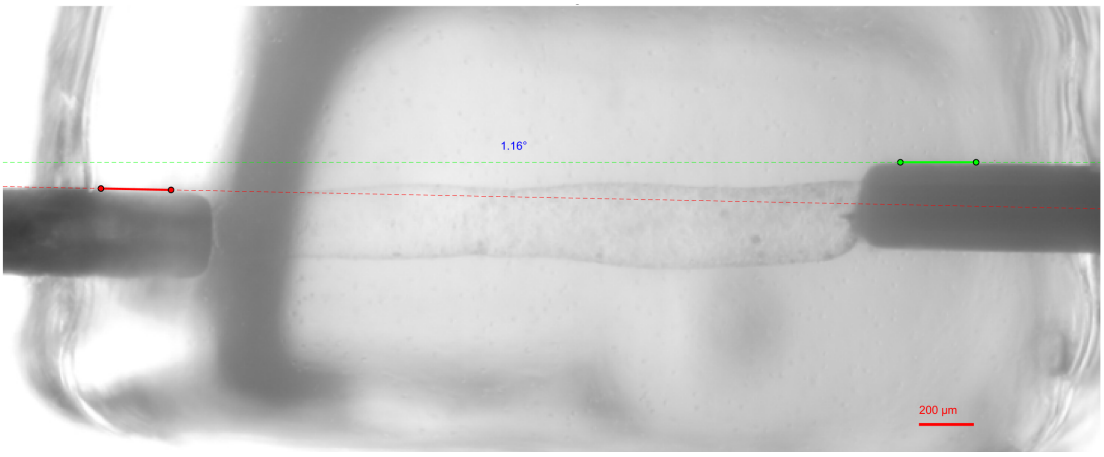


Figure C.20: Angle between needles of test 7

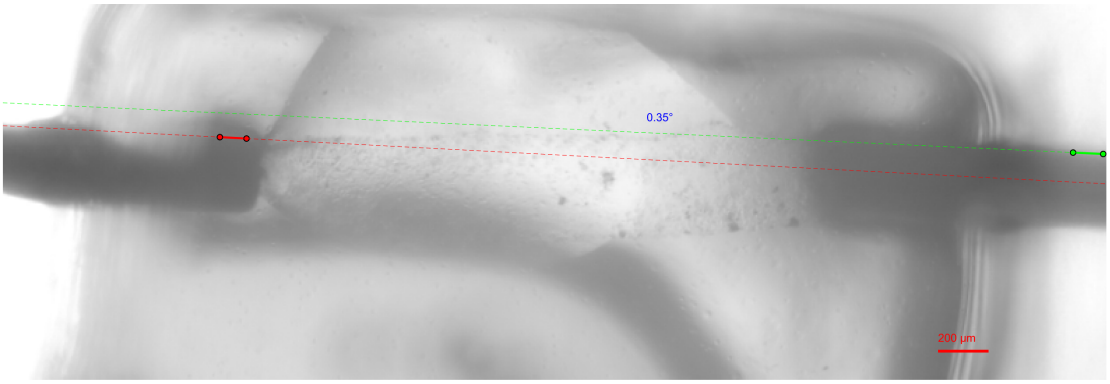


Figure C.21: Angle between needles of test 8

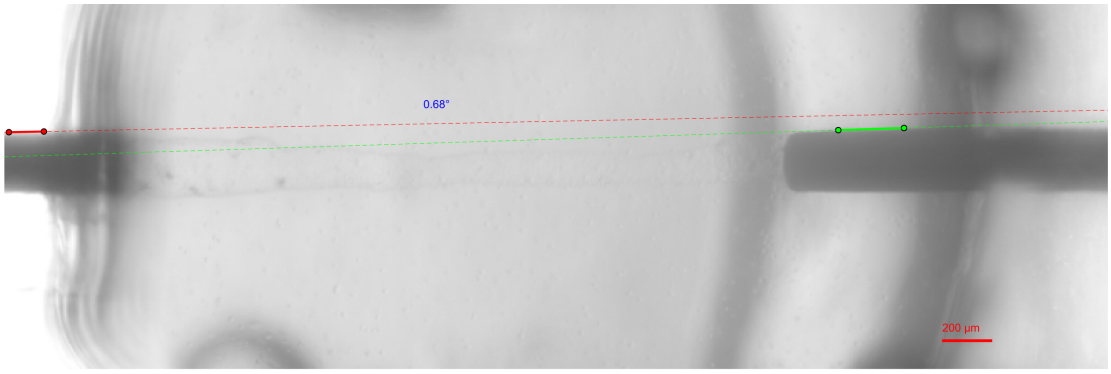


Figure C.22: Angle between needles of test 9

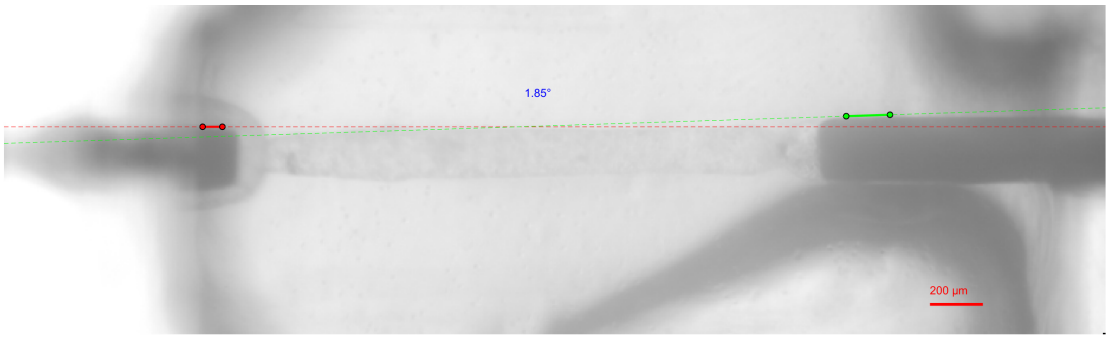


Figure C.23: Angle between needles of test 10

# D Scripts

## D.1 G-code: Square

```
; GENERAL :
N14                ; set line numbers for error logging - Slic3r version
M772 S1            ; reset metrics and arm automatic reporting
M627 X0 Y0 Z0 J-500 K5                 ; setup abort action
M107               ; fans/UV           ; off
M106 C255          ; fans/UV           ; set to 0-255 range
G53                ; clear offsets
G21                ; units             : mm
G91                ; coordinatess      : relative
G0 Z30             ; drop bed
G90                ; coordinates       : absolute
M229 E1 D1         ; enable E-values (volumetric) ;E1: Specifies the first extruder.
; TEMP CONTROL :
M104 T11 S90      ; head temp    : set, no wait
G28 X0 Y0          ; home, goto   : X and Y
M109 T11 S90      ; head temp    : set and wait
;G4 S20 ;wait for 120seconds
T0                 ; use FIRST tool position from the left
; \\\\\\\\\\\\\\\   END HYREL HEADER for a 16A with a Heated Head in T0/T11 - 2021.02.24   //////
G21 ; set units to millimeters
G90 ; use absolute coordinates
M82 ; use absolute distances for extrusion !!!!!!!!!!
G92 E0 ; reset extrusion distance !!!!!!!!!!
;announce new layer <0>
;---
;M756 S0.25
;M790 ;execute any new layer actions
;---
G1 X0.00 Y0.00 F180 ;start point
G1 Z0.20 F180.000 E-2; move to next layer
G1 X0.000 Y0.000  E3 F560.000; move to first point of the square
G1 X0.000 Y30.000 E6 F560.000 ; move to second point (along X)
G1 X20.000 Y30.000 E9 F180; move to third point (along Y)
```

```
G1 X20.000 Y0.000 E12 ; move to fourth point (along -X)
G1 X0.000 Y0.000 E15 ; move to first point (along -Y)
G1 E-6 F180 ; Retract the filament slightly
G92 E0 ; Zero the extruder
G1 Z30 F1200 ; Raise the print head
M104 S0 T11; Turn off extruder heater
;M140 S0; bed uit
G28 X0 Y0; home axis
M84 ; Disable motors
; End of G-code
```

## D.2 G-code: line

```
; GENERAL :
N14                ; set line numbers for error logging - Slic3r version
M772 S1            ; reset metrics and arm automatic reporting
M627 X0 Y0 Z0 J-500 K5                 ; setup abort action
M107               ; fans/UV           ; off
M106 C255          ; fans/UV           ; set to 0-255 range
G53                ; clear offsets
G21                ; units             : mm
G91                ; coordinatess      : relative
G0 Z30             ; drop bed
G90                ; coordinates       : absolute
M229 E1 D1         ; enable E-values (volumetric) ;E1: Specifies the first extruder.
; TEMP CONTROL :
M104 T11 S90      ; head temp    : set, no wait
G28 X0 Y0          ; home, goto   : X and Y
M109 T11 S90      ; head temp    : set and wait
;G4 S20 ;wait for 120seconds
T0                 ; use FIRST tool position from the left
; \\\\\\\\\\\\\\\   END HYREL HEADER for a 16A with a Heated Head in T0/T11 - 2021.02.24   //////
G21 ; set units to millimeters
G90 ; use absolute coordinates
M82 ; use absolute distances for extrusion !!!!!!!!!!
G92 E0 ; reset extrusion distance !!!!!!!!!!
;announce new layer <0>
```

## D.3 Matlab code: Distance Y-axis capillaries

```
clear; close all; clc;

Test = '10';

% Step 1: Load the Image
[filename, pathname] = uigetfile({'*.png;*.jpg;*.jpeg;*.tif;*.bmp', 'Image Files'}, 'Select an Image');
if isequal(filename, 0)
    disp('No file selected. Exiting...');
    return;
end

% Read the image
img = imread(fullfile(pathname, filename));

% Convert to grayscale
if size(img, 3) == 3
    grayImg = rgb2gray(img);
else
    grayImg = img;
end

% Choose which of those three images has best visible lines:
% Option 1: Display the grayscale image
figure;
imshow(grayImg);
title('Loaded Image');

% Option 2: Enhance the contrast
enhancedImg = imcomplement(mat2gray(grayImg));
figure;
imshow(enhancedImg);
title('Enhanced Image');

 % Option 3: Edge Detection using Canny (Optional)
% edges = edge(enhancedImg, 'Canny');
% figure;
 %imshow(edges);
 %title('Edge Detection');

% Set the scale (pixels per micrometer)
disp('Click two points on the image to set the scale (known distance in micrometers)');
[x, y] = ginput(2);
if length(x) < 2 || length(y) < 2
    error('You must select two points to set the scale.');
end
```

```
46
47 knownDistance = input('Enter the known distance between these two
       points in micrometers: ');
48 if isempty(knownDistance) || knownDistance <= 0
49     error('Invalid distance. Please enter a positive number.');
50 end
51
52 pixelDistance = sqrt((x(2) - x(1))^2 + (y(2) - y(1))^2);
53 pixelsPerMicrometer = pixelDistance / knownDistance;
54 fprintf('Scale set: 1 micrometer = %.2f pixels\n',
       pixelsPerMicrometer);
55
56 % Add scale bar to the image
57 scaleBarLengthMicrometers = 200.0; % Length of scale bar in
       micrometers
58 scaleBarLengthPixels = scaleBarLengthMicrometers *
       pixelsPerMicrometer;
59
60 % Adjust the position of the scale bar
61 scaleBarX = size(img, 2) - 120; % Adjusted X position
62 scaleBarY = size(img, 1) - 20; % Y position
63
64 % Draw the scale bar on the image
65 hold on;
66 line([scaleBarX, scaleBarX + scaleBarLengthPixels], [scaleBarY,
       scaleBarY], 'Color', 'r', 'LineWidth', 3);
67 text(scaleBarX, scaleBarY - 10, sprintf('%d m',
       scaleBarLengthMicrometers), 'Color', 'r', 'FontSize', 12);
68
69 % Save the image with drawn lines and scale bar
70 saveas(gcf, 'Image_without_lines.png');
71 disp('Image saved as "Image_without_lines.png"');
72
73 % Draw the first line using right mouse clicks, press Enter when done
74 disp('Draw the first line using right mouse clicks, press Enter when
       done...');
75 h1 = drawpolyline('Color', 'r');
76 line1 = h1.Position;
77
78 % Draw the second line using right mouse clicks, press Enter when
       done
79 disp('Draw the second line using right mouse clicks, press Enter when
       done...');
80 h2 = drawpolyline('Color', 'g');
81 line2 = h2.Position;
82
83 % Determine the common x-range for both lines
84 commonXRange = max(min(line1(:,1)), min(line2(:,1))):min(max(line1
       (:,1)), max(line2(:,1)));
```

```
85
86 % Interpolate both lines to have as many points as the common x-range
87 line1InterpY = interp1(line1(:,1), line1(:,2), commonXRange);
88 line2InterpY = interp1(line2(:,1), line2(:,2), commonXRange);
89
90 % Calculate the distance between the two lines on the y-axis for each
       x value
91 distancesY = abs(line1InterpY - line2InterpY) / pixelsPerMicrometer;
92
93 % Remove NaN values from distancesY
94 distancesY = distancesY(~isnan(distancesY));
95
96 % Determine the total length of the common X-range in micrometers
97 xAxisLengthMicrometers = (max(commonXRange) - min(commonXRange)) /
       pixelsPerMicrometer;
98
99
100 % Calculate mean, standard deviation, min, max, median, and IQR
       distances
101 meanDistanceY = mean(distancesY);
102 stdDistanceY = std(distancesY);
103 minDistanceY = min(distancesY);
104 maxDistanceY = max(distancesY);
105 medianDistanceY = median(distancesY);
106 iqrDistanceY = iqr(distancesY);
107
108 % Display the results
109 fprintf('Total X-axis length: %.2f micrometers\n',
       xAxisLengthMicrometers);
110 fprintf('Mean Distance (Y): %.2f micrometers\n', meanDistanceY);
111 fprintf('Standard Deviation (Y): %.2f micrometers\n', stdDistanceY);
112 fprintf('Minimum Distance (Y): %.2f micrometers\n', minDistanceY);
113 fprintf('Maximum Distance (Y): %.2f micrometers\n', maxDistanceY);
114 fprintf('Median Distance (Y): %.2f micrometers\n', medianDistanceY);
115 fprintf('Interquartile Range (IQR) (Y): %.2f micrometers\n',
       iqrDistanceY);
116
117 % Save the image with drawn lines and scale bar
118 saveas(gcf, 'Image_with_lines.png');
119 disp('Image saved as "Image_with_lines.png"');
120
121 % Save the data to an Excel file
122 data = table({'Mean Distance (micrometers)';
123               'Standard Deviation (micrometers)';
124               'Minimum Distance (micrometers)';
125               'Maximum Distance (micrometers)';
126               'Median Distance (micrometers)';
127               'Interquartile Range (IQR) (micrometers)';
128               'Pixels per Micrometer';
```

```
129                 'X-axis Length (micrometers)'}, ...
130                [meanDistanceY;
131                 stdDistanceY;
132                 minDistanceY;
133                 maxDistanceY;
134                 medianDistanceY;
135                 iqrDistanceY;
136                 pixelsPerMicrometer;
137                 xAxisLengthMicrometers], ...
138                'VariableNames', {'Metric', 'Value'});
139 line1Table = array2table([commonXRange' line1InterpY'], '
    VariableNames', {'X', 'Y'});
140 line2Table = array2table([commonXRange' line2InterpY'], '
    VariableNames', {'X', 'Y'});
141 distancesTable = array2table(distancesY', 'VariableNames', {'
    Distance_Y'});
142
143 writetable(data, ['line_data_' Test '.xlsx'], 'Sheet', 'Statistics');
144 writetable(line1Table, ['line_data_' Test '.xlsx'], 'Sheet', 'Line1')
    ;
145 writetable(line2Table, ['line_data_' Test '.xlsx'], 'Sheet', 'Line2')
    ;
146 writetable(distancesTable, ['line_data_' Test '.xlsx'], 'Sheet', '
    Distances_Y');
147 disp(['Data saved to "line_data_' Test '.xlsx"']);
148
149 % Create a boxplot of the distances on Y-axis with outliers
150 figure;
151 boxplot(distancesY);
152 xlabel(['Capillary ', Test]);
153 ylabel('Distance (micrometers)');
154 title(['Boxplot of Distances between Lines, Capillary ', Test]);
155 grid on;
156 saveas(gcf, 'boxplot_with_outliers.png');
157 disp('Boxplot with outliers saved as "boxplot_with_outliers.png"');
158
159 % Create a boxplot of the distances on Y-axis without outliers
160 figure;
161 boxplot(distancesY, 'whisker', 1.5, 'Symbol', '');
162 xlabel(['Capillary ', Test]);
163 ylabel('Distance (micrometers)');
164 title(['Boxplot of Distances between Lines, Capillary ', Test]);
165 grid on;
166 saveas(gcf, 'boxplot_without_outliers.png');
167 disp('Boxplot without outliers saved as "boxplot_without_outliers.png
    "');
```

## D.4 Matlab code: Angular difference injection needles

```
clear; close all; clc;

% Step 1: Load the Image
[filename, pathname] = uigetfile({'*.png;*.jpg;*.jpeg;*.tif;*.bmp', 'Image Files'}, 'Select an Image');
if isequal(filename, 0)
    disp('No file selected. Exiting...');
    return;
end

% Read the image
img = imread(fullfile(pathname, filename));

% Convert to grayscale if needed
if size(img, 3) == 3
    grayImg = rgb2gray(img);
else
    grayImg = img;
end

% Display the grayscale image
figure;
imshow(grayImg);
title('Loaded Image');

% Set the scale (pixels per micrometer)
disp('Click two points on the image to set the scale (known distance in micrometers)');
[x, y] = ginput(2);
if length(x) < 2 || length(y) < 2
    error('You must select two points to set the scale.');
end

knownDistance = input('Enter the known distance between these two points in micrometers: ');
if isempty(knownDistance) || knownDistance <= 0
    error('Invalid distance. Please enter a positive number.');
end

pixelDistance = sqrt((x(2) - x(1))^2 + (y(2) - y(1))^2);
pixelsPerMicrometer = pixelDistance / knownDistance;
fprintf('Scale set: 1 micrometer = %.2f pixels\n', pixelsPerMicrometer);

% Add scale bar to the image
scaleBarLengthMicrometers = 200.0; % Length of scale bar in micrometers
```

```
43 scaleBarLengthPixels = scaleBarLengthMicrometers *
       pixelsPerMicrometer;
44
45 % Adjust the position of the scale bar
46 scaleBarX = size(img, 2) - 120; % Adjusted X position
47 scaleBarY = size(img, 1) - 20; % Y position
48
49 % Draw the scale bar on the image
50 hold on;
51 line([scaleBarX, scaleBarX + scaleBarLengthPixels], [scaleBarY,
       scaleBarY], 'Color', 'r', 'LineWidth', 3);
52 text(scaleBarX, scaleBarY - 10, sprintf('%d m ',
       scaleBarLengthMicrometers), 'Color', 'r', 'FontSize', 12);
53
54 % Draw the first line using right mouse clicks, press Enter when done
55 disp('Draw the first line using right mouse clicks, press Enter when
       done...');
56 h1 = drawline('Color', 'r');
57 line1 = h1.Position;
58
59 % Draw the second line using right mouse clicks, press Enter when
       done
60 disp('Draw the second line using right mouse clicks, press Enter when
        done...');
61 h2 = drawline('Color', 'g');
62 line2 = h2.Position;
63
64 % Calculate the angle between the two lines and extend them with
       dashed lines on both sides
65 vector1 = line1(2,:) - line1(1,:);
66 vector2 = line2(2,:) - line2(1,:);
67 angleBetweenLines = atan2d(norm(cross([vector1 0], [vector2 0])), dot
       (vector1, vector2));
68
69 % Extend lines with dashed lines on both sides
70 hold on;
71 plot([line1(1,1) - vector1(1)*100, line1(1,1) + vector1(1)*100], [
       line1(1,2) - vector1(2)*100, line1(1,2) + vector1(2)*100], '--r');
72 plot([line2(1,1) - vector2(1)*100, line2(1,1) + vector2(1)*100], [
       line2(1,2) - vector2(2)*100, line2(1,2) + vector2(2)*100], '--g');
73
74 % Find intersection point
75 intersection = line1(1,:) + (line2(1,:) - line1(1,:)) * (dot(vector1,
        vector2) / dot(vector1, vector1));
76
77 % Draw an arc to represent the angle
78 theta = linspace(0, deg2rad(angleBetweenLines), 100);
79 arcX = intersection(1) + 20 * cos(theta);
80 arcY = intersection(2) + 20 * sin(theta);
```

```
81 plot(arcX, arcY, 'r');
82
83 % Display the angle on the figure
84 text(mean([line1(1,1), line2(1,1)]), mean([line1(1,2), line2(1,2)]) -
       20, sprintf('%.2f  ', angleBetweenLines), 'Color', 'b', 'FontSize
      ', 12);
85
86 % Save the image with drawn lines and scale bar
87 saveas(gcf, 'Image_with_lines_and_angle.png');
88 disp('Image saved as "Image_with_lines_and_angle.png"');
```

## D.5 Matlab code: positional offset injection needles

```
clear; close all; clc;

% Step 1: Load the Image
[filename, pathname] = uigetfile({'*.png;*.jpg;*.jpeg;*.tif;*.bmp', 'Image Files'}, 'Select an Image');
if isequal(filename, 0)
    disp('No file selected. Exiting...');
    return;
end

% Read the image
img = imread(fullfile(pathname, filename));

% Convert to grayscale if needed
if size(img, 3) == 3
    grayImg = rgb2gray(img);
else
    grayImg = img;
end

% Display the grayscale image
figure;
imshow(grayImg);
title('Loaded Image');

% Set the scale (pixels per micrometer)
disp('Click two points on the image to set the scale (known distance in micrometers)');
[x, y] = ginput(2);
if length(x) < 2 || length(y) < 2
    error('You must select two points to set the scale.');
end

knownDistance = input('Enter the known distance between these two points in micrometers: ');
if isempty(knownDistance) || knownDistance <= 0
    error('Invalid distance. Please enter a positive number.');
end

pixelDistance = sqrt((x(2) - x(1))^2 + (y(2) - y(1))^2);
pixelsPerMicrometer = pixelDistance / knownDistance;
fprintf('Scale set: 1 micrometer = %.2f pixels\n', pixelsPerMicrometer);

% Add scale bar to the image
scaleBarLengthMicrometers = 200.0; % Length of scale bar in micrometers
```

```
scaleBarLengthPixels = scaleBarLengthMicrometers *
    pixelsPerMicrometer;

% Adjust the position of the scale bar
scaleBarX = size(img, 2) - 120; % Adjusted X position
scaleBarY = size(img, 1) - 20; % Y position

% Draw the scale bar on the image
hold on;
line([scaleBarX, scaleBarX + scaleBarLengthPixels], [scaleBarY,
    scaleBarY], 'Color', 'r', 'LineWidth', 3);
text(scaleBarX, scaleBarY - 10, sprintf('%d m',
    scaleBarLengthMicrometers), 'Color', 'r', 'FontSize', 12);

% Click on two points to draw horizontal lines
disp('Click on two points to draw horizontal lines...');
[x, y] = ginput(2);

% Draw horizontal lines at the clicked points and mark the points
line1Y = y(1);
line2Y = y(2);
line([0, size(img, 2)], [line1Y, line1Y], 'Color', 'r', 'LineWidth',
    2);
line([0, size(img, 2)], [line2Y, line2Y], 'Color', 'g', 'LineWidth',
    2);
plot(x(1), y(1), 'ro');
plot(x(2), y(2), 'go');

% Draw a dashed line between the green and red lines
line([x(1), x(1)], [line1Y, line2Y], 'Color', 'b', 'LineStyle', '--')
    ;

% Calculate the distance on Y-axis between the two horizontal lines
distanceY = abs(line1Y - line2Y) / pixelsPerMicrometer;

% Display the distance on Y-axis on the figure
midpointX = size(img, 2) / 4; %It is displayed on a 1/4 now
text(midpointX, mean([line1Y, line2Y]), sprintf('%.2f m', distanceY
    ), 'Color', 'b', 'FontSize', 12);

% Save the image with drawn lines and scale bar
saveas(gcf, 'Image_with_horizontal_lines_and_distance.png');
disp('Image saved as "Image_with_horizontal_lines_and_distance.png"')
    ;
```

# E Literature review

# Design of a model mimicking the Alveolar-Capillary Barrier

Literature review

Paulien Laninga

to be publicly defended on:
Friday January 18, 2024 at 2:00 PM.

TU Delft
Delft University of Technology

# Contents

**Abstract**

This paper identifies a research opportunity and outlines a plan to improve the modelling of the alveolar-capillary barrier. Several long-on-a-chip devices have been developed to model the alveolar-capillary barrier. However, incorporating all the mechanical properties of the biological environment into a model remains a challenge. The models currently in use are identified and analysed. It is found that most models use monolayers of endothelial cells rather than a cylindrical shape like that of capillaries. To better mimic the barrier, vascularisation of the models could be a potential improvement. The consideration of vascularised organs-on-a-chip models leads to the choice of designing pre-structured channels in the hydrogel to facilitate perfusion of the vessels. Several fabrication methods to obtain micro-scale channels, which are already used to create vessels, will be compared. This research will focus on sacrificial molding as it has been shown to give the most relevant result. A design plan will be presented to integrate vascularisation and cyclic stretching into an alveolar-capillary barrier model.

# 1 Introduction

Environmental pollution triggers inflammatory responses in the lungs that may contribute to the development of chronic lung disease. Understanding and predicting the progression of chronic lung diseases is important to provide appropriate care. Appropriate cellular models are needed to improve knowledge and understanding of the underlying functional mechanisms of these cellular responses. The use of lung-on-a-chip could provide a significant improvement in mimicking the human lung compared to other models. However, several drawbacks and limitations need to be overcome. The structural and dynamic properties of the model should be improved. Erasmus MC and TU Delft are collaborating to obtain more dynamic and physiologically relevant models. The models will be used to study the effect of environmental pollution on the alveolar-capillary barrier. This research focuses on improving models of the alveolar-capillary barrier. It will start with a literature review to analyse currently used models, look for research potential and then provide a research plan.

# 2 Alveolar-capillary barrier

The lungs have a large interface with the outside world. This interface consists of the permeable alveolar-capillary barrier, which plays a crucial role in the functioning of the lungs by ensuring the exchange of gases and nutrients between the blood capillaries and the alveoli [1]. The exchange of O2 and CO2 across the barrier is due to diffusion [2]. The barrier also plays an important role in protecting the body from harmful substances. To gain more knowledge about a good model, the structure, dimensions and dynamics of the human barrier are analysed.

## 2.1 Histology of the alveolar-cappillary barrier

Figure 1 shows a schematic representation of an alveolus. It has the shape of a sphere with air inside and is surrounded by four blood vessels, the cross-section of which can be seen. Inside the alveoli a macrophage is visualised, which play an important role in immunity and immune responses [3]. A mitochondrion is also visualised in the alveoli, they have a critical function in energy production, are essential for nutrient and oxygen sensing and regulate critical cellular processes including cell death and inflammation [4]. We can then take a closer look at the barrier between the alveolus and a capillary. This barrier consists of a respiratory membrane, which is made up of two basement membranes and an interstitial space that separates the epithelial cells from the endothelial cells. The human respiratory membrane has an average thickness of 1.1µm ± 0.1, but the gas exchange region is smaller, with a thickness of 0.62 µm ± 0.04 [1][5][6]. The two basement membranes within the airway membrane are the endothelial and epithelial basement membranes, these membranes line the basal side of the epithelial and endothelial tissues.

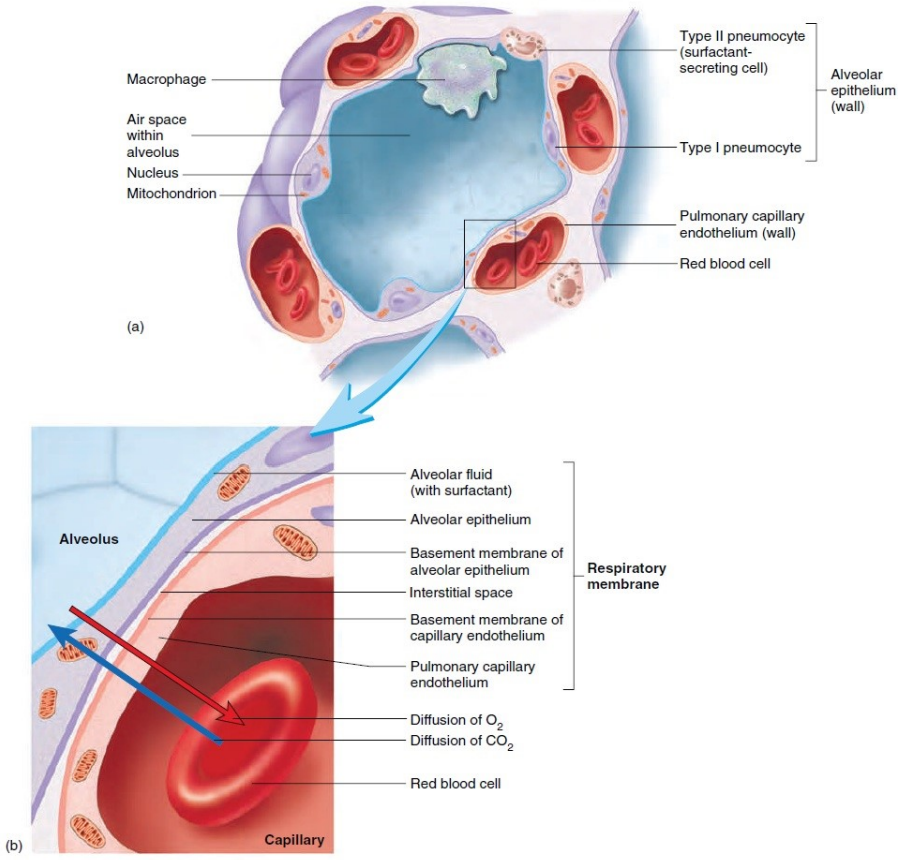


Figure 1: Alveolar barrier, figure adapted from Seeley R. et al 2002 [7]

### 2.1.1 Basement membrane of aveolar epithilial

The epithelial basement membrane consists of three layers, a basal lamina, a layer of epithelial cells and the epithelium [8]. There are two types of epithelial cells, type I pneumocytes and type II pneumocytes. On average there are 47 type 1 cells covering 95% of the surface area in the alveoli and 92 of the smaller type II cells per alveoli[9]. Type I cells are ultra-thin and wide, with a diameter of about 50 to 100 $\mu$m [10]. They facilitate the rapid diffusion of oxygen and carbon dioxide from the air to the erythrocytes in the capillaries because of their flat and plate-like structure. In addition, type I cells cannot replicate and are susceptible to toxic injury. [9][11]. Type II cells are cubic and exist in clusters[2], they have a diameter of about 10 $\mu$m[10]. They are sensitive to membrane stiffness and surface architecture[12]. Type II cells can rebuild the epithelial layer when type I cells are injured[2]. Type II alveolar epithelial cells secrete surfactant, a surface-active agent. It forms a biophysically active thin and continuous film that can reduce surface tension[13]. There is a surface tension at the gas-liquid interface because the liquid molecules are more attracted to each other than the gas molecules. The surfactant reduces this cohesion of water molecules, resulting in a lower surface tension, so less force is needed to expand the lungs and it prevents the alveoli from collapsing [14] [9]. [11]. Another function of surfactant is the protective layer of the mucous membrane (muscus), which is important for immune defence [1][13]. The surfactant film plays a critical role in particle movement and retention properties. The surfactant also contains several immunocompetent cells such as resident macrophages, dendritic cells and neutrophils[15]. The surfactant can be taken up by type II cells or macrophages for degradation. Macrophages, also known as dust cells, are the last line of defence and can remove or sequester unwanted particles, dust or bacteria. They are present in both alveolar and inter-alveolar spaces [11]. The liquid lining layer has an estimated mean thickness of about 200nm in the rat lung[13]. Another part of the epithelial basement membrane is the basal lamina which is a layer of extracellular matrix and has a thickness of 50nm[16].

### 2.1.2 Interstitial space

Collagen fibrils, elastic fibres or fibroblasts can be found at the junction between the basal lamina and the stroma. Fibroblasts are cells that can directly connect the endothelium to the epithelium through openings in the basement membranes. They also produce and maintain the ECM, others have mainly contractile properties, these are called myofibroblasts.[13][12]. In some parts of the airway, the basement membranes are fused. When the basement membranes are in direct contact, there is no supporting tissue, which reduces the thickness to 0.1-1.5$\mu$m and facilitates gas exchange [16][11].

The interstitial space and partly the basement membranes consist of extracellular matrix (ECM), which contains collagen and elastin fibres [1][9]. The ECM is porous and provides structural support for cells. Some reports on animal lungs show that there are two different pore sizes in the membrane, most pores have a diameter of less than 2.5nm and a small fraction have pores larger than 400nm[6][17]. Due to the structural support of ECM, the stiffness of human alveolar tissue is in the range of 1-2kPa [6][8].

### 2.1.3 Capillary endothelial basement membrane

The basement membrane of the capillary endothelium contains endothelial cells that form the capillary network used to deliver nutrients and oxygen to other parts of the body. This network contains capillaries with a diameter of approximately 6-8$\mu$m [18] [19][20]

### 2.1.4 Pores of Kohn

The lung contains many alveoli, between the alveoli there are Kohn's pores with a diameter of 10-15µm.[11]. The pores are bordered by extensions of type I pneumocytes.[21]. It was thought that these pores allowed air to flow from one alveolus to another to equalise air pressure and for communication between adjacent alveoli. However, several studies show that these pores are normally filled with alveolar lining fluid, preventing air flow between alveoli, and are thought to provide collateral ventilation only under extreme conditions such as terminal bronchiole blockage [22]. [23]. Another hypothesis is that Kohn's pores provide a portal for macrophage movement between alveoli.[23].

## 2.2 Dynamics of the barrier

The tracheais a large organ that expands during breathing. This movement is controlled by the diaphragm. This happens in several stages. The first phase is inhalation, when the air we breathe in enters the lungs. The last phase is when the air is expelled from the lungs. The change in volume of the lungs depends on the intensity of breathing and this is characterised by quiet breathing and labored breathing [7]. During quiet breathing, the person is at rest and has 10-12 breaths per minute, which corresponds to a frequency of 0.2 Hz[9].

### 2.2.1 Pressure

During the phases of breathing, the pressure in the alveoli changes. During inhalation, the volume of the lungs increases as the diaphragm descends. This descent causes the elastic fibres of the alveoli to expand. This descent causes the elastic fibres in the alveoli to expand. This expansion causes a drop in alveolar pressure to about 130 Pa, which is below atmospheric pressure during quiet breathing. The pressure difference causes air to flow into the lungs. This inhalation continues until the pressure in the alveoli is equal to the pressure outside the body, which is normally atmospheric pressure. During exhalation, the volume of the lungs decreases as the diaphragm relaxes and rises and the elastic fibres in the alveoli passively contract. This results in a higher pressure of about 130 Pa above atmospheric pressure in the alveoli. Air is expelled from the alveoli and out of the lungs. At the end of expiration, the pressure in the alveoli returns to atmospheric pressure. [14] [7] [11].

### 2.2.2 Expension

During breathing, the lung tissue expands. There have been several studies of this expansion of the alveoli. J.B. Forrest researched guinea pig lungs and showed that the volume of the alveoli increases linearly with the lung volume [24]. In another study, using optical sectioning microscopy, it was observed that in the rat lung, the alveoli have an uneven expansion, with both segments of a single alveolus being considered as individual cells. It has been observed that type I epithelial cells have a greater expansion than type II cells[25]. In dog lungs, it has been measured by stereoscopic radiography that bronchial length and diameter are proportional to the change in the cube root of absolute lung volume[26]. However, to estimate average tissue strain, it is assumed that the linear dimensions of lung tissue scale isotopically with change in the cube root of lung volume. According to this assumption, the corresponding strain is approximately 4% during normal tidal lung inflation, 12% during deep inspiration or a sigh, and 25% at vital capacity. [27] [28] [29] [30].

### 2.2.3 Gas exchange and blood flow

For optimal gas exchange across the barrier, there should be a balance between ventilation, gas volume and perfusion. Gas volume is controlled by changing bronchial diameter while blood flow is controlled by changing arteriolar diameter. Optimal gas exchange is essential to prevent oxygen deprivation of body tissues. Equilibrium is reached after 0.25s of diffusion across the respiratory membrane, whereas a red blood cell spends only about 0.75s in the pulmonary capillary[14]. Blood flow in capillaries causes shear stress on the endothelial cells, which is in the range of 0.1-1 $N/m^2$[31].

# 3 Alveolar-capillary barrier in vitro or LOC

Several types of models are currently used in LOC research. These can be divided into static models, models including strain, models including flow and models integrating both stretching and flow.

## 3.1 Static models

A static air-liquid interface is a model that can be used to study the alveolar-capillary barrier. The figure 2 shows an example of a static ALI model. First, a fluid containing epithelial cells is placed in the upper compartment so that the epithelial cells are immersed. The medium above the cells is then removed and the apical surface of the epithelium is exposed to air. Nutrients are then supplied from the basolateral side. Culturing the cells with ALI results in more physiological phenotypes.[31] The interfaces between the different cell types in the model are enabled by the porous membrane. Recently, hydrogels have been incorporated into ALI models, resulting in a more 3D structuring of the cells, and it arranges interstitial cells such as fibroblasts into the microenvironment.[31] This device also allows co-culture with endothelial cells.

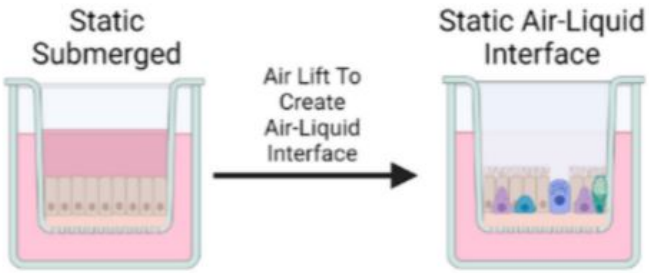


Figure 2: A illustration of a static ALI model [31]

Static models can also be fabricated with bioprinting. Horváth et al. used 3D bioprinting to produce an model of the barrier, consisting of endothelial cells, basement membrane and epithelial cells. Their research demonstrated the viability of the cells and showed that this technique allows the automated and reproducible creation of a thin layer of cells that can be used to create a static alveolar-capillary barrier [32].

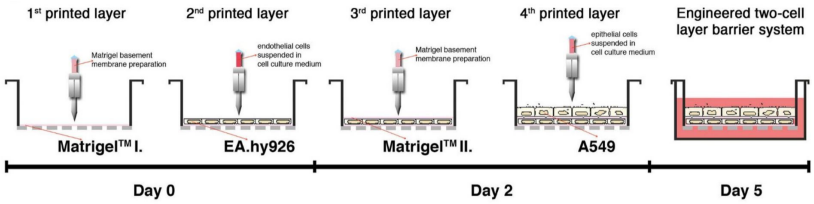


Figure 3: Schematic illustration of bioprinting an alveolar-capillary barrier model[32]

Having an ALI interface is an important aspect of models mimicking the alveolar-capillary barrier because of the cell differentiation. Static models used 2D monolayers of epithilial cells and endothilial cells, it can also be co-cultured with other cells. But those static models have no stretching and flow so we will not analyse those further.

## 3.2 Models including stretching

The mechanical effect of breathing is also included in some of the models used today. Cyclic stretching is applied to models with a fabricated membrane on which two monolayers of epithelial and endothelial cells are cultured. Polydimethylsiloxane (PDMS) is often used to create a membrane. PDMS has good mechanical, optical and biocompatible properties and is often used to make a porous membranes.

However, the material has some biological limitations, distorting the biochemical environment through high adsorption and absorption of small molecules.
The model created by Zamprong et al. is analysed further because they achieved deflection in three dimensions and used a different membrane material. They produced a biological, stretchable and biodegradable membrane made from collagen and elstin, proteins of the lung ECM. Using material similar to ECM better mimics the biological environment, as ECM also provides the structural basis for cell growth in humans. However, applying cyclic mechanical stretching to such a thin membrane of ECM molecules is technically challenging, so they used a gold mesh to overcome this.

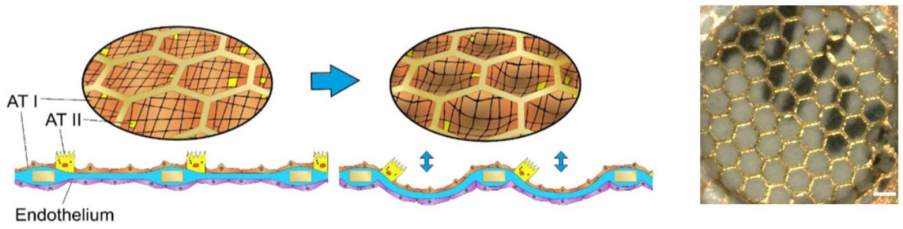


Figure 4: Biodegradable and stretchable membrane designed by Zamprogno et al. [33]

Its design is shown in figure 4. It is fabricated using a bottom-up approach fabrication technique by drop casting a CE solution onto a gold mesh. The solution spreads out and is held in place by surface tension. The gold mesh acts as a framework. It has a pore size of 260 µm and supports an array of 40 alveoli. The mesh has a diameter of 2mm and is 18µm thick, allowing cells to be cultured on both sides. The gold mesh has been treated with 5% 3-aminopropyltriethoxysilane and 0.1% glutaraldehyde to ensure attachment of the membrane. The mesh consists of an array of 40 regular hexagons with sides of 130µm and walls of 30µm width. The water in the CE solution evaporates and the suspended membrane begins to form. Collagen molecules self-assemble into fibrils, which provide the structural support, as in ECM. After drying, the membrane was integrated into a microfluidic chip. The membrane is stretched by applying negative pressure to the basolateral side. This results in a homogeneous deflection in three dimensions. At 2 kPa the radial strain reached 9.1% ± 2.5%. When epithelial cells were seeded on the mesh, 4.0 kPa was needed to induce a linear strain of 10%. Changing the ratio of the protein concentration changed the stiffness of the membrane. Their membrane is produced by a simple method and the thickness, composition and stiffness can be easily changed. The thinnest membrane they obtained had a thickness of 4.5 ± 0.8 µm. The barrier was maintained for up to three weeks. An advantage is that the CE membrane did not require precoating before cell seeding. Their model is used with primary patient lung alveolar epithelial cells and primary lung endothelial cells, which makes this result particularly relevant to our research [33].

Creating a homogeneous deflection in three dimensions is a feature we wanted to incorporate into our design. Using the pressure differential to stretch the barrier is the only method found that achieves this. This makes it a promising method to include in our design. The results of their mechanical properties, such as the increase in stiffness after epithelial cells are seeded onto the mesh, will also be taken into account during the design phase of our model.

## 3.3 Models inlcuding flow

Blood flow has been shown to affect vascular homeostasis, including the inflammatory response of endothelial cells; the inflammatory response is an important consideration in our model [34][35]. Creating flow in the static models shown in the section 3.1 can be done using rocking platforms. This is a simple method of creating a flow that results in shear stress on the wall of the endothelial cells. The flow generated by a rocking platform is bidirectional, unlike the unidirectional flow in a body. It has recently been shown that cells cultured with bidirectional flow have a significant delay in the extravasation of immune cells compared to cells cultured with unidirectional flow [36]. So we need to look at models that have unidirectional flow, which will be discussed in the next sections.

## 3.4 Models including stretching and flow

A commercially available model has been developed by Huh et al. and is shown in figure 5. In this device, cell culture of the monolayer is done by flowing liquid into the channel instead of using a pipette. Again, PDMS is used to make a membrane that is 10$\mu$m thick and has 10$\mu$ wide pentagonal pores. To mimic respiration, a strain of 5-15% was applied to the membrane. The cell remained viable for more than two weeks.

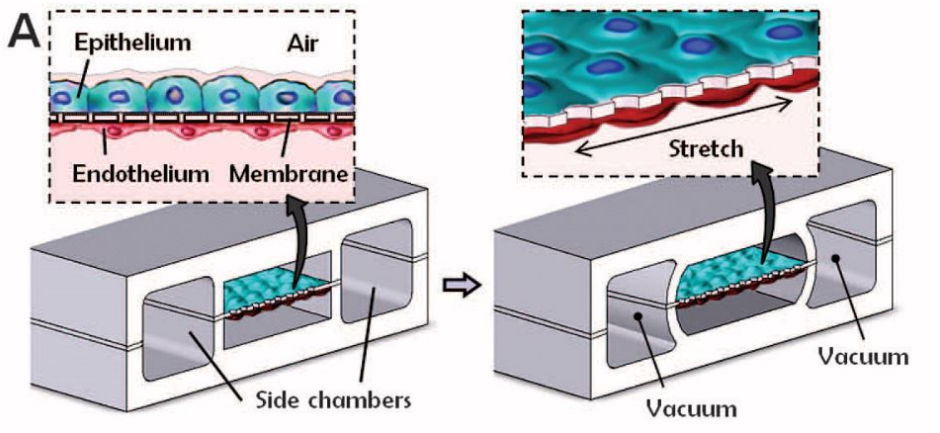


Figure 5: Device to model alveolar-capillary barrier created by Huh et al.[37]

Using this model, it was shown that membrane stretching leads to distortion of the cell shape. Stretching also affected the epithelial and endothelial uptake of nanoparticles and stimulated their transport across the barrier. When the strain was combined with a shear stress of 1.5 Pa on the endothelial cells, the transport rate of the nanoparticles increased.

## 3.5 Evaluation LOC models

Several types of research discussed above have shown us not only the importance of integrating flow and strain into the model, but also the importance of mimicking flow and strain correctly. The strain on an alveolar-capillary barrier is triaxial, this strain is achieved in the model of Zamprong et al. and discussed in section 3.2. This stretching method is taken into account in the design of our model. Flow is also included in alveolar models, but does not fully mimic the biological environment as endothelial cells are only cultured as a monolayer rather than vessels. If we consider also other LOC and OOC rather than only alveolar models, more knowledge about vascularization can be obtained. In the next chapter, chapter 4, vascularized Lung-on-a-chip (LOC) models will be analysed.

# 4 Vascularization of LOC

Growing endothelial cells in ECM hydrogels results in this self-assembled blood vessel. A random network can be formed or a specific structure can be created by using a scaffold.

## 4.1 Random vascularization

Vasculogenesis and angiogenesis are two biological processes that lead to the formation of blood vessels in vivo. Vasculogenesis is a process by which new blood vessels are formed, typically during embryonic development, and angiogenesis is the formation of new blood vessels from pre-existing vessels[38]. These biological processes can be used to generate a random network of vessels smaller than 100$\mu$m[39]. Most models that use vascularization to vascularize a spheriod, these methods are not applicable to our application. Two models could be relevant, these will be analysed and discussed.

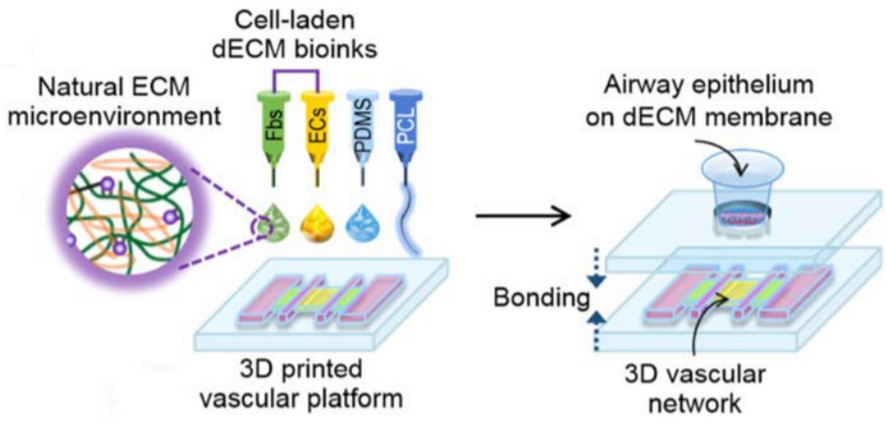


Figure 6: Vascularized network integrated with airway epithelium model created by Park et al.[40]

First, Park et al. developed a vascular platform that was fabricated in a one-step process using a 3D cell printing system. They then printed endothelial cells and fibroblasts, using decellularised extracellular matrix bioink, into a specific polycaprolactone frame, as shown in figure 6. There is a niche in the frame where the vascular network is formed. On top of this frame, an airway model was assembled with the printed vascular platform. Interestingly, this created a functional interface between the airway epithelium and the vascular network[40].

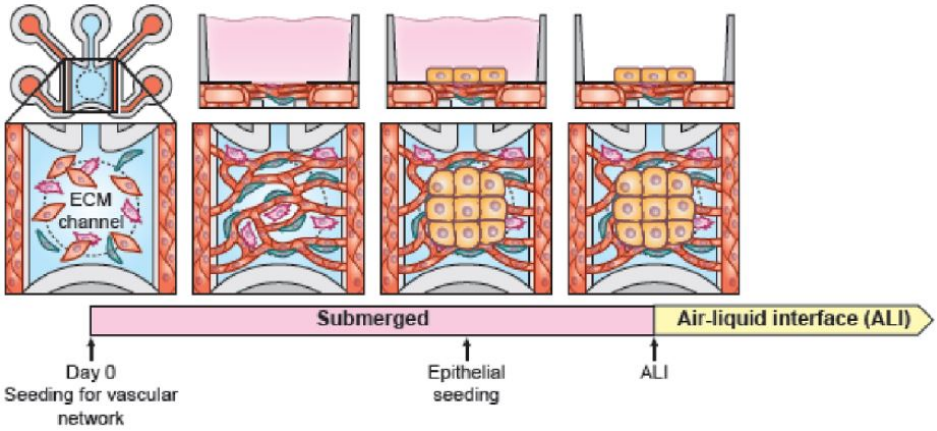


Figure 7: Vascularized network integrated with alveolar or bronchiolar model created by Jung et al.[41]

Jung et al. used a different method to integrate vascularization into LOC. They developed the model on a 64-chip microfluidic plate-based platform, allowing for high throughput screening. They

describe two models, a vascularized alveolar model and a vascularized bronchiolar model. They claimed to have shortened the maturation time for their small airway epithelial cells, which are cells in the bronchiolar capillary junction of the lung. Their transdifferentiation time was reduced to just two weeks after ALI. They hypothesise that this is due to a more efficient nutrient supply and better cell-cell crosstalk because no scaffold or permeable membrane was incorporated. Whether this would also be the case with alveolar cells cannot be concluded from their research. Also, the viability and perfusion time of the alveolar model is not specifically mentioned.

They analysed the perfusability with fluoroscopy and the vascular network remained perfusable for two weeks after the ALI induction. The main channels on the side of the device detached from the wall after three weeks (post-seeding). This could be due to the non-physiological angle of the channel and high shear stress and flow. A decrease in the diameter of the main vessels was observed, this decrease was probably the reason for the timeline limitation. Another interesting observation was that the flow of the vascular bed can be up to 50% of the flow through the main channels. I include this observation in my conclusion. [41].

## 4.2 Evaluation of vascularization of LOC

It can be concluded that vascularized LOCs increased the physiological relevance of the model. However, perfusability remains a challenge. My interpretation is as follows. A randomly self-assembled network perfused by larger vessels needs a high pressure to keep the network perfused, because the network has much smaller diameters and non-optimal streamlined channels, it will lead to a high resistance. This is supported by the last observation. This high pressure is likely to damage the vessels and also challenge the remaining perfusable network. By creating a pre-structured network of vessels, this could result in a longer perfusion time for the vessels. To gain more knowledge on how to create such a network, we will look at models based on scaffold vascularization. Several models will be analysed, including their fabrication method and performance.

# 5 Scaffold based vascularization

Scaffold based vascularization allows the alignment of vessels and can be used to promote perfusion and better cellular organisation. Alignment of the vessels could improve the reproducibility and lifetime of a model compared to a random network of vessels. Several methods are used to create microchannels, followed by successful vascularization, and these methods are analysed and compared. Note that none of the models discussed are used to vascularize an alveolar model.

## 5.1 Fabrication methods scaffolds

### 5.1.1 Bioprinting

Bioprinting is one of the techniques used to create blood vessels. Only a few printing methods have successfully produced vascularized constructs, such as extrusion bioprinting and stereolithography [42]. The ability to create iterative prototypes and models at low production cost and time is a well-known advantage of 3D printing. Almost any geometry can be created due to the availability of modelling software [43]. Bioprinting allows for precise placement of cells without the need for a mold or material removal. And even if there is a need for a support structure, then multi-materials can be used to achieve this. These aspects make the technique promising. However, 3D printing with biological material has specific requirements, such as the strength and permeability of biological tissues. The modification of 3D printing techniques to make them applicable to biological systems has been slow due to these specific requirements. Another challenge is to create an environment in which cells will adopt[43].

There are two different methods used in bioprinting: direct and indirect printing. In direct printing, the deposited material contains cells that will form the vascular network and this is deposited on a surface [44]. In indirect printing, the printed material is a guide for cells that are subsequently seeded [43]. Uniaxial channels can be formed in hydrogels by extrusion of a sacrificial material. The endothelial cells could be located within the sacrificial material or introduced after channel formation. By varying the nozzle diameter and extrusion rate the vessel wall thickness and lumen diameter can be determined. The composition of the used bio-ink used affects the cell viability and material extrusion. The parameters of the bioinks are optimised to improve cell viability [44].

For both types of bioprinting the material is a compromise between ease of use and the biocompatibility. Natural polymers or decellularised ECM are often preferred for their biocompatibility. Using both, have proven to be promising, but their use in bioprinting is still limited. Due to the required mechanical properties that determine their printability, they require highly engineered set-ups. These mechanical properties of the printed material include viscosity, density, surface tension, cross-linking properties, stiffness and degradation profiles [42][45].

Although bioprinting is one of the most promising fabrication methods, we will not explore it further. This is because bioprinting is not yet an available fabrication method at TU Delft.

### 5.1.2 Needle molding

One of these techniques is needle molding. Needle molding is an early used technique. Hydrogel is casted around a removable needle. A channel is formed and can be connected to a flow loop to allow perfusion [44]. Chrobak et al. described the formation, perfusion and maturation of microvascular tubes in vitro. They used a coated stainless steel needle to create tubes 5-7mm long and 55-120µm in diameter. The tubes increased to 75-150µm after maturation. These increasing diameters are related to the gelling temperature. On days 1-2 the tubes contracted, this was considered as a defect and was prevented by gelling the collagen at 23°C. On days 3-7 the tubes expanded, this 'defect' could not be prevented, but it was concluded that expansion of the tubes required a confluent endothelial lining. They persisted for at least 5 days and often much longer, some tubes persisted for 3 weeks. Because of the constant perfusion in their tubes, they were able to improve the barrier function by delivering albumin to the ECs [46]. Needle modelling is a relatively cheap and simple method, but is often limited to the construction of single tubular mesochannels without branches. As a result, it fails to recapitulate the resolution and complexity of the microvasculature [44]. In our model, simplicity is a goal and therefore it could be an interesting fabrication method. Recently, Park et al. have shown that it is possible to use needle insertion to create microvasculature by angiogenesis. Their setup is shown in figure 8. They investigated strategies to create vascularized lung cancer-on-a-chip (VLCC). Two 500µm diameter channels were created with needles in a hydrogel based on decellularised lung

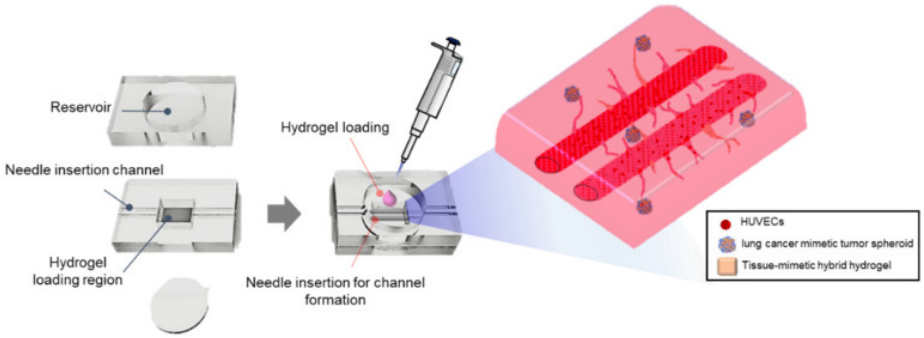


Figure 8: Setup of needle method created by Park at el. [47]

extracellular matrix (ldECM). After endothelialisation with HUVECs, two large perfusable vessels resembling arterioles were formed. A capillary network structure was formed between the two large stable blood vessels. The diameter of these capillaries was not reported [47].

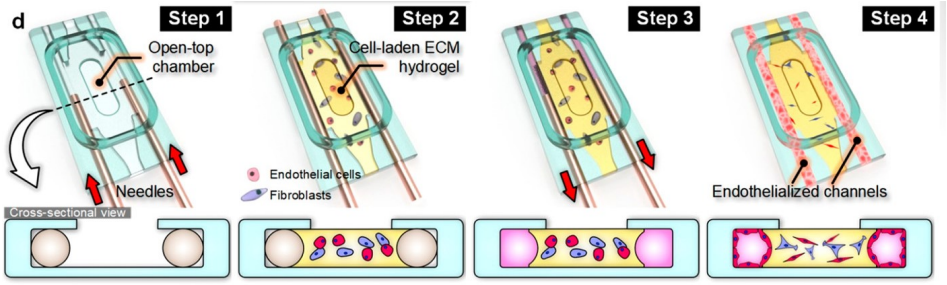


Figure 9: Setup of needle method created by Paek at el. [48]

Paek et al. also uses needle molding in combination with a PDMS mold. This process is shown in figure 9. The needle, with a diameter of 400µm, was inserted into microchannels inside the PDMS mold. ECM hydrogel precursor solution mixed with suspension of primary human vascular endothelial cells and fibroblasts was injected into the culture chamber. After gelling of the suspension, the needles were removed to create hollow circular channels, which were seeded with vascular endothelial cells to form an endothelium on the luminal surface. The viability of their channels and network was maintained for more than 14 days.

### 5.1.3 Sacrificial molding

Sacrificial molding is another technique used to create mesovasculature [44]. Shimizu et al. have made a mold of polyvinyl alcohol (PVA) and placed it in an ECM consisting of transglutaminase (TG) crosslinked gelatin. The mold dissolves after rinsing with hot water, leaving microchannels with a diameter of 300µm. The mold was tested with simultaneous perfusion and stretching. Three days after seeding, GFP-HUVECs covered the entire inner surface of the microchannel and formed an endothelial tube during perfusion. Cell viability after more than four days was not reported. The stretching motion was an uniaxial and was performed at 2.5% to 10% strain at 1Hz[49]. Interesting is their flow analysis during perfusion and stretching. During stretching, they observed the affected behaviour of the flow inside the microchannel. Due to the volume change caused by stretching, an oscillatory flow was seen in the microchannel. However, this was observed in channels with a diameter of 560µm. It cannot be concluded that the same effect will occur in a channel with a different diameter. The alignment of the HUVECs after application of fluid shear stress and mechanical stretch stress was also examined. The HUVECs appeared to align clearly with the direction of the flow and the vertical direction of the stretching motion[49]. Miller et al, also used a sacrificial mold. They used a biocompatible sacrificial material, a glass made from inexpensive carbohydrates. They 3D printed a carbohydrate glass lattice and encapsulated it with living cells in the ECM. Water flow dissolved the lattice. Then HUVECs were then seeded into the lumen to form a vascular architecture. The HUVECs were attached for one

hour in static culture. They reached confluence within one day as shown in figure 10. They formed vessels with a diameter of 150µm to 750µm. It was not mentioned how long the network remained perfusable, but images show an intact lumen with a diameter of around 150µm after 9 days in culture. Their method is not very time-consuming. The steps in their process: cell encapsulatoin, lattice in ECM prepolymer, ECM crosslinking and glass dissolution, take only a few minutes[50].

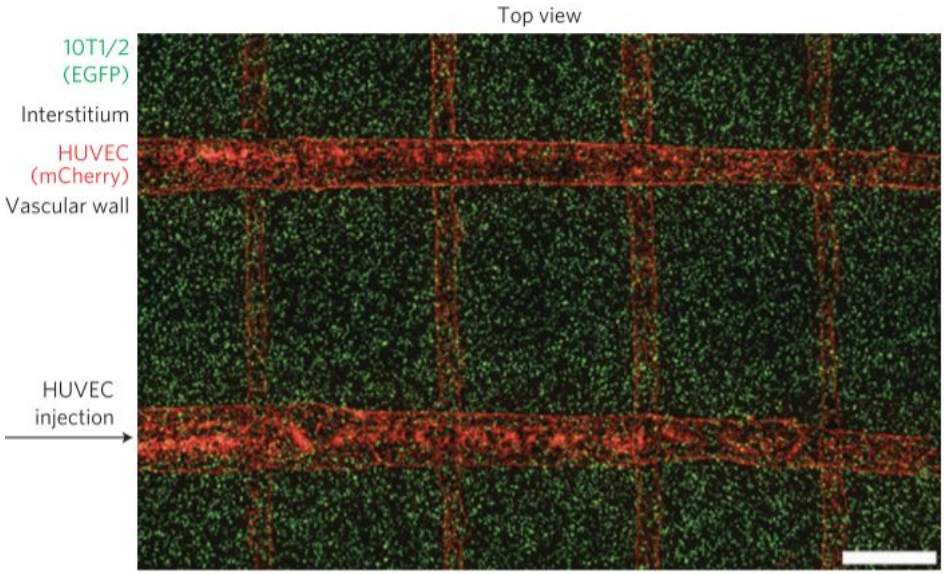


Figure 10: Vascular architecture form after sacrificial molding by Miller et al. after one day of culture. Scale bar, 1mm. [50]

### 5.1.4 Scaffold-wrapping

The scaffold-wrapping method is another technique that can create scaffolds or channels with a cylindrical structure and desired pattern [51]. In this method, a mold is encapsulated with endothelial cells by vasculogenesis. The scaffold is then degraded resulting in a perfusable vascular network. Recently Ying-Ting Lin et al, used this method. They used photolithography to create a fibrin scaffold, shown in figure 11 that was wrapped by HUVECs and encapsulated in collagen gel. After plasmin treatment,

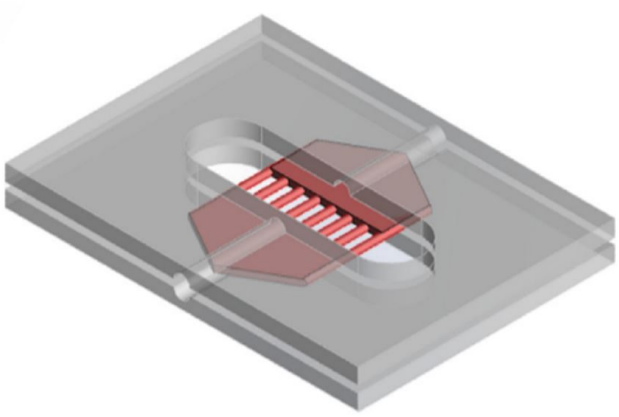

Figure 11: Scaffold structure used for scaffold-wrapping designed by Lin et al.[52]

a perfusable vessel lumen was created. The vessel had a diameter of 30µm. After degradation of the scaffold it remained perfusable for only 2 days. An advantage of this method is that the diameter of

the vessels can be precisely determined[52]. The challenge is to allow the cells to attach to the collagen and maintain their shape after degradation of the scaffold [51]. This scaffold wrapping method lasted 9 days in total. On day 7, the fibrin scaffold degraded and the lumen stayed perfusable for two days[52]. So, this is a time-consuming process compared to the needle molding method.

### 5.1.5 Molds with closed channels

Molds are also used to produce channels. These are often made from PDMS and fabricated using soft lithography techniques[53]. Closed channels can be created by stacking two layers of PDMS and seeded with ECs. Fluid flow can be easily controlled by channel dimensions and flow rates. An advantage of using PDMS is its biocompatibility and optical transparency. A disadvantage is the non-selective absorption of oxygen and other hydrophobic molecules[44]. For our application, the absorption of small molecules can affect our research results. Lithogrophy can also be used with hydrogel materials. This provides a more biologically relevant environment, which benefits the viability of the ECs. Bischel et al. used a PDMS mold with channels fabricated by soft lithography, shown in figure 12. The channels are filled with ECM hydrogel consisting of type I collagen and Matrigel. This resulted in a circular lumen

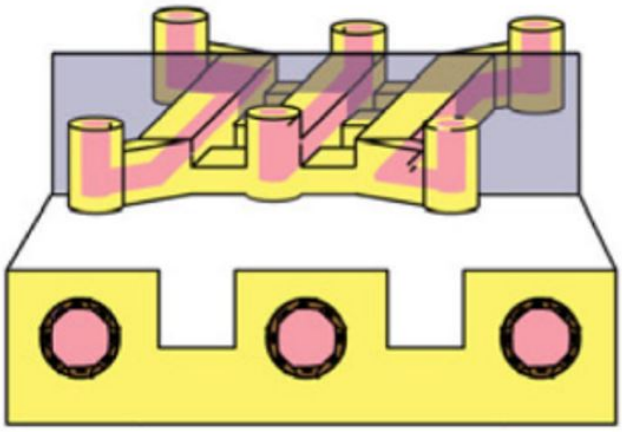

Figure 12: PDMS mold with three channels filled with hydrogel designed by Bischel et al.[54]

structure lined with endothelial cells to mimic a vascular structure with a diameter of 256µm. The viability of the cells after 48 hours is not mentioned[54]. The use of soft lithography molds facilitates the creation of more complex geometries.

## 5.2 Culturing cells

To create vessel, human umbilical vein endothelial cells (HUVECs) are being cultured in a hydrogel mimicking the ECM. Impartant information about the cell culturing is collected and discussed in this chapter.

### 5.2.1 Hydrogels

All of the above methods use hydrogels to mimic the ECM. The composition of these hydrogels varies. Park et al. varied the concentration of their hydrogel. They found that angiogenesis and cell viability were enhanced by the mechanical and biochemical properties of the ldECM-based hydrogel, which depended on the hydrogel ratio and concentration. They compared the properties of the ldECM-based hydrogel with those of collagen/fibrin hydrogel. Their setup is shown in figure 8. Cell viability was highest at 2% ldECM, which has a similar stiffness to the collagen/fibrin hydrogel. Pro-angiogenic activity was highest at 1% ldECM, but this concentration had lower cell viability and lower stiffness. Stiffness is probably not the only parameter influencing viability and pro-angiogenic activity. After comparing the 25:75 ldECM/collagen hydrogel with the 1% ldECM-100 hydrogel, they hypothesised

that the difference in microstructure also had an effect. The Young's modulus of 1% ldECM is 2.21 ± 0.23 kPa [47].

### 5.2.2 Seeding cells

For cultering cells several methods are used. One of the options culturing under constant perfusion. Several models discussed use this method. To describe this method, the exact procedure for seeding the model created by Peak at al., shown in figure 9, will be discussed.

After the removal of the needle, the channels were washed once with EGM-2. A suspension of 10 µL of HUVEC suspension ($1 \times 10^7$ cells/mL) was then introduced into the channels, allowing the cells to attach to the channel surface for 3 hours. A continuous flow of culture medium was then pumped through the channels at a volumetric flow rate of 70µL/h [48]. This is a fast and relatively simple method.

Another option is to rotate the channel as the cells are cultured. Park et al. endothelialised the channels formed by the mandrills with RFP HUVECs at $7 \times 10^6$ cells/mL and then rotated them at 10 rotations/h for 1 h at 37 ∘C[47]. Not many models use this seeding method, so it will not be used for our research plan, but could be an alternative option if the previous methods fail.

### 5.2.3 Diameters

Chrobak et al. investigated whether tubes with smaller initial diameters were viable. They concluded that the smallest tube that could be seeded and sustain flow had an initial diameter of 55$\mu$m. These tubes would have expanded to 70-75$\mu$m. However, the HUVECs grew in aggregates that spanned the lumen. This resulted in reduced flow and the cells died within three days [46]. Lin et al. showed that their scaffold wrapping method was successful in creating small vessels with a diameter of less than 30$\mu$m. However, after degradation of the fibrin scaffold in the collagen gel, the network was perfusable for only 2 days.

# 6 Discussion and conclusion scaffold based vascularization

Information and data from several articles will be compared with each other. This is done to make conclusions about the diameters of the created vessel, the used fabrication method and the used hydrogels.

## 6.1 Diameter channels

Research which compares the diameters of channels to cell viability or perfusability is not found. Therefore the data found in several articles is compared to each other and is shown in table 1. In several articles, a specific day is mentioned on which the cells are alive or show an intact vessel. But in almost none of the articles is mentioned at what day the cells died or when the vessels started clogging or leaking. That is why no firm conclusions can be drawn from the collected data. For our research, the diameter is an important parameter and therefore the corresponding performance should be determined. This will be one of the steps in the development of our final design.

| Diameter | Viability | Perfusablility | Source |
|---|---|---|---|
| 500 $\mu$m | At least 4 days | At least 7 days | Park et al. [47] |
| 400 $\mu$m | At least 14 days | At least 7 days | Paek et al. [48] |
| 300-400$\mu$m | At least 14 days | At least 4 days | Shimizu et al. [49] |
| 150-750 $\mu$m | At least 9 days | - | Miller et al. [50] |
| 256 $\pm$21$\mu$m | At least 2 days | At least 2 days | Bischel et al. [54] |
| 75-150 $\mu$m | - | At least 1 week, some 3 weeks | Chrobak et al. [46] |
| $\leq$55$\mu$m | maximum of three days | - | Chrobak et al. [46] |
| $\leq$30$\mu$m | - | for 2 days | Lin et al. [52] |

Table 1: Diameters of the obtained vessels and their performance

Vessels with diameters in the range of 300-500$\mu$m show the longest proven viability and perfusability time. This range might therefore be a good range to start in our process. To mimic the lung capillaries, having diameters of around 8$\mu$m, as stated before, obtaining smaller vessels is preferred. Data might indicate that keeping a good performance with vessels with a diameter of 30-50$\mu$m is more challenging. This is likely more challenging due to clogging. However, a diameter of 75$\mu$m seems to have shown a relatively good performance. Indicating that it is interesting to create more data about the performance of vessels with a diameter in the range of 30-75$\mu$m.

## 6.2 Fabrication method

Four fabrication methods successfully created channels in which vessels have been created. Table 2 provides an overview of those fabrication methods and the diameters of the vessels which were created afterwards.

| Fabrication method | Diameter | Source |
|---|---|---|
| Sacrificial molding | 150-750 $\mu$m | Miller et al. [50] |
| Sacrificial molding | 300-400$\mu$m | Shimizu et al. [49] |
| Scaffold wrapping | $\leq$30 $\mu$m | Lin et al. [52] |
| Needle molding | $\leq$55$\mu$m and 75-150 $\mu$m | Chrobak et al. [46] |
| Needle molding | 400$\mu$m | Paek et al. [48] |
| PDMS mold, soft lithography | 256 $\pm$21$\mu$m | Bischel et al.[54] |

Table 2: Fabrication method and the diameters of the obtained vessels

From table 2 it can be concluded that needle molding and scaffold wrapping obtained vessels with the smallest diameters. However scaffold wrapping is a sensitive time-consuming and biological process and has not proven to be able to create vessels which sustained for a long time. Therefore this fabrication method is not preferred.

As discussed in section 6.1, creating vessels with a wide range of diameters is needed to obtain information about the performance of the vessels. Sacrificial molding and needle molding obtained the largest range of vessel diameters. With lithography, PDMS mold can be fabricated in a wide range of sizes. It is important to take into account that it is not known if vessels having a wide range can be formed in those molds. So, sacrificial and needle molding might be preferred over channels in a pdms mold. Another advantage of using sacrificial or needle molding is having a channel in hydrogel. This can be made of only biological components and it prevents the membrane from being in contact with PDMS.

Two fabrication methods remain interesting. With needle molding it is not an option to obtain every structure we would like but a big advantage of needle molding is the relatively easy and fast fabrication process. Therefore we can use this method to obtain in a short time more information about the process of creating a vessel. Such as, which diameter(s) give good performance, which hydrogel to use and look into other parameters that influence vessel formation. The other remaining method is sacrificial molding. An aspect of this method is that the mold is degraded with the perfusion of water. An advantage is that after the mold is degraded the perfusion of the cell suspension can take place. Moreover, the structure of the mold can be made such that the diameter of the channel is larger at the position where it is connected to the inlet, making it easier to handle this method. Also, multiple channels can be connected to one inlet and one outlet. This method has also proven to be successful in several types of hydrogels, making it an option to use our preferred hydrogel.

### 6.2.1 Sacrificial molding

Two sacrificial materials, shown in table 3 are found to be used for our application. The used material influences the complexity of the printing process and the diameter which can be achieved. Therefore the process of both materials is discussed.

| sacrificial material | diameter | Source |
|---|---|---|
| Carbohydrate glass | 150-750 $\mu$m | Miller et al. [50] |
| Polyvinyl alcohol (PVA) | 300-400$\mu$m | Shimizu et al. [49] |

Table 3: Used sacrificial material to create channels used to create vessels

Carbohydrate is a mixture of 25g glucose, 53g sucrose, 10g dextran and 50 ml reverse osmosis water. The mixture was heated to 165 °C to remove most of the water before was printed with a fused deposition modelling (FDM) at 110°C under nitrogen pressure through a steel nozzle having an inner diameter of 1.2mm and 0.84mm. The structure is then vitrified to 50° and immersed in a solution of poly(D-lactide-co-glycolide) (PDLGA) in chloroform for 5 min. The mixture is rapidly cooled down below its glass transition temperature and forms a glassy amorphous solid. It can then be used or it can be stored at 45°C or in a vacuum chamber to protect it from ambient moisture. The ECM was dispensed around the created lattice and after crosslinking it was immersed in an aqueous solution and the lattice was dissolved within minutes. Because the lattice was coated with PDLGA the dissolved carbohydrates could easily flow out through the channels [50].
For the fabrication of the PVA mold also a FDM 3D printer was used. Two filaments were used, one with the composite of PVA and one for the PVA mold. The nozzle had a temperature of 190° and a diameter of 200 $\mu$m. A TG gelatin pre-gel solution formed the bottom layer after it was cooled on ice. The PVA mold was placed on top of it then more TG gelatin pre-gel solution embedded the mold before it was solidified. Then it was placed in a drying oven in 31 ° for 2 hours to activate the enzyme, probably being PVAase (polyvinyl alcohol hydrolase). The TG gelatin gel was cut at the ends of the PVA mold and hot water was used to dissolve any remainder of the PVA mold. Because of the swelling of the mold in the ECM-based scaffold a minimum diameter of $\sim$300$\mu$m was obtained. The PVA mold absorbed water and swelled while the TG gelatin gel solidified. [49]

Both fabrication methods use a FDM (Fused Deposition Modeling) 3D printer, but the temperature of the material as it is deposited is a big difference. This fabrication processes can take place at the TU Delft, however printing at 190° might be challenging as it is closer to the limitations of the available 3D printer. The vessels made with carbohydrate glass were smaller than those made with PVA mold.

Also, after the PVA was printed it swelled while with carbohydrate glass a smaller channel diameter was obtained than the used nozzles. Those results are related to the material properties and the settings of the 3D printer such as flow rate and pressure. It should be determined which properties and settings are desired. Due to the result obtained in those articles and because the fabrication with a carbohydrate glass mold is less challenging, this method is preferred.

## 6.3 Hydrogel

Hydrogels are used to mimic ECM and several types of hydrogels are used. Their results are shown in table 4. A wide range of materials are used but no firm conclusion can be made. However, hydrogels with fibrin show good results. But not only the composition of hydrogels is important. The mechanical properties of hydrogels, such as microstructure, density and stiffness are important parameters to take into account. Those parameters not only affect the perfusion and viability of the cells but also the angiogenic activity shown by Park et al. which was discussed in section 5.2.1 [47]. Our priority is to create strong aligned vessels rather than a random vascularized network. Optimal parameters to achieve this are not found. Important to take into account is that the stiffness of human alveolar tissue is in the range of 1-2kPa [6][8].

| Hydrogel | Cells | Viability | Perfusablility | Source |
|---|---|---|---|---|
| Fibrinogen solution mixed with thrombin | HUVECs | At least 14 days | At least 7 days | Paek et al. [48] |
| Fibrin mixed with type I collagen | hAMECs | Over 40 days | - | Paek et al. [48] |
| PEG hdyrogel | HUVECs | at least three days | - | Miller et al. [50] |
| Agarose | HUVECs | At least 8 days | - | Miller et al. [50] |
| Fibrin gel (10mg $ml^{-}1$) | HUVECs | - | At least 9 days | Miller et al. [50] |
| Collagen gel | HUVECs | - | At least 1 week | Chrobak et al. [46] |
| Collagen I with plasmin and VitroGel | HUVECs | - | For 2 days | Lin et al. [52] |
| TG gelatin* | HUVECs | - | At least for 4 days | Shimizu et al. [49] |
| Collagen I with 25% Matirgel | HUVECs | At least for 2 days | At least for 2 days | Bischer et al. [54] |

Notes: * Pre-gel solution of transglutaminase cross-linked gelatin

Table 4: Hydrogels compared with viability of the cells and perfusion of the vessel

# 7 Research proposal

## 7.1 Research potential

Incorporating the mechanical parameters experienced by the cells, such as strain and blood flow, is important in mimicking the alveolar-capillary barrier. As discussed in chapter 3, different models have been developed and some are commercially available. These models can be static or have unidirectional strain combined with flow. A model developed by Jung et al., combines a random vascularized network with epithelial cells. This is already an improvement in models because vascularization better mimics the alveolar tissue than a monolayer of endothelial cells. However, creating a perfusable vascularized network is challenging and therefore a pre-patterned structure for the vessels is preferred. Scaffold based vascularized models will also provide more control over the mechanical parameters in a LOC model, particularly, the hemodynamics. Having a pre-patterned vascular structure in alveolar-capillary barrier is, to my knowledge, not been created yet. So, the research potential I have found is to create networked, cylindrical microfluidic channels, vascularize those channels and implement them with an ALI monolayer of alveolar epithelial cells creating an alveolar-capillary barrier. Another research potential is to stretch this membrane by applying pressure difference, causing tri-axial strain of the membrane.

Before obtaining this model, more research should be done to obtain the information needed for designing our model. As discussed in section 6.1 it is not known what diameter provides good performances related to the cell viability and perfusibility of the channel. Also, the diameter which can be obtained with sacrificial molding can be more explored. This is linked to the hydrogel and the sacrificial material used for the mold. The composition of a hydrogel with the optimal channel forming and a possible trade off between angiosese is also unknown, but this will not be part of our focus.

## 7.2 Research question

The research potential mentioned above in section 7.1 lead to the following reserearch question and its sub-questions:
**Can vascularization, using sacrificial molding, and cyclic stretching, using a pressure differential, be integrated into an aveoli-on-a-chip?**

- How to vascularize hollow channels in hydrogels?
  - Which hydrogel should be used?
- How to fabricate channels with diameters ranging from 30-300$\mu$m with sacrificial molding?
  - What sacrificial material should be used?
- Can a pressure differential be used for the cyclical stretching of the alveolar-capillary-barrier?
  - How to integrate epithelial cells having an air-liquid interface and vascularized endothelial cells?

## 7.3 Requirements and objectives

Several requirements need to be considered when answering the research question and sub-questions mentioned in the 7.2 section. These requirements will be used to set the objectives. The goal of the device is to create models of an alveolar-capillary barrier to study the effect of pollution on the barrier. Therefore, the model should replicate the biological environment of the tissue and be reproducible. It should also be possible to manufacture the device at TU Delft and use it at Erasmus MC, preferably with optimal adaptation to existing processes.

Reproducing the biological environment of the tissue is important because of the cellular response to, for example, shear stress or strain. The mechanical properties we want to include in our model are listed in the table 5. Several of these properties are based on the findings in chapter 2.

| Requirements biological model | Value |
|---|---|
| Shear stress on endothelial cells | 0.1-1 $N/m^2$ |
| Stiffness of tissue | 1-2kPa |
| Strain tissue | 10-20% |
| Stretching frequency | 0.2 Hz |
| Perfusability of the vessels | Two weeks |

Table 5: Requirements biological environment of the model

The stiffness of the lung tissue is 1-2kPa, but this is not a requirement of the stiffness of our device or base. The base can have a higher stiffness in the range of 100 MPa, like that of PDMS, because it is still possible to obtain a strain around 10% and this will make the device more robust [55]. So, in addition to the requirements of the biological environment of the tissue model, there are also requirements of the device. To study the cellular response to environmental stress, the cellular response is assessed optically, for example with fluoroscopy, an optically transparent device is needed. To perfuse the channels, the channels need to be connected to a pump. When stretching the barrier with a pressure differential, the device should have a base with mechanical properties that create the desired stretch in the tissue.

| Device requirements |
|---|
| Optical transparency |
| Connection pump to the channels |
| Functional base to obtain 10-20% strain of the tissue |
| Reproducible model |

Table 6: Requirements device

In order to meet these requirements, several objectives need to be set.

- Develop a 3D printed sacrificial material with a cylindrical simple structure.
- Evaluate the dissolution of the sacrificial material within a hydrogel.
- Evaluate a cell seeding method to vascularize channels.
- Evaluate the optimal hydrogel and diameter to prolong the perfusibility of vessels.
- Determine whether vessels remain perfusable for at least two or even four weeks.
- Evaluate the vascularization of a more complex structure using sacrificial molding.
- Implement vascularization on ALI cultured alveoli epithilial cells.
- Develop a device with a functional base that can be actuated by pressure potential.
- Evaluate the performance of the model.

## 7.4 Methodology and risk mitigation

The methodology shows the approach to achieving our objectives. Risk mitigation was taken into account in determining the approach to our design. Cell culture is a process that can take several days. Testing the performance of a device will therefore be a time-consuming process. In particular, vascularization is one of our biggest risks. Evaluating a method to vascularize channels might take a lot of time or might not succeed at all. So our strategy is to work on a mechanical challenge in parallel with a biological evaluation.

Developing a 3D printed sacrificial material with a desired structure is a mechanical challenge while evaluating the optimal hydrogel and diameter is a biological challenge. It is desirable to start the evaluation of the cell seeding method, hydrogel and diameter as fast as possible and not be dependent on the success of the sacrificial molding. Therefor, the first step is to create channels with a simpler fabrication method. As discussed in section 6.2 needle molding is a relatively simpler method. The

left side of the scheme in figure 13 shows how some of the biological objectives can be achieved while gaining expertise in sacrificial casting. There are several aspects to gaining this expertise. Firstly, the material should be chosen, carbohydrate glass might be obvious, but more research should be done on alternative materials such as PVA. As a first step, this material should be printed in a straight line, once this is achieved it can be dissolved and a more complex structure can be printed. A more complex structure is one with multiple channels that convert and divert, leading to an inlet and an outlet of the channels.

One of the risks in this design phase is the inability to create vascularized channels with sacrificial modelling. This may be because the sacrificial material fails to print or dissolve. The device is then designed using needle molding as the manufacturing technique. In this case, the left side of the scheme will be followed, providing an alternative research outcome. A disadvantage could be that a less complex channel structure can be formed, but it allows the implementation of vascularization in our model. Another objective is to determine whether perfusability can be maintained for at least two or four weeks. If the vessel remains perfusable for 4 weeks, which would be an excellent result, then this will allow the start of ALI at the same time as the vascularization of the channels. If the vessels remain perfusable for 2 weeks or less, an option may be found in delaying the dissolution of the sacrificial and postponing the vascularization of the channels. The study the maximal perfusable time of the vessels will take a lot of "waiting" time, which can be used to design a functional base of the device. The last step of our research, after the integration of all the features, is the evaluation of our model. This evaluation can be done by validating the barrier functions and cell viability using fluoroscopy.

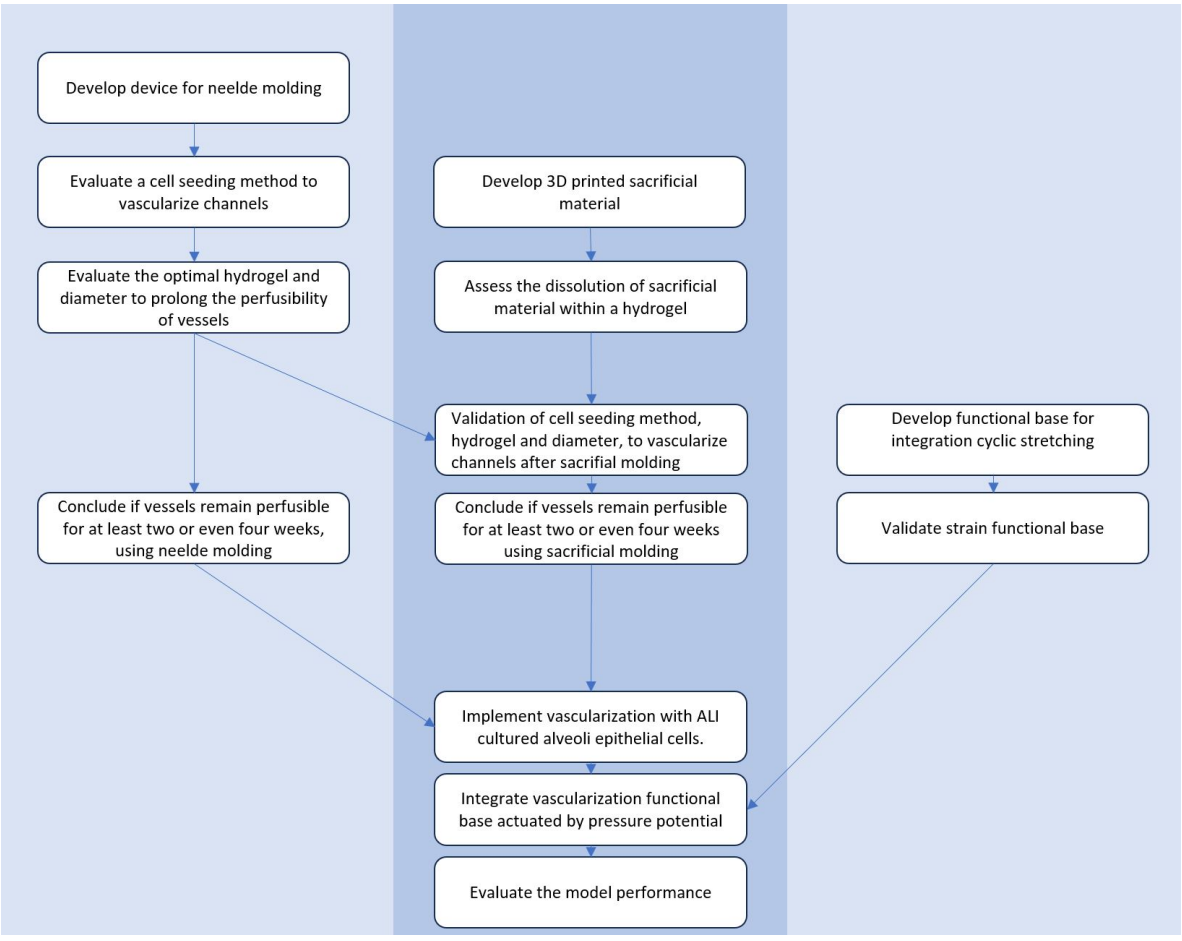


Figure 13: Methodology

## 7.5 Planning research

Figure 14 shows the planning of the research, it includes several milestones. The first milestone is to determine the composition of the hydrogel and the diameters of the channels. The second milestone is to determine whether vessel formation is successful and, if so, to determine the maximum duration of vessel integrity. Then there are two milestones at the beginning of May. One is to determine if vascularization of the channels created by sacrificial molding can be achieved. The other milestone is to validate whether the desired strain can be achieved with the developed base. Then, in early July, the big milestone is set to determine whether the device, once integrated, will result in a well-replicated and reproducible model. The results of this research will then be written and the milestone for completion of the report will be set at the end of July.

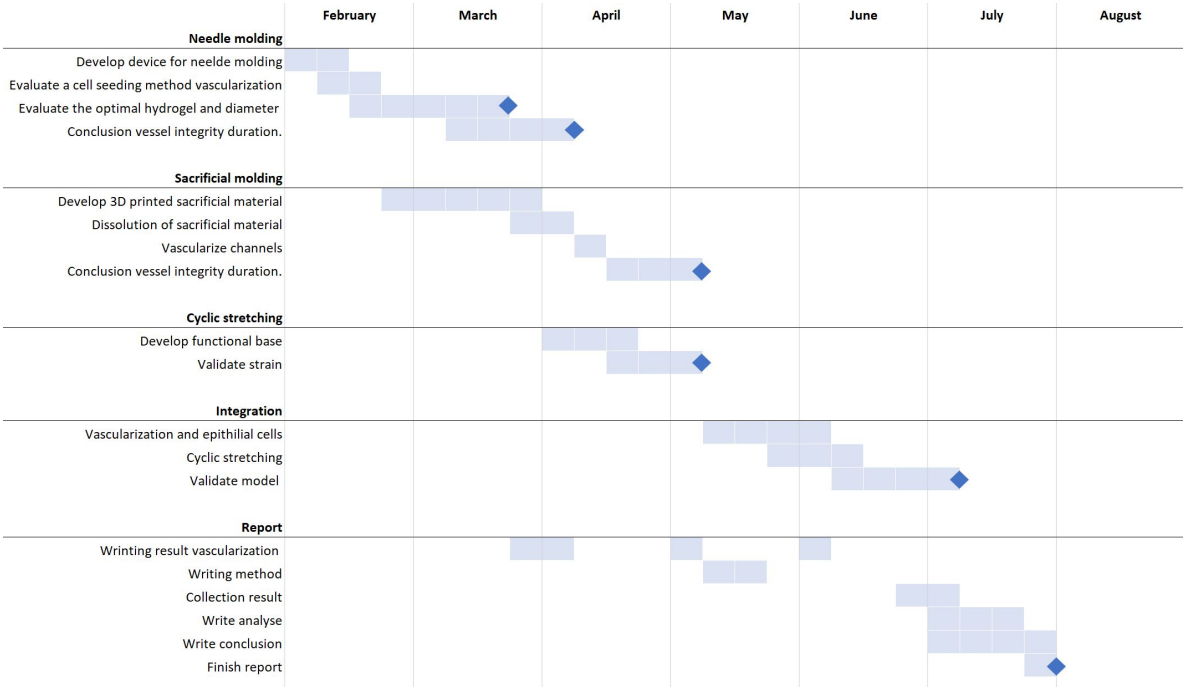


Figure 14: Research planning

# References


[1] A. Kadyrova, P. Kanabekova, A. Martin, D. Begimbetova, and G. Kulsharova, "Evaluation of membranes for mimicry of an alveolar-capillary barrier in microfluidic lung-on-a-chip devices," 2022. [Online]. Available: https://doi.org/10.1016/j.matpr.2022.05.582

[2] W. F. Boron and E. L. Boulpaep, *Medical physiology, 2e updated edition e-book: with student consult online access*. Elsevier health sciences, 2012.

[3] M. A. Elhelu, "The role of macrophages in immunology," *Journal of the National Medical Association*, vol. 75, p. 314, 3 1983. [Online]. Available: /pmc/articles/PMC2561478/?report=abstracthttps://www.ncbi.nlm.nih.gov/pmc/articles/PMC2561478/

[4] S. M. Cloonan and A. M. Choi, "Mitochondria in lung disease," *The Journal of Clinical Investigation*, vol. 126, pp. 809–820, 3 2016.

[5] P. Gehr, M. Bachofen, and E. R. Weibel, "The normal human lung: Ultrastructure and morphometric estimation of diffusion capacity'," *Respiration Phyvsiology*, vol. 32, pp. 121–140, 1978.

[6] A. Doryab, S. Tas, B. Taskin, L. Yang, A. Hilgendorff, J. Groll, D. E. Wagner, and O. Schmid, "Review www.afm-journal.de evolution of bioengineered lung models: Recent advances and challenges in tissue mimicry for studying the role of mechanical forces in cell biology," 2019. [Online]. Available: https://onlinelibrary.wiley.com/doi/10.1002/adfm.201903114

[7] S. R. R. S. T. D. and T. P., *Essentials of anatomy and physiology (4th ed.)*. McGraw-Hill., 2002.

[8] N. Khalilgharibi and Y. Mao, "Cite this article," 2021.

[9] O. T. Guenat and F. Berthiaume, "Incorporating mechanical strain in organs-on-a-chip: Lung and skin," *Biomicrofluidics*, vol. 12, p. 42207, 2018. [Online]. Available: https://doi.org/10.1063/1.5024895

[10] E. D. Crandall, M. A. Matthay, and S. Garfinkel, "Alveolar epithelial transport," *https://doi.org/10.1164/ajrccm.163.4.2006116*, vol. 163, pp. 1021–1029, 12 2012. [Online]. Available: www.atsjournals.org

[11] Y. S. Khan and D. T. Lynch, *Histology, Lung*. StatPearls Publishing, Treasure Island (FL), 2022. [Online]. Available: http://europepmc.org/books/NBK534789

[12] A. Doryab, M. B. Taskin, P. Stahlhut, A. Schröppel, D. E. Wagner, J. Groll, and O. Schmid, "A biomimetic, copolymeric membrane for cell-stretch experiments with pulmonary epithelial cells at the air-liquid interface," *Advanced Functional Materials*, vol. 31, 3 2021.

[13] L. Knudsen and M. Ochs, "The micromechanics of lung alveoli: structure and function of surfactant and tissue components the structural components for gas exchange," *Histochemistry and Cell Biology*, vol. 150, pp. 661–676, 2018. [Online]. Available: https://doi.org/10.1007/s00418-018-1747-9

[14] E. N. Marieb and K. Hoehn, *Human Anatomy and Physiology, 11th edition*. Pearson, 2018.

[15] S. Upadhyay and L. Palmberg, "Air-liquid interface: Relevant in vitro models for investigating air pollutant-induced pulmonary toxicity," 2018. [Online]. Available: https://academic.oup.com/toxsci/article/164/1/21/4925479

[16] E. R. Weibel, "Respiration physiology 11, 54-75," 1970.

[17] C. Hermans and A. Bernard, "Pneumoproteinaemia: a new perspective in the assessment of lung disorders," *European Respiratory Journal*, vol. 11, pp. 801–803, 4 1998. [Online]. Available: https://erj.ersjournals.com/content/11/4/801https://erj.ersjournals.com/content/11/4/801.abstract

[18] M. G. Levitzky, *Blood Flow to the Lung*. New York, NY: McGraw-Hill Education, 2017. [Online]. Available: accessmedicine.mhmedical.com/content.aspx?aid=1160936239

[19] D. F. Tees, P. Sundd, and D. J. Goetz, "A flow chamber for capillary networks: Leukocyte adhesion in capillary-sized, ligand-coated micropipettes," *Principles of Cellular Engineering*, pp. 213–231, 1 2006.

[20] E. R. Weibel, "Lung morphometry: the link between structure and function introduction: searching for the structural basis of lung physiology."

[21] C. Desplechain, B. Foliguet, E. Barrat, G. Grignon, and F. Touati, "Les pores de kohn des alveoles pulmonaires," *Clinical Respiratory Physiology*, vol. 19, pp. 59–68, 1983.

[22] W. Mitzner, "Mechanics of the lung in the 20 th century."

[23] K. Shang, M. Fu, R. Morent, al, G. Fu, W. Cai, C. Kan, M. J. Oldham, and O. R. Moss, "Pores of kohn: forgotten alveolar structures and potential source of aerosols in exhaled breath optical study of the ultrasonic formation process of noble metal nanoparticles dispersed inside the pores of monolithic mesoporous silica pores of kohn: forgotten alveolar structures and potential source of aerosols in exhaled breath," *Journal of Breath Research J. Breath Res*, vol. 13, p. 21003, 2019. [Online]. Available: https://doi.org/10.1088/1752-7163/ab0524

[24] J. B. Forrest, "533 with 6 text-figure8 the effect of changes in lung volume on the size and shape of alveoli," *J. Physiol*, vol. 210, pp. 533–547, 1970, [forrest 1970]¡br/¿¡br/¿Opzoek of de 4

[25] C. E. Perlman and J. Bhattacharya, "Alveolar expansion imaged by optical sectioning microscopy," *J Appl Physiol*, vol. 103, pp. 1037–1044, 2007. [Online]. Available: http://www.

[26] J. M. B. Hughes, F. G. Hoppin, and J. Mead, "Effect of lung inflation on bronchial length and diameter in excised lungs," *JOURNAL OF APPLIED PHYSIOLOGY*, vol. 32, 1972.

[27] C. M. Waters, E. Roan, and D. Navajas, "Mechanobiology in lung epithelial cells: Measurements, perturbations, and responses," 2012, bron 3 van Guenat 2018, waters 2012 (wat weer bron 3 van nissar is)¡br/¿Dit is ook bron 24 van Doryab,2019]¡br/¿dit is de bron als het goed is over linear strain of 4

[28] A. Gump, L. Haughney, and J. Fredberg, "Relaxation of activated airway smooth muscle: relative potency of isoproterenol vs. tidal stretch," *Journal of applied physiology (Bethesda, Md. : 1985)*, vol. 90, pp. 2306–2310, 2001. [Online]. Available: https://pubmed.ncbi.nlm.nih.gov/11356796/

[29] E. Roan and C. M. Waters, "What do we know about mechanical strain in lung alveoli?" *Am J Physiol Lung Cell Mol Physiol*, vol. 301, pp. 625–635, 2011, [Roan,2011]¡br/¿¡br/¿Bron 24, van Doryab, 2019 wat bron 15 is van Sophhie¡br/¿. [Online]. Available: http://www.ajplung.org

[30] J. J. Fredberg, D. Inouye, B. Miller, M. Nathan, S. Jafari, S. H. Raboudi, J. P. Butler, and S. A. Shore, "Airway smooth muscle, tidal stretches, and dynamically determined contractile states," *American journal of respiratory and critical care medicine*, vol. 156, pp. 1752–1759, 1997. [Online]. Available: https://pubmed.ncbi.nlm.nih.gov/9412551/

[31] T. J. Bennet, A. Randhawa, J. Hua, K. C. Cheung, T. J. . Bennet, A. . Randhawa, J. . Hua, K. C. Cheung, T.-L. Hackett, and E. T. Osei, "Airway-on-a-chip: Designs and applications for lung repair and disease," *Cells 2021, Vol. 10, Page 1602*, vol. 10, p. 1602, 6 2021, [Bennet 2021]. [Online]. Available: https://www.mdpi.com/2073-4409/10/7/1602/htmhttps://www.mdpi.com/2073-4409/10/7/1602

[32] L. Horvath, Y. Umehara, C. Jud, F. Blank, A. Petri-Fink, and B. Rothen-Rutishauser, "Engineering an in vitro air-blood barrier by 3d bioprinting," *Scientific Reports 2015 5:1*, vol. 5, pp. 1–8, 1 2015, [Horvath 2015]¡br/¿¡br/¿. [Online]. Available: https://www.nature.com/articles/srep07974

[33] P. Zamprogno, S. Wüthrich, S. Achenbach, G. Thoma, J. D. Stucki, N. Hobi, N. Schneider-Daum, C. M. Lehr, H. Huwer, T. Geiser, R. A. Schmid, and O. T. Guenat, "Second-generation lung-on-a-chip with an array of stretchable alveoli made with a biological membrane," *Communications biology*, vol. 4, 12 2021. [Online]. Available: https://pubmed.ncbi.nlm.nih.gov/33547387/

[34] S. Pun, L. C. Haney, and R. Barrile, "Modelling human physiology on-chip: Historical perspectives and future directions," *Micromachines*, vol. 12, 10 2021, [pun '21].

[35] A. O. Stucki, J. D. Stucki, S. R. R. Hall, M. Felder, Y. Mermoud, R. A. Schmid, T. Geiser, and O. T. Guenat, "From chip-in-a-lab to lab-on-a-chip: towards a single handheld electronic system for multiple application-specific lab-on-a-chip (asloc)," vol. 15, p. 1302, 2014, [Stucki, 2015]¡br/¿Aangeraden door Urs op 20-08-23¡br/¿. [Online]. Available: www.rsc.org/loc

[36] L. van Os, J. Yeoh, G. Witz, D. Ferrari, P. Krebs, Y. Chandorkar, S. Zeinali, A. Sengupta, and O. T. Guenat, "Immune cell extravasation in an organ-on-chip to model lung inflammation," *European Journal of Pharmaceutical Sciences*, vol. 187, p. 106485, 8 2023.

[37] D. Huh, B. D. Matthews, A. Mammoto, M. Montoya-Zavala, H. Y. Hsin, and D. E. Ingber, "Reconstituting organ-level lung functions on a chip," *Science*, vol. 328, pp. 1662–1668, 6 2010.

[38] B. Vailhé, D. Vittet, and J. J. Feige, "In vitro models of vasculogenesis and angiogenesis," *Laboratory Investigation 2001 81:4*, vol. 81, pp. 439–452, 4 2001. [Online]. Available: https://www.nature.com/articles/3780252

[39] A. Monteduro, S. Rizzato, G. C. Biosensors, ..., and undefined 2023, "Organs-on-chips technologies–a guide from disease models to opportunities for drug development," *Elsevier*, 2023. [Online]. Available: https://www.sciencedirect.com/science/article/pii/S0956566323002130?casa_token=_AdRGw2f9NsAAAAA:Io2SdfY8p4N-JSQQF48OdXi3m6GC8RIFgx4bvTPJvlIlG_UApR-6bMcN5kY2tKS-js9r5TjYNOG0

[40] "Development of a functional airway-on-a-chip by 3d cell printing," 2018, [Ju Young Park 2019]. [Online]. Available: https://doi.org/10.1088/1758-5090/aae545

[41] O. Jung, Y. T. Tung, E. Sim, Y. C. Chen, E. Lee, M. Ferrer, and M. J. Song, "Development of human-derived, three-dimensional respiratory epithelial tissue constructs with perfusable microvasculature on a high-throughput microfluidics screening platform," *Biofabrication*, vol. 14, p. 025012, 2 2022, [Jung 2022]. [Online]. Available: https://iopscience.iop.org/article/10.1088/1758-5090/ac32a5https://iopscience.iop.org/article/10.1088/1758-5090/ac32a5/meta

[42] L. Bova, F. Billi, and E. Cimetta, "Mini-review: advances in 3d bioprinting of vascularized constructs," *Biology Direct*, vol. 15, pp. 1–5, 12 2020. [Online]. Available: https://biologydirect.biomedcentral.com/articles/10.1186/s13062-020-00273-4

[43] D. Sharma, D. Ross, G. Wang, W. Jia, S. J. Kirkpatrick, and F. Zhao, "Upgrading prevascularization in tissue engineering: A review of strategies for promoting highly organized microvascular network formation," *Acta Biomaterialia*, vol. 95, pp. 112–130, 9 2019, [sharma, 2019]¡br/¿¡br/¿4.3.1 micro-scaffold based prevascularization¡br/¿4.3.2. Microfluidics devices for structured microvessel formation and in vitro bio-mechanism detection .

[44] S. Fleischer, D. N. Tavakol, and G. Vunjak-Novakovic, "From arteries to capillaries: approaches to engineering human vasculature," *Advanced functional materials*, vol. 30, 9 2020, [Fleischer 2020]. [Online]. Available: /pmc/articles/PMC7942836//pmc/articles/PMC7942836/?report=abstracthttps://www.ncbi.nlm.nih.gov/pmc/articles/PMC7942836/

[45] H. Grover, C.-P. Spatarelu, K. De'De', S. Zhao, K. Yang, Y. S. Zhang, Z. Chen, H. Grover, C.-P. Spatarelu, K. De'De', S. Zhao, K. Yang, Y. S. Zhang, and Z. Chen, "Vascularization in 3d printed tissues: emerging technologies to overcome longstanding obstacles," *AIMS Cell and Tissue Engineering 2018 3:163*, vol. 2, pp. 163–184, 2018. [Online]. Available: http://www.aimspress.com/article/doi/10.3934/celltissue.2018.3.163http://www.aimspress.com/rticle/doi/10.3934/celltissue.2018.3.163

[46] K. M. Chrobak, D. R. Potter, and J. Tien, "Formation of perfused, functional microvascular tubes in vitro," 2006. [Online]. Available: www.elsevier.com/locate/ymvre

[47] S. Park, T. H. Kim, S. H. Kim, S. You, and Y. Jung, "Three-dimensional vascularized lung cancer-on-a-chip with lung extracellular matrix hydrogels for in vitro screening," *Cancers*, vol. 13, 8 2021. [Online]. Available: https://pubmed.ncbi.nlm.nih.gov/34439103/

[48] J. Paek, S. E. Park, Q. Lu, K. T. Park, M. Cho, J. M. Oh, K. W. Kwon, Y. S. Yi, J. W. Song, H. I. Edelstein, J. Ishibashi, W. Yang, J. W. Myerson, R. Y. Kiseleva, P. Aprelev, E. D. Hood, D. Stambolian, P. Seale, V. R. Muzykantov, and D. Huh, "Microphysiological engineering of self-assembled and perfusable microvascular beds for the production of vascularized three-dimensional human microtissues," *ACS Nano*, vol. 13, pp. 7627–7643, 7 2019. [Online]. Available: https://pubs.acs.org/doi/full/10.1021/acsnano.9b00686

[49] A. Shimizu, W. H. Goh, S. Itai, M. Hashimoto, S. Miura, and H. Onoe, "Lab on a chip devices and applications at the micro-and nanoscale ecm-based microchannel for culturing in vitro vascular tissues with simultaneous perfusion and stretch †," vol. 20, 2020.

[50] J. S. Miller, K. R. Stevens, M. T. Yang, B. M. Baker, D. H. T. Nguyen, D. M. Cohen, E. Toro, A. A. Chen, P. A. Galie, X. Yu, R. Chaturvedi, S. N. Bhatia, and C. S. Chen, "Rapid casting of patterned vascular networks for perfusable engineered three-dimensional tissues," *Nature Materials 2012 11:9*, vol. 11, pp. 768–774, 7 2012, [jardan s. miller 2012]. [Online]. Available: https://www.nature.com/articles/nmat3357

[51] Y.-T. Tung, C.-C. Chang, J.-C. Ju, and G.-J. Wang, "Fabrication of a reticular poly(lactide-co-glycolide) cylindrical scaffold for the in vitro development of microvascular networks," *Science and Technology of Advanced Materials*, vol. 18, pp. 163–171, 2017. [Online]. Available: http://dx.doi.org/10.1080/14686996.2016.1278351

[52] Y. T. Lin, Y. T. Tung, J. Y. Wong, and G. J. Wang, "Fabrication of perfusable microvessel networks by mimicking in vivo vasculogenesis using a novel scaffold-wrapping method," *Materials and Design*, vol. 227, p. 111707, 3 2023, [Lin 2023].

[53] S. Dávila, J. Cacheux, and I. Rodríguez, "Microvessel-on-chip fabrication for the in vitro modeling of nanomedicine transport," 2021, davila 2021. [Online]. Available: https://doi.org/10.1021/acsomega.1c00735

[54] L. L. Bischel, E. W. Young, B. R. Mader, and D. J. Beebe, "Tubeless microfluidic angiogenesis assay with three-dimensional endothelial-lined microvessels," *Biomaterials*, vol. 34, p. 1471, 2 2013. [Online]. Available: /pmc/articles/PMC3529167//pmc/articles/PMC3529167/?report=abstracthttps://www.ncbi.nlm.nih.gov/pmc/articles/PMC3529167/

[55] J. Shrestha, S. R. Bazaz, H. A. Es, D. Y. Azari, B. Thierry, M. E. Warkiani, and M. Ghadiri, "Lung-on-a-chip: the future of respiratory disease models and pharmacological studies," *Critical reviews in biotechnology*, vol. 40, pp. 213–230, 2 2020. [Online]. Available: https://pubmed.ncbi.nlm.nih.gov/31906727/